

https://dspace.org/

Postcranial osteology of the neotype specimen of Massospondylus carinatus Owen, 1854 (Dinosauria: Sauropodomorpha) from the upper Elliot formation of South Africa

Barrett, Paul M.; Chapelle, Kimberley E.J.; Staunton, Casey K.; Botha, Jennifer; Choiniere, Jonah N.

2019-04
Evolutionary Studies Institute
https://hdl.handle.net/10539/26829

Downloaded from a DSpace repository. https://dspace.org/

Postcranial osteology of the neotype specimen of *Massospondylus carinatus* Owen, 1854 (Dinosauria: Sauropodomorpha) from the upper Elliot formation of South Africa

Paul M. Barrett[1,2*] §, Kimberley E.J. Chapelle[2], Casey K. Staunton[2], Jennifer Botha[3] & Jonah N. Choiniere[2]

[1]*Department of Earth Sciences, Natural History Museum, Cromwell Road, London SW7 5BD, U.K.*

[2]*Evolutionary Studies Institute, University of the Witwatersrand, Private Bag 3, WITS 2050, Johannesburg, South Africa*

[3]*Department of Karoo Palaeontology, National Museum, PO Box 266, Bloemfontein 9300, South Africa*

Received 2 September 2018. Accepted 30 January 2019

Massospondylus carinatus Owen, 1854, from the earliest Jurassic upper Elliot Formation of South Africa, was one of the first dinosaurs to be described from Gondwana. It has been incorporated into numerous phylogenetic, palaeobiological and biostratigraphic analyses, is often viewed as an exemplar for understanding sauropodomorph anatomy and is a key taxon in studies of early dinosaur evolution. Since its initial description, numerous specimens have been referred to this species, ranging from isolated postcranial elements to complete skeletons with three-dimensional skulls. In addition, *M. carinatus* has been identified in areas outside of the main Karoo Basin. Surprisingly, however, there have been few attempts to define the taxon rigorously, so that the basis for many of these referrals is weak, undermining the utility of this abundant material. Here, we provide the first detailed postcranial description of the neotype specimen of *M. carinatus*, use it as a basis for diagnosing the species on the basis of cranial, axial and appendicular characters, demonstrate that it represents an adult individual on the basis of osteohistology, and discuss ways in which these data can assist in providing a better understanding of Karoo-aged African dinosaur faunas.

Keywords: *Massospondylus carinatus*, Massospondylidae, Sauropodomorpha, upper Elliot Formation, postcranial anatomy, osteohistology, taxonomy.

Palaeontologia africana 2019. ©2019 Paul M. Barrett, Kimberley E. J. Chapelle, Casey K. Staunton, Jennifer Botha & Jonah N. Choiniere. This is an open-access article published under the Creative Commons Attribution 4.0 Unported License (CC BY4.0). To view a copy of the license, please visit http://creativecommons.org/licenses/by/4.0/. This license permits unrestricted use, distribution, and reproduction in any medium, provided the original author and source are credited.
The article and five supplements are permanently archived at: http://wiredspace.wits.ac.za/handle/10539/26829

INTRODUCTION

Massospondylus carinatus Owen, 1854 was one of the first dinosaurs to be named from the southern hemisphere and since its initial description numerous complete skeletons, including skulls, and thousands of isolated elements have been referred to this taxon (e.g. Cooper 1981; Kitching & Raath 1984; Gow *et al*. 1990). *M. carinatus* is a non-sauropod sauropodomorph that is best known from the latest Triassic/earliest Jurassic upper Elliot and Clarens formations (upper Stormberg Group) of the Karoo Basin in South Africa and Lesotho (e.g. Kitching & Raath 1984; Gow *et al*. 1990; Sues *et al*. 2004; Knoll 2005; Chapelle & Choiniere 2018), but additional material has also been reported from the Forest Sandstone and Mpandi formations of the mid-Zambezi, Mana Pools and Tuli basins in Zimbabwe (e.g. Attridge 1963; Raath *et al*. 1970; Bond 1973; Cooper 1981; Munyikwa 1997), which are thought to be correlative with upper Stormberg Group sediments (e.g. Johnson *et al*. 1996; Bordy & Catuneanu 2001; Catuneanu *et al*. 2005). Indeed, *Massospondylus* specimens are so abundant that it was designated the nominal taxon for the uppermost biostratigraphical range zone within the Karoo Supergroup of South Africa (*Massospondylus* Range Zone: Kitching & Raath 1984). It has also been used to infer correlations between Gondwanan basins, both regionally (Bond 1965; Cooper 1981) and internationally (Apaldetti *et al*. 2011).

As a result of these discoveries, *M. carinatus* is potentially one of the best-represented early dinosaurs and has formed the basis for numerous palaeobiological studies on locomotion (Bonnan & Senter 2007), growth rates (Chinsamy 1993; Erickson *et al*. 2001), tooth replacement (D'Emic *et al*. 2013), ontogeny (Gow 1990; Gow *et al*. 1990; Reisz *et al*. 2005, 2010) and nesting behaviour (Kitching 1979; Zelenitsky & Modesto 2002; Reisz *et al*. 2012). It has also been an important exemplar in broader studies of early dinosaur herbivory, palaeoecology and faunal studies (e.g. Raath 1974; Cooper 1981; Galton 1985a; Crompton & Attridge 1986; Gow *et al*. 1990; Barrett 2000; Knoll 2005; Barrett & Upchurch 2007; Butler *et al*. 2013).

*Author for correspondence. E-mail: p.barrett@nhm.ac.uk

***Palaeontologia africana* 53: 114–178 — ISSN 2410-4418 [Palaeontol. afr.] Online only**
Permanently archived on the 29th of April 2019 at the University of the Witwatersrand, Johannesburg, South Africa.
The article and five supplements are permanently archived at: http://wiredspace.wits.ac.za/handle/10539/26829

Finally, due to the completeness of many referred specimens, *M. carinatus* is frequently included in phylogenetic analyses of early sauropodomorph and early dinosaur interrelationships (e.g. Yates 2004, 2007a; Smith & Pol 2007; Upchurch *et al*. 2007; Sertich & Loewen 2010; Yates *et al*. 2010; Apaldetti *et al*. 2011, 2013; Otero & Pol 2013; Baron *et al*. 2017; Chapelle & Choiniere 2018). Most of these recent works recover *M. carinatus* within a small, but globally distributed, clade (the eponymous Massospondylidae) that usually also includes *Adeopapposaurus*, *Coloradisaurus*, *Glacialisaurus*, *Leyesaurus* and *Lufengosaurus*, although clade membership varies between analyses.

For many years it was assumed that *M. carinatus* was the only sauropodomorph dinosaur from the upper Stormberg Group (Kitching & Raath 1984; Lucas & Hancox 2001; Knoll 2005). However, a range of other taxa spanning the sauropodomorph tree have now been named from this unit including *Aardonyx celestae* (Yates *et al*. 2010), *Antetonitrus ingenipes* (Yates & Kitching 2003), *Arcusaurus pereirabdalorum* (Yates *et al*. 2011), *Ignavusaurus rachelis* (Knoll 2010), *M. kaalae* (Barrett 2009) and *Pulanesaura eocollum* (McPhee *et al*. 2015) (see review in McPhee *et al*. 2017). As a result, the former practice of referring all sauropodomorph specimens recovered from the upper Stormberg Group to *Massospondylus* by default is no longer tenable (Barrett 2004, 2009; Yates *et al*. 2004; McPhee *et al*. 2017).

In addition to material from southern Africa, specimens from other Late Triassic and Early Jurassic deposits elsewhere have been referred to *Massospondylus*, though not to *M. carinatus*. From India, these include the type specimens of *M. rawesi* Lydekker, 1890a and *M. hislopi* Lydekker, 1890a, from the Lameta Beds (Maastrichtian) and Lower Maleri Formation (late Carnian–early Norian), respectively. *M. rawesi*, represented by an isolated tooth, is currently regarded as a *nomen dubium* (an indeterminate theropod dinosaur; e.g. Carrano *et al*. 2010), whereas *M. hislopi*, which was based on an isolated vertebra, lacks any features supporting its validity and is also regarded as a *nomen dubium* (Sauropodomorpha indet.: von Huene 1906; Galton & Upchurch 2004). Another specimen from the Upper Maleri Formation (late Norian–Rhaetian) formerly referred to *Massospondylus* sp. (Kutty *et al*. 1987) is now considered to represent an indeterminate guaibasaurid sauropodomorph (Novas *et al*. 2011).

Other reported occurrences of *Massospondylus* sp. from outside southern Africa were used previously to support global biostratigraphic correlations for the Early Jurassic (e.g. Attridge *et al*. 1985) but these have since been shown to represent other sauropodomorph taxa. A crushed, but almost complete, skull associated with fragmentary postcranial material from the Kayenta Formation (Sinemurian–Pliensbachian) of the U.S.A. (Attridge *et al*. 1985) has now been referred to *Sarahsaurus aurifontanalis* (Rowe *et al*. 2011), while a complete skull and partial skeleton from the Cañón del Colorado Formation (Lower Jurassic) of Argentina has been designated the holotype of *Adeopapposaurus mognai* (Martínez 2009). Finally, Cooper (1981) suggested that the Early Jurassic Chinese genera *Lufengosaurus* and *Yunnanosaurus* should be regarded as junior synonyms of *Massospondylus*, vastly expanding the geographic range of the genus, but the numerous differences between these taxa clearly support their generic separation (Young 1941, 1942; Galton & Upchurch 2004; Barrett *et al*. 2005, 2007). These historical misidentifications result, at least in part, from the lack of published, comparative information on *Massospondylus* specimens from the type area.

Surprisingly, in spite of its prominence in palaeobiological, biostratigraphical and systematic studies, there has been relatively little work on the anatomy and taxonomy of *Massospondylus carinatus* and there have been few attempts to diagnose the taxon or to establish clear criteria for referring additional material to its hypodigm. Most earlier descriptions were based on isolated remains whose associations and exact provenance were unknown (e.g. Owen 1854; Seeley 1895a; von Huene 1906; Haughton 1924), although a proliferation of new *Massospondylus* species names also appeared at this time (see Galton & Cluver [1976] and Cooper [1981] for reviews; see Discussion, below). There were few additional studies until more complete specimens were discovered from the 1960s onward, primarily through the efforts of A.W. Crompton, C.E. Gow and R.M.H Smith at the Iziko South African Museum, J.W. Kitching of the University of the Witwatersrand and W.J. de Klerk of the Albany Museum, all working in the main Karoo Basin of South Africa, with additional collections being made from the upper Elliot and Clarens formations of Lesotho by several French and Anglo/South African expeditions (e.g. Ellenberger *et al*. 1964; Attridge & Charig 1967; Anonymous 1969). Nevertheless, these new discoveries did not spur any thorough treatments of the taxon. Indeed, for several decades, the main published source of information on *M. carinatus* was Cooper's (1981) monograph, which is based upon a variety of specimens collected from several different Zimbabwean localities and formations. Although this became the standard reference work on *M. carinatus*, it has not yet been demonstrated that this Zimbabwean material is conspecific with that from the main Karoo Basin (or that the Zimbabwean specimens represent a single taxon).

Some recent work has attempted to evaluate the vast amount of material referred to *Massospondylus carinatus*, in order to more adequately characterize the taxon. Gow *et al*. (1990) published a brief account of several complete and partially complete skulls that they referred to *M. carinatus* (including what was to become the neotype, BP/1/4934, as well as BP/1/4376, BP/1/4779, BP/1/4930, BP/1/4998, BP/1/5241 and several other cranial fragments) alongside a more targeted description of isolated braincase material (BP/1/5231, BP/1/5276: Gow 1990). However, these skulls were not illustrated or described in detail until the publication of Sues *et al*. (2004), who also proposed the first detailed diagnosis of the taxon, which was based solely on cranial characters. In all of these publications, the variations in cranial proportions and anatomy observed within this large sample were ascribed to plastic deformation or other preservational differences and the potential of these features for taxonomic or palaeobiological



Figure 1. Neotype skeleton of *Massospondylus carinatus* (BP/1/4934) in left lateral (**A**) and right lateral (**B**) views. Scale bars = 50 mm. (Continued on p. 117.)

purposes were unexplored (although Gow *et al*. [1990] speculated that differences in cranial robusticity might reflect sexual dimorphism). Additional information on palatal and mandibular anatomy was provided by Barrett & Yates (2006) based on another referred specimen (SAM-PK-K1314). Barrett (2004, 2009) erected a new species, *M. kaalae*, based on a small, disarticulated partial skull (SAM-PK-K1325) that possessed distinctive braincase anatomy, and also referred an additional skull to *M. carinatus* (SAM-PK-K7904). The most comprehensive account, however, is that of Chapelle & Choiniere (2018) who used computed tomographic (CT) scanning to produce three-dimensional, bone-by-bone descriptions of every preserved element in the skull of BP/1/5241. Chapelle & Choiniere (2018) rejected the diagnostic features proposed by Sues *et al*. (2004), though without justification, and proposed two other characters of the braincase and palate as potentially distinctive (see Emended Diagnosis, below). None of these papers provided any discussion of the postcrania, although several of these skulls are preserved as part of complete, or partially complete, skeletons (e.g. BP/1/4934, BP/1/4779, BP/1/5241, SAM-PK-K1314).

Other recent studies on *Massospondylus carinatus* have included descriptions of the clavicle in BP/1/5241 (Yates & Vasconcelos 2005) and those of eggs, nests and embryos (e.g. BP/1/5347: Kitching 1979; Zelenitsky & Modesto 2002; Reisz *et al*. 2005, 2010, 2012). The referral of the latter to *M. carinatus* requires confirmation, however, as the single autapomorphy used to support this suggestion has been shown to be unreliable (Chapelle & Choiniere 2018; see below); moreover, reliance upon provenance arguments to verify this identification are no longer tenable in light of our new understanding of upper Elliot Formation sauropodomorph diversity (see above).

Here, we present the first full description of the postcranial skeleton of the neotype specimen of *Massospondylus carinatus* (BP/1/4934: Fig. 1), complementing previous publications on its cranial anatomy (Gow *et al*. 1990; Sues *et al*. 2004). We use this information to propose an emended diagnosis for this species, with the aim of providing a firm anatomical and taxonomic baseline that will enable others to assess referral of additional individuals to this taxon and for adjudicating on the various synonymies that have been proposed (e.g. Seeley 1895a; Galton & Cluver 1976; Cooper 1981; Galton 1990; Galton & Upchurch 2004).

MATERIALS AND METHODS

Owen (1854) based his description of *Massospondylus carinatus* on five isolated vertebrae that he had received as part of a shipment of 56 fossil reptile bones from the Orpen family earlier that year. These specimens were from the farm Beauchef Abbey 215 in the Harrismith District, Free State Province, South Africa (Owen 1854; Seeley 1895a; Kitching & Raath 1984) and although the

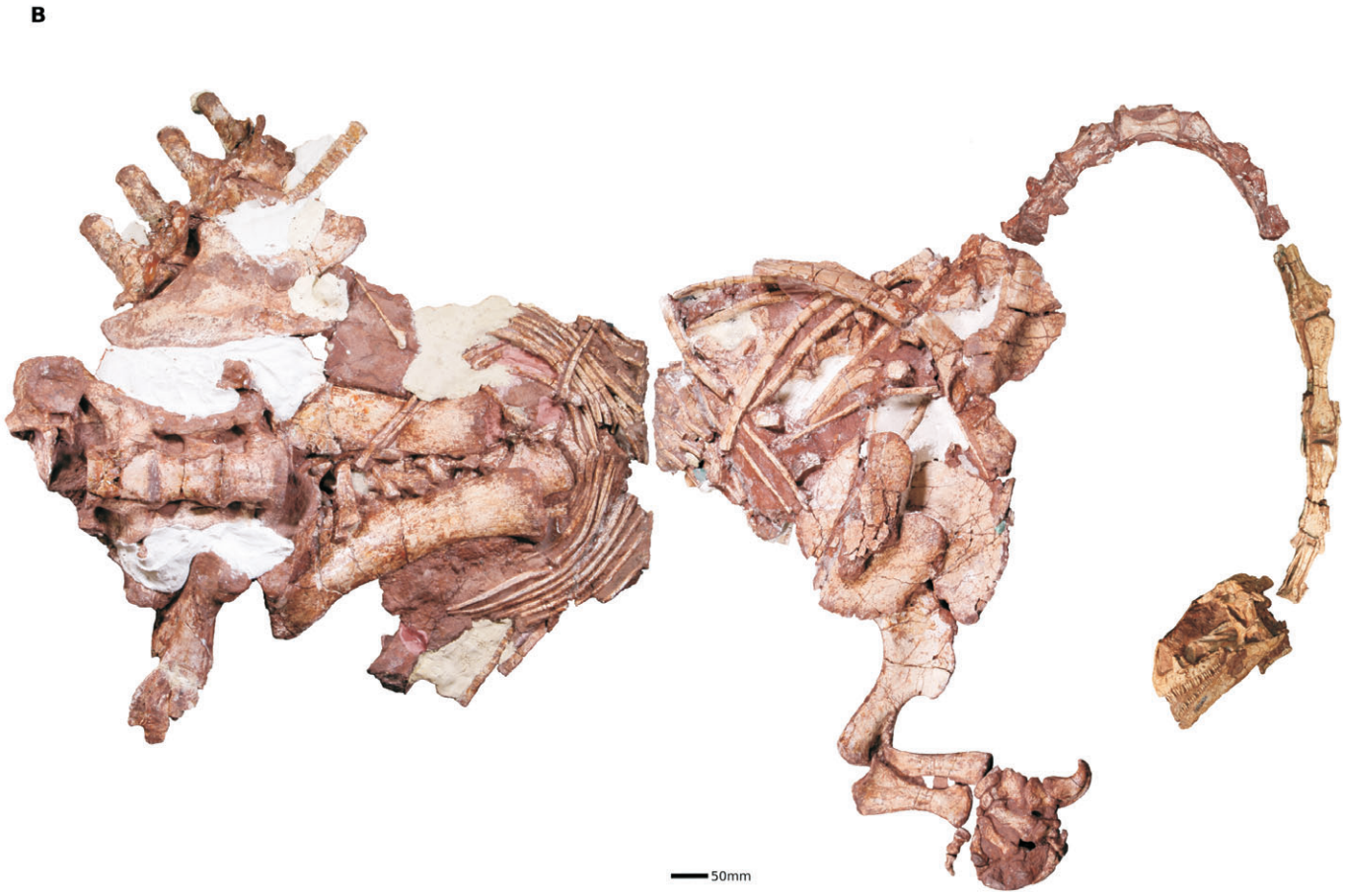


Figure 1 (continued).

exact horizon was not recorded only the upper Elliot Formation is accessible at this locality (Kitching & Raath 1984). Owen (1854) regarded these vertebrae as caudals, but Seeley (1895a) demonstrated that they were cervicals and provided the first revision of the genus. Owen (1854) also referred 13 other isolated specimens, including other vertebrae, limb and girdle material to his new taxon, though tentatively. As no holotype was designated these five cervical vertebrae formed the syntype series of *M. carinatus*. Unfortunately, all of these specimens were destroyed when the Hunterian Museum of the Royal College of Surgeons was hit during a bombing raid on London on 19th May 1941, although illustrations of the original material (Lydekker 1890b; Seeley 1895a; von Huene 1906) and plaster casts survive (SAM-PK-C958–62, NHMUK PV R1312 and R3027–8; see Yates & Barrett 2010).

As examination of these casts and illustrations did not reveal any diagnostic features, and as the original specimens were no longer accessible, Yates & Barrett (2010) formally proposed BP/1/4934 as a neotype for *M. carinatus*, following the earlier suggestions of Sues *et al.* (2004) and Barrett (2009). This proposal avoided the difficulties that would have been inherent in designating *M. carinatus* a *nomen dubium*, given its widespread familiarity and entrenchment within the published literature (see above and Yates & Barrett 2010). Further details of the taxonomic history of *Massospondylus*, including discussion of its other nominal species, can be found in Seeley (1895a), Cooper (1981) and Yates & Barrett (2010).

BP/1/4934 (nicknamed 'Big Momma', although the sex is unknown) is the largest and most complete individual known, includes an almost complete skull and a partial, articulated postcranial skeleton, and has been widely cited in the literature as an exemplar of *M. carinatus* (e.g. Gow *et al.* 1990; Sues *et al.* 2004: Fig. 1). Indeed, this specimen is probably the most complete skeleton of any non-sauropod sauropodomorph from Africa and has been on public display in the J.W. Kitching Gallery of the Evolutionary Studies Institute (ESI) of the University of the Witwatersrand since 1990 (Graham *et al.* 2018).

Numerous non-sauropod sauropodomorphs have been described in the past 20 years and the number of valid taxa has more than doubled since the last major taxonomic review of this group (Galton & Upchurch 2004). The anatomy of these animals varies considerably from small, omnivorous bipeds very close to the base of the dinosaur tree (e.g. *Buriolestes*: Cabreira *et al.* 2016) to large-bodied obligate herbivores that are much closer to sauropod origins (e.g. *Melanorosaurus*: Yates 2007a). Consequently, comprehensive comparisons between *Massospondylus* and all of these taxa are neither practical nor taxonomically informative, because as an early diverging massopodan *Massospondylus* is not regarded as either a particularly primitive or derived sauropodomorph. Here, we restrict the majority of our comparisons to those taxa that have been most frequently proposed as close relatives of *M. carinatus* (i.e. putative members of Massospondylidae: e.g. Smith & Pol 2007; Yates 2007; Apaldetti *et al.* 2011, 2013; Chapelle & Choiniere 2018), including *Adeo-*

papposaurus mognai, *Coloradisaurus brevis*, *Ignavusaurus rachelis*, *Leyesaurus marayensis*, *Lufengosaurus huenei*, *Sarahsaurus aurifontanalis* and *Seitaad ruessi* (see below). Anatomical terminology for vertebral laminae and fossae follows Wilson (1999, 2012) and Wilson *et al*. (2011).

In order to facilitate the following description, BP/1/4934 has been re-prepared and remounted, with each of its individual blocks protected by bespoke 'Epoplast' clamshell jackets (see Graham *et al*. 2018 for details). Surface models of the specimen were produced using photogrammetric techniques (Mallison & Wings 2014) and are available as .obj files with .png textures in the Supplementary Information (Supplementary Models 1–5). We used a Canon 760D cropped frame sensor body equipped with a Tamron 14–30 mm full frame lens (effective focal length of 22.4–48 mm) to take pictures of sections of the specimen from a variety of angles. Images were stored as .jpg files and imported into AgiSoft Photoscan Pro (AgiSoft PhotoScan Professional (Version 1.2.6) retrieved from http://www.agisoft.com/downloads/installer/ for model reconstruction. Models were made by aligning single chunks (single-surface models) or multiple chunks (multiple surface models), with the following workflow batch settings: align photos with highest accuracy; optimize alignment; build dense cloud with high quality; build mesh with high facecount; build texture. All parameters not specified were left as defaults. An .html file containing our batch processing workflow is available in the Supplementary Information.

In order to investigate the ontogenetic status of BP/1/4934 we conducted an osteohistological analysis. Due to the neotype status of the specimen, and the lack of a complete femur, only small portions of the right humerus and left femur were sampled. Thin-sectioning was conducted at the National Museum, Bloemfontein, using standard osteohistological methods following Botha-Brink *et al*. (2018). Osteohistological terminology follows that of Francillon-Vieillot *et al*. (1990) and de Ricqlès *et al*. (1991).

LOCALITY AND HORIZON

BP/1/4934 was collected in March 1980 from the upper Elliot Formation of Bormansdrift 133 Farm, in the Clocolan District, Free State Province, by Lucas Huma and James Kitching (see Kitching & Raath 1984 for locality details). This farm has yielded additional upper Elliot Formation tetrapod material, including the cynodont *Pachygenelus* and other sauropodomorph remains (Kitching & Raath 1984). It is also the type locality of the early turtle *Australochelys africanus* (Gaffney & Kitching 1994). No specific coordinate data were recorded during the collection of the specimen but the collections catalogue of the Evolutionary Studies Institute states that the specimen was 'bisected by a cross-cutting dolerite dyke, and a sample of this dyke is retained in the collections'.

One of us (J.N.C.) has visited Bormansdrift 133 and can confirm that only upper Elliot Formation sediments are exposed there. Moreover, only one small hill on this farm preserves suitable outcrop for fossil prospecting and it is cross-cut by a prominent, narrow dyke. During field investigations in 2016 and 2017, significant vertebrate remains were collected from this hill at approximately 28.962739°S, 27.430377°E, at an elevation of 1712 m, and we consider this area to be the most likely source of the neotype (Fig. 2). This site is capped by a prominent sandstone ridge that is either uppermost Elliot or Clarens formation, whose bottom contact lies at 1717 m. A short distance from this site, also on Bornmansdrift 133, an unquestionable Clarens/upper Elliot contact is present at 1737 m. Therefore, we regard the stratigraphic position of BP/1/4934 as being situated within the upper Elliot Formation, somewhere between 5–25 m below its contact with

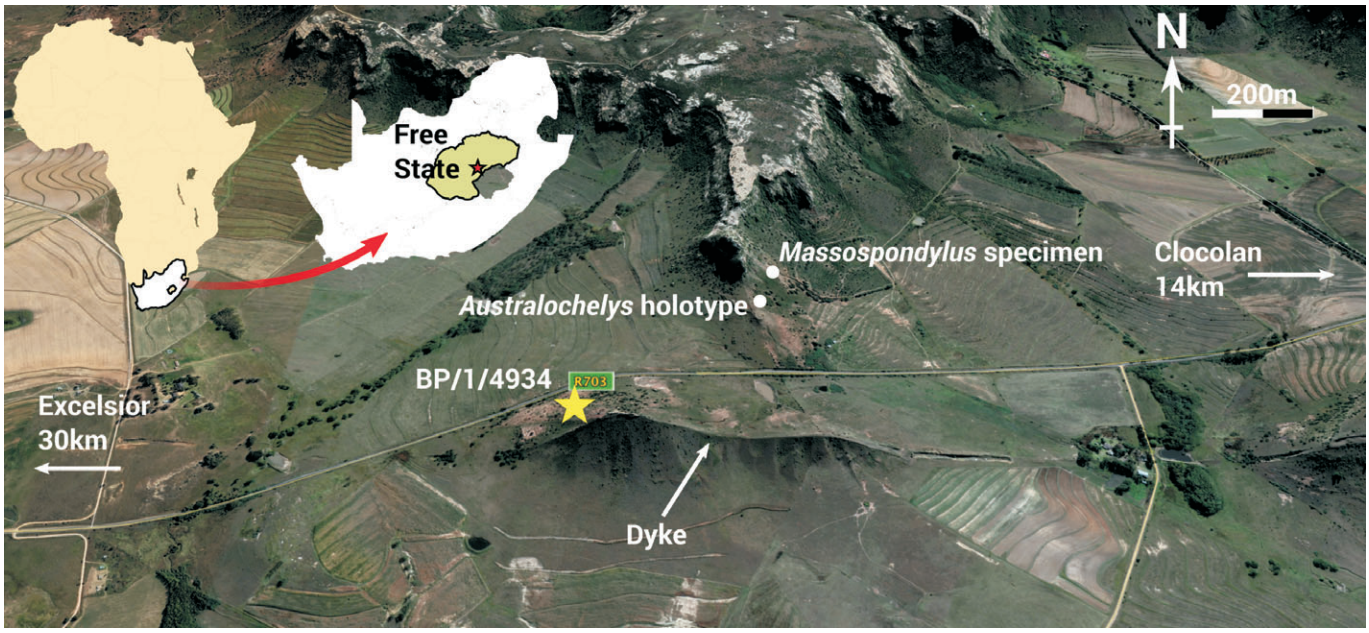


Figure 2. Locality map for the neotype skeleton of *Massospondylus carinatus* (BP/1/4934), which was excavated from the upper Elliot Formation of Bormansdrift 133 Farm, Clocolan District, Free State Province, South Africa. Insets show the location of South Africa and Free State Province, respectively. Note the prominent dyke that marks the position of the type locality. Map image downloaded from GoogleEarth.

the Clarens Formation. In the Clocolan region, the upper Elliot Formation is approximately 80 m thick and, therefore, BP/1/4934 can be placed confidently within the uppermost 25% of the upper Elliot Formation.

The age of the upper Elliot Formation has been debated, with earlier authors assuming that the entire Stormberg Group was Late Triassic in age (e.g. Haughton 1924). However, over the past three decades most authors have agreed that the Elliot Formation straddles the Triassic/Jurassic boundary (TJB), primarily on the basis of biostratigraphic correlations using fossil vertebrates (Olsen & Galton 1984; Lucas & Hancox 2001). As a result, the lower Elliot Formation has been regarded as Late Triassic (potentially Norian/Rhaetian) in age, whereas the upper Elliot Formation has been considered to be Early Jurassic (Hettangian–Sinemurian) (Olsen & Galton 1984; Lucas & Hancox 2001; Knoll 2004, 2005; Olsen *et al*. 2011). Until recently, no absolute age constraints were available for the units within the Stormberg Group due to a lack of interbedded tuff layers and/or marine intercalations, but application of magnetostratigraphy to the Elliot Formation across the main Karoo Basin has indicated that the TJB lies higher in the section that previously appreciated (Sciscio *et al*. 2017). Rather than falling between the lithological divisions of the lower and upper Elliot Formation, the TJB appears to lie within the upper Elliot Formation, suggesting that the lower part of the upper Elliot is Rhaetian in age, while its upper part is Early Jurassic (Hettangian–Sinemurian) (Sciscio *et al*. 2017). As the neotype locality lies within in the upper part of the upper Elliot Formation, we regard is as earliest Jurassic in age.

SYSTEMATIC PALAEONTOLOGY

Dinosauria Owen, 1842
Saurischia Seeley, 1887 (sensu Baron *et al*. 2017)
Sauropodomorpha von Huene, 1932

MASSOSPONDYLIDAE von Huene, 1914 (sensu Sereno 1998)

Definition: The most inclusive clade containing *Massospondylus carinatus* Owen, 1854, but not *Plateosaurus engelhardti* von Meyer, 1937 or *Saltasaurus loricatus* Bonaparte & Powell, 1980 (Sereno 1998).

Comment: The family Massospondylidae was proposed by von Huene (1914) for the reception of three taxa: *Massospondylus carinatus*, *M. harriesi* and *Aetonyx palustris*. Of these, only *M. carinatus* is currently recognized as a valid taxon, with the other two taxa considered junior synonyms of *M. carinatus* (Cooper 1981). Sereno (1998) provided a stem-based definition for the clade Massospondylidae, using *Plateosaurus* as an external non-sauropod sauropodomorph specifier, which was subsequently amended to include *Saltasaurus* as a second external sauropod specifier, and this definition is followed herein. Sereno (1999) was the first to identify a massospondylid clade in a formal phylogenetic analysis, which included *Massospondylus* and *Yunnanosaurus*. Some subsequent analyses failed to recover a massospondylid clade, rendering Massospondylidae monotypic (e.g. Galton & Upchurch 2004; Upchurch *et al*. 2007), but the majority of recent phylogenetic analyses have identified a monophyletic Massospondylidae that usually includes *M. carinatus*, *Coloradisaurus* and *Lufengosaurus* and a variable number of other taxa (e.g. Yates 2003, 2004, 2007a; Yates & Kitching 2003; Smith & Pol 2007; Martínez 2009; Apaldetti *et al*. 2011, 2013; Novas *et al*. 2011; Otero & Pol 2013; Chapelle & Choiniere 2018). However, many of these publications misattribute the current definition of Massospondylidae to either Yates (2003) or Yates (2007b), who did not define the clade in either publication, rather than to Sereno's (1998) original definition.

MASSOSPONDYLUS CARINATUS Owen, 1854
Figures 1 and 3–28

Neotype: BP/1/4934, a partially complete skeleton including skull, but lacking most of the hind limbs and tail (Fig. 1).

Locality and horizon: Bormansdrift 133 Farm, Clocholan District, Free State Province, South Africa. Uppermost part of the upper Elliot Formation, Stormberg Group (Hettangian–Sinemurian; Sciscio *et al*. 2017).

Emended diagnosis (based on autapomorphies): basipterygoid processes diverge at an angle of <60°; anterior cervical centra with elongation ratios (centrum length/anterior centrum height) of >7.0; neural spines of anterior cervical vertebrae bear hook-like expansions anteriorly; distal scapula blade with small dorsal and large ventral expansions; deltopectoral crest extends for ~60% of humeral length; ulna length/humerus length ratio ≤0.6; anterior surface of distal pubes flat and unexpanded.

ANATOMICAL DESCRIPTION

BP/1/4934 is almost fully articulated, with many of the individual bones preserved in life position, and it has been prepared in relief, with most of the skeleton remaining at least partially embedded in matrix (Fig. 1). Consequently, the majority of postcranial elements cannot be examined in three dimensions as some remain partially obscured by matrix, while overlapping bones hide others. This also constrains the number of measurements that can be taken, but those available are presented in Tables 1–9. The specimen is usually stored or displayed lying on its right-hand side, so the bones on this side of the skeleton have been difficult to access. However, the recent construction of 'Epoplast' clamshell jackets now enables detailed examination of these previously inaccessible elements (Graham *et al*. 2018). As preserved, BP/1/4934 is approximately 3.5 m in length; if it had similar proportions to other closely related sauropodomorphs (e.g. *Lufengosaurus*) this suggests an overall body length of ~5 m.

During its excavation and preparation BP/1/4934 was divided into several blocks (Graham *et al*. 2018). In addition to the skull, which can be removed from the specimen, these comprise: 1) the anterior cervicals; 2) the posterior cervicals; 3) an anterior thoracic block containing the anterior dorsal series, pectoral girdles, parts of the right forelimb, and numerous ribs; and 4) a posterior thoracic block that includes the posterior dorsal series, sacrum, anterior caudal caudal vertebrae, the gastral basket, pelvic girdles, the partial left femur, and numerous

ribs. Several other postcranial elements, including the left humerus, left and right radius and ulna, right manual phalanges, and various partial metatarsals and pedal phalanges, have been prepared out more fully and are each visible in multiple views. The articulated left manus remains embedded in matrix as a small separate block but its component parts are visible in at least palmar and dorsal views (see below). Numerous indeterminate limb bone, rib, gastral and vertebral fragments also form part of the specimen but offer no additional information and are not considered further herein.

Axial column

The atlas and the axis intercentrum are missing, but the rest of the presacral vertebral column is well preserved and forms an almost complete, articulated series. Following preparation, the axial skeleton was divided among several different skeletal blocks. As currently displayed, most of the axial column is visible in either dorsal or left lateral view, but each of these blocks can be rotated to reveal details of their other surfaces. The anterior-most block contains cervical vertebrae (Cv) 2–5, which are preserved in articulation, though the posterior-most part of Cv5 is missing. Moving posteriorly, the second block contains Cv6–Cv10 preserved in articulation. The anterior-most part of Cv6 is missing and this block also includes the anterior-most part of dorsal (D) 1 (the prezygapophyses and anterior-most part of the centrum). Cv10 has a transitional 'cervicodorsal' morphology (see below) but is considered to be part of the neck due to the morphology of the associated rib. A large block containing the anterior part of the thorax includes D1–D7 in articulation, together with the anterior-most part of D8. The posterior thoracic block includes D8–D14, which all are preserved in articulation except for D14, which is visible in anterior view. Sacrals (S) 1–3 are in contact with the left ilium, which largely obscures them in left lateral view, but these can be observed on the reverse side of the posterior thoracic block. Five caudal vertebrae (Cd) are preserved: one that lies out of articulation in a position immediately behind the sacrum, and an additional four articulated vertebrae that have been displaced and rotated so that that are visible in right lateral view. All of the preserved caudals are from the proximal part of the tail, but it is not clear if they are Cd1–Cd5 or if these represent other proximal caudals. Numerous fragments of ribs, gastralia and vertebral processes are also associated with the specimen, but these offer little additional information and are stored separately.

Cervical vertebrae

There are 10 cervical vertebrae, as also occurs in *Lufengosaurus* (IVPP V15; Young 1941) and *Sarahsaurus* (Rowe *et al*. 2011), but in contrast to *Adeopapposaurus*, which possesses 11 cervicals (Martínez 2009). The cervical vertebrae have experienced minimal crushing, but some distortion has occurred, particularly in the anterior cervicals, and the presence of matrix and the cervical ribs obscures other features (Figs 3–7). There is little or no offset between the anterior and posterior articular surfaces of Cv2–5, but this might be the result of deformation. A small offset is present in the other cervicals (where visible), as the centrum is slightly downcurved posteriorly so that the dorsal margin of the posterior articular surface is situated slightly ventral to that of the anterior articular surface in lateral view. The neurocentral junctions can be traced in Cv2–7 due to a marked break-in-slope between the lateral margin of the neural arch and the centrum, which produces a distinct 'stepped' morphology. This feature is due to the laterally swollen bases of the neural arch pedicles, which overhang the dorsolateral surfaces of the centra, a morphology that also produces an acute slit-like depression along the neurocentral junction in all cervicals, including the axis and Cv10, which is also present in *Adeopapposaurus* (R. Martínez, pers. comm., July 2018) and to some extent in *Leyesaurus* (C. Apaldetti, pers. comm., August 2018), but that is absent in *Coloradisaurus* (Apaldetti *et al*. 2013) and *Lufengosaurus* (IVPP V15). The neurocentral junctions appear to be partially fused in the anterior cervicals and fully fused in the middle to posterior cervicals (but the lateral surfaces of Cv8–10 are obscured by matrix). In all cervicals, the base of the neural arch does not extend for the full length of the centrum: there are short gaps between the anterior and posterior margins of the neural arch and the anterior and posterior margins of the centrum. The neural arch increases in relative and absolute height along the series, whereas the centra remain long and low. The presence/absence of hyposphenes/hypantra cannot be determined due to the close apposition of the vertebrae in the articulated column. The shape and size of the neural canal is not discernable in any of the cervicals (with the exception of the axis), but the shallow depth of the neural arch indicates that it must have been a small, dorsoventrally narrow opening. Measurements of the cervical vertebrae are provided in Table 1.

Axis – Small parts of the anterior-most centrum and neural arch are missing, including the anterior-most margin of the neural spine, but otherwise the axis is complete and three-dimensional. A small, flat sliver of bone on the right anterolateral surface of the centrum might represent part of an atlantal neural arch (Fig. 3; Supplementary Model 1).

In lateral view, the centrum is elongate and dorsoventrally low, with a minimum centrum length/height ratio of 4.36, which is similar to the ratio of ~4.0 reported for *Leyesaurus* (Apaldetti *et al*. 2011), but longer than that for either *Adeopapposaurus* (~3.5: Martínez 2009) or *Lufengosaurus* (~2.6: IVPP V15). The lateral surfaces of the centrum are gently concave anteroposteriorly and convex dorsoventrally along their entire lengths and they lack pneumatic foramina and fossae (Fig. 3A). No nutrient foramina are present. The lateral surfaces are divided from the ventral surface by a distinct break in slope, which forms a ridge that extends for the entire length of the centrum and gives the centrum a sub-quadrate cross-section. Small protuberances situated at the mid-height of the centrum at the junction between the anterior and lateral surfaces are interpreted as parapophyses and these structures contact the heads of the cervical ribs.

In ventral view, the centrum has an elongate, narrow,

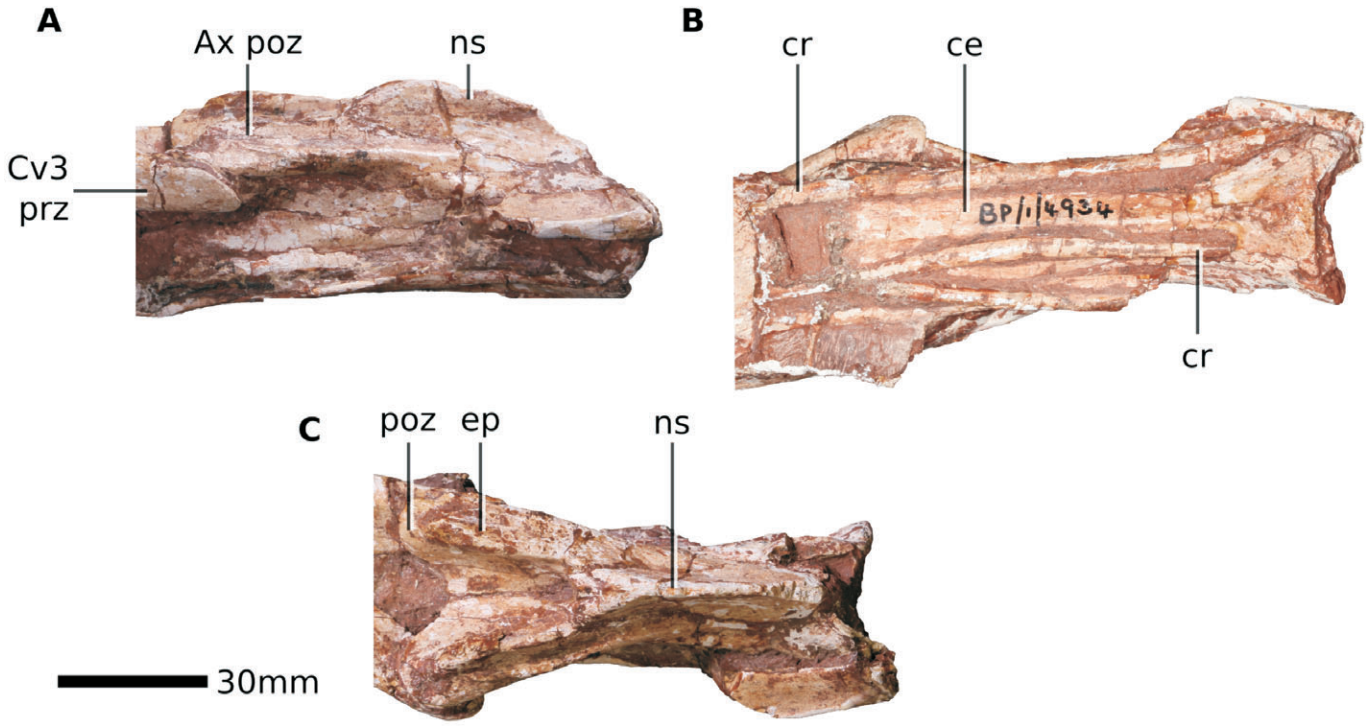


Figure 3. Axis of *Massospondylus carinatus* (BP/1/4934) in right lateral (**A**), ventral (**B**) and dorsal (**C**) views. Anterior is to the right in all images. Scale bar = 30 mm.

Table 1. Measurements of cervical vertebrae in BP/1/4934. All measurements are in mm. Those marked with an asterisk are minima due to breakage. Some measurements were not possible due to either extensive breakage or the presence of matrix/overlapping elements.

	CL	ACH	ACW	PCH	PCW	NSL	NSH	VH	CL/ACH
Axis	96*	22	31	–	–	48*	10	32	4.36
Cv3	135	18	30	18	33	81*	–	37	7.5
Cv4	152	20	33	20	38	80*	16	40	7.6
Cv5	–	19	35	–	–	–	16	–	–
Cv6	–	–	–	28	52	85*	14	57	–
Cv7	149	25	44	29	58	74*	20	60	5.96
Cv8	137	29	49	37	61	75*	26	–	4.72
Cv9	123	34	53	37	68	56*	27	68	3.62
Cv10	120*	29	59	–	71	34	29	68	4.14

hourglass-shaped outline (Fig. 3B). The anterior margin of the centrum expands toward the articular surface, but the lateral margins constrict immediately posterior to this point to form the narrowest point of the centrum (around one-quarter of the length of the centrum from the anterior end). Posteriorly, the lateral margins diverge slightly, so that the posterior part of the centrum expands towards the posterior articular surface. A sharp, well-defined midline keel arises from a point immediately posterior to the anterior margin of the centrum and extends posteriorly to terminate just anterior to its posterior margin, as also occurs in *Adeopapposaurus* (Martínez 2009), *Leyesaurus* (Apaldetti *et al*. 2011) and *Lufengosaurus* (IVPP V15). In *M. carinatus*, the keel is sharp and prominent anteriorly, but is reduced in prominence posteriorly, becoming a low rounded ridge. The keel divides the ventral surface into two equally sized portions, which are slightly concave anteriorly, due to the ventral projection of the keel and the curvature of the anterior articular surface, but which are flat posteriorly.

The anterior articular surface of the centrum is damaged, but the preserved portion shows that it was wider than high (see Table 1); the posterior articular surface is completely obscured by matrix and the presence of Cv3 and no details are available.

The neural arch is elongate and low (Fig. 3A). The anterior neural canal opening has an approximately triangular outline, which is widest ventrally. The neural spine is a low, transversely thin, ridge-like structure with a narrow triangular transverse cross-section and flat lateral surfaces, as in *Leyesaurus* (Apaldetti *et al*. 2011). In lateral view, the postzygapophyses of *M. carinatus* extend only a few millimetres beyond the posterior articular surface of the centrum. They are almost horizontally inclined, but their articular surfaces are oriented slightly posterolaterally. The dorsal margins of each postzygapophysis bear a strong, ridge-like epipophysis, which gives the postzygapophyses a triangular transverse cross-section. The epipophysis terminates anterior to the apex of the postzygapophysis and does not overhang its posterior margin, as also occurs in *Adeopapposaurus* (Martínez 2009) and *Leyesaurus* (Apaldetti *et al*. 2011). In dorsal view, the

postzygapophyses diverge at an angle of approximately 30° (Fig. 3C). As in *Adeopapposaurus* and *Leyesaurus* (Martínez 2009; Apaldetti *et al*. 2011), in *M. carinatus* the articular surfaces of the postzygapophyses expand medially so that they almost meet at the midline, leaving only a narrow slit between them. As a result, the postzygapophyses and the posterior margin of the neural spine frame a deep triangular sulcus, at the anterior apex of which a small, postspinal fossa. The postspinal fossa is elliptical in outline with its long axis directed dorsoventrally. No diapophysis is visible. Distinct neural arch laminae are absent, although the lateral margin of the postzygapophysis could be regarded as an incipient lamina as it is continuous with a low ridge that extends onto the lateral surface of the neural arch. However, it is not clear if this structure is equivalent to either a postzygodiapophyseal lamina (PODL) or a spinopostzygapophyseal lamina (SPOL) as it connects to neither the spine nor the diapophysis. The same structure is also present in *Adeopapposaurus* (Martínez 2009). Similar features have been described as SPOLs in *Leyesaurus*, as in the latter case they merge clearly with the neural spine (Apaldetti *et al*. 2011).

Two pairs of cervical ribs are associated with the axis and are visible in ventral view (Fig. 3B). The lateral-most ribs appear to be those borne by the axis: their anterior ends are in close contact with the anterolateral margins of the centrum. The other pair of ribs probably represent those of the atlas. All of the ribs are elongate (length of the incomplete right axis rib = 97 mm), thin (maximum shaft diameter = 4 mm) and have cylindrical transverse cross-sections. They maintain approximately the same diameter along their entire length and are not expanded anteriorly in their proximal articular region, nor do they taper appreciably posteriorly. There is no evidence that the anterior articular surface was subdivided into a tuberculum and capitulum, but this area is damaged in both ribs present. The posterior ends of the ribs extend only a short distance beyond the posterior surface of the centrum, just reaching the level of the anterior margin of Cv3, but not underlapping the following vertebra, though they are broken posteriorly and may have extended slightly further.

Anterior cervicals (Cv3–Cv5)–In Cv3–5, the anterior and posterior articular surfaces are obscured by matrix and/or by the presence of other vertebrae. Cv3 is complete, with the exception of the neural spine, which has been broken close to its base; Cv4 is missing small portions of the right postzygapophysis and the posterior part of the neural spine; and Cv5 lacks the tip of the left prezygapophysis and the posterior part of the vertebra. These three vertebrae are essentially identical in morphology, differing only in small details, which are noted below (Figs 4–5; Supplementary Model 1).

In lateral view, the centra are exceptionally elongate and low (Figs 4A, 5A), and Cv3 and Cv4 possess centrum length/height ratios of 7.5 and 7.6, respectively (see Table 1: not ~4.0 as stated in Apaldetti *et al*. 2011). This exceeds the maximum cervical vertebral elongation ratios present in all other putative massospondylid taxa, including *Adeopapposaurus* (~5.0: Martínez 2009), *Coloradisaurus* (~3.8: Apaldetti *et al*. 2013), *Leyesaurus* (~5.0: Apaldetti *et al*. 2011) and *Lufengosaurus* (~3.3: IVPP V15), and is regarded as an autapomorphy of *M. carinatus*. In all three vertebrae, the anterior articular surface is wider than high and has a sub-elliptical outline with its long axis oriented horizontally. The lateral surfaces of the centra lack pneumatic foramina and nutrient foramina; the broken cross-section of the centrum in Cv5 confirms that internal pneumatic spaces were absent. As mentioned above, the neural arch overhangs the lateral surface of the centrum to create a dorsoventrally narrow, slit-like depression that extends along the central part of the neurocentral junction (Figs 4A–C, 5A): this depression is dorsoventrally tallest centrally and tapers anteriorly and posteriorly. The remainder of each centrum's lateral surface is gently concave anteroposteriorly and dorsoventrally. The lateral surfaces of the centra are separated from their ventral surfaces by distinct breaks of slope that form ventrolateral ridges, giving the centra sub-rectangular transverse cross-sections. As with the axis, there is no clear parapophysis, but a low swelling situated close to the anteroventrolateral corner of the centrum, which is usually encrusted with matrix, probably represents this process.

In ventral view, the centra of Cv3–5 have elongate, hourglass-shaped outlines (Figs 4D, 5B). The narrowest point of the centrum occurs further posteriorly than in the axis, at a point approximately 39% (Cv3) to 46% (Cv4) of the length of the centrum from its anterior margin. A midline keel is present in all three vertebrae: in Cv3 this extends for almost the full length of the centrum, but it does not reach the anterior- or posterior-most margins of the bone, whereas in Cv4 the keel is absent from the posterior one-third of the centrum (Figs 4D, 5B). In Cv3 and Cv4, the keel is most prominent in the centre of the centrum and is less pronounced both anteriorly and posteriorly. Similar keels are present in *Adeopapposaurus* and *Lufengosaurus* (Martínez 2009; Young 1951; IVPP V15), but in *Leyesaurus* these keels are restricted to the anterior part of the centrum (Apaldetti *et al*. 2011). In *M. carinatus*, the ventral margins of the anterior and posterior articular surfaces are both gently convex, giving the vertebra an almost dumbbell-shaped outline (Figs. 4D, 5B). The posterior articular surface is slightly wider than the anterior surface.

In lateral view, the prezygapophyses extend for a considerable distance anterior to the centrum and extensively overlap the posterior part of the preceding vertebra (Figs 4A–C, 5A), as also occurs in *Adeopapposaurus* and *Leyesaurus* (Martínez 2009; Apaldetti *et al*. 2011), but unlike the shorter prezygapophyses of *Coloradisaurus* (Apaldetti *et al*. 2013). In *M. carinatus*, the prezygapophyses are oriented horizontally, terminate in bluntly tapering rounded tips and their articular surfaces face dorsomedially (Figs 4A–C, 5A). In dorsal view, they diverge from each other at an angle of approximately 30° and their bases are connected via a transverse web of bone that lies anterior to the base of the neural spine, forming a distinct interprezygapophyseal lamina (IPRL) (Figs 4E, 5C), as also occurs in *Adeopapposaurus* (R. Martínez, pers. comm., July 2018) and *Leyesaurus* (C. Apaldetti, pers. comm., August

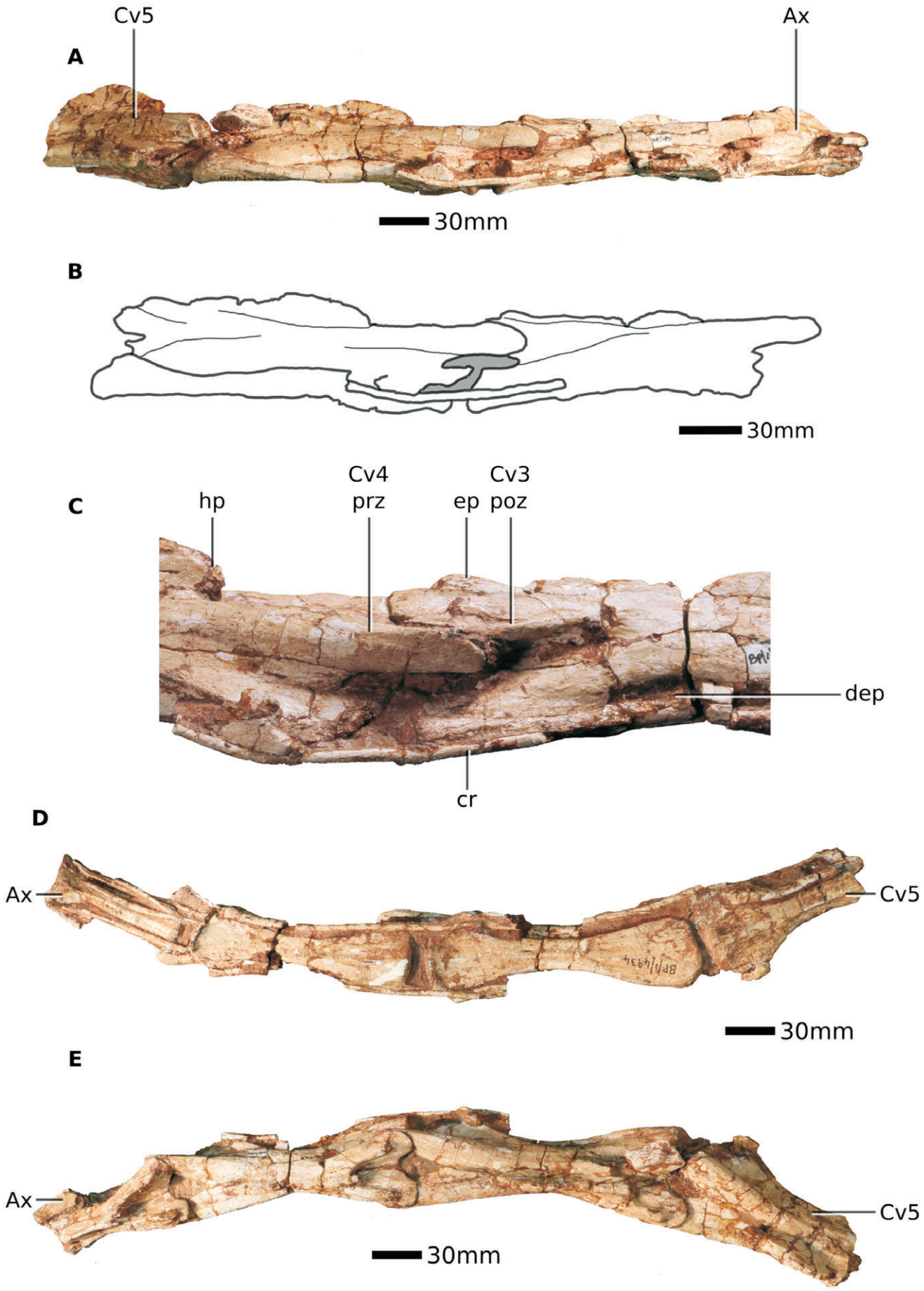


Figure 4. Anterior cervical vertebrae (axis to Cv5) of *Massospondylus carinatus* (BP/1/4934). **A**, axis and Cv3–5 in right lateral view; **B**, interpretative line drawing of Cv3 and Cv4 in right lateral view; **C**, close-up of the posterior end of Cv3 and anterior end of Cv4 in right lateral view; **D**, axis and Cv3–5 in ventral view; **E**, axis and Cv3–5 in dorsal view. Anterior is to the right in all images. Scale bars = 30 mm.

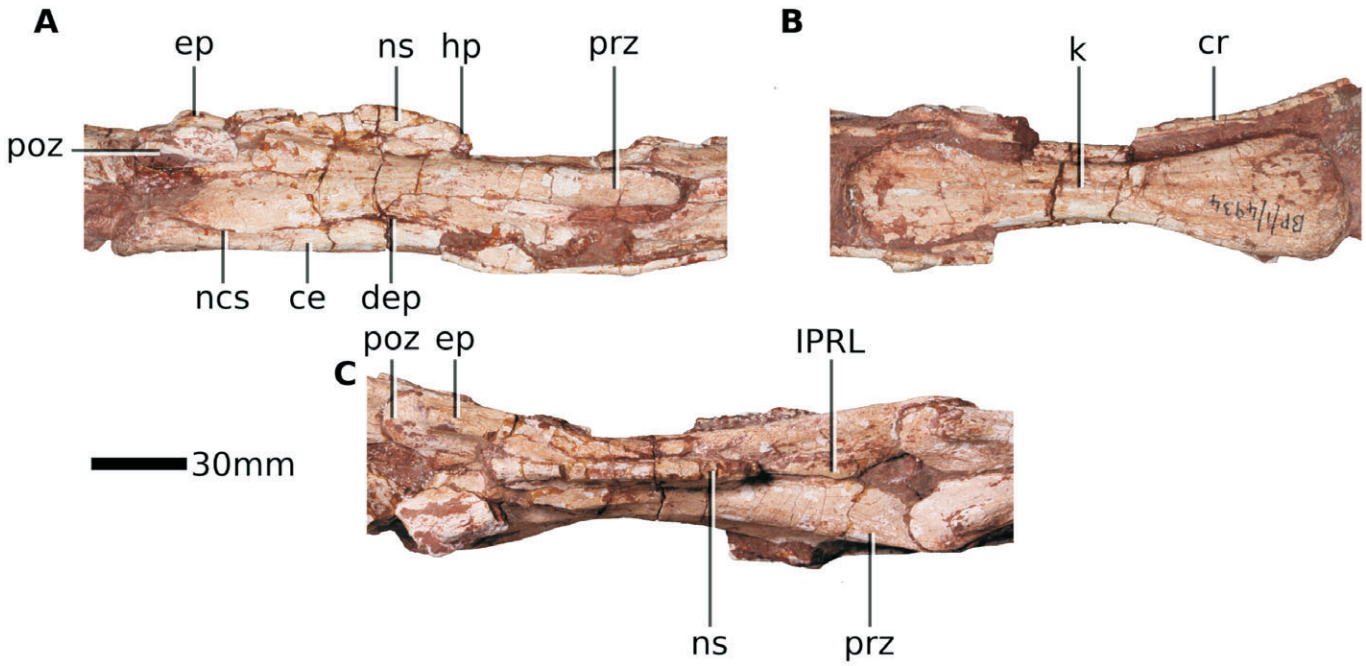


Figure 5. Cervical vertebra 4 (Cv4) of *Massospondylus carinatus* (BP/1/4934) in right lateral (**A**), ventral (**B**) and dorsal (**C**) views. Anterior is to the right in all images. Scale bar = 30 mm.

2018). This lamina is relatively short anteroposteriorly in Cv3 of *M. carinatus*, but more extensive in Cv4 and Cv5 (Fig. 5C). The prezygapophyses have a triangular transverse cross-section and their dorsal margins form a rounded ridge that extends for a short distance on to the lateral margin of the neural arch. In all three vertebrae, the anteroventrolateral corner of the neural arch flares laterally, at a point immediately ventral to point at which the prezygapophysis merges with the rest of the neural arch, to form a short, wing-like, anterolaterally projecting diapophysis that forms the articulation for the cervical rib tuberculum (Figs 4A–C, 5A). However, although a diapophysis is present, it does not support any well-developed laminae: the low flanges of bone arising from it anteriorly and posteriorly do not connect to any other landmarks but merge smoothly into the sides of the neural arch.

The postzygapophyses of Cv3 and Cv4 are essentially identical to those of the axis. In lateral view, they extend horizontally and bear prominent ridge-like epipophyses on their dorsal margins (Figs 4A–C, 5A,C), which terminate prior to the end of the process and do not overhang it, as also occurs in *Adepapposaurus* and *Leyesaurus* (Martínez 2009; Apaldetti *et al*. 2011). In *M. carinatus*, the postzygapophyses are shorter than the prezygapophyses and terminate at a point approximately level with the posterior margin of the centrum (Figs 4A–C, 5A). In dorsal view, the postzygapophyses diverge from each other at an angle of approximately 60° (Figs 4E, 5C). Their articular facets expand medially, forming extensive rounded processes that almost meet at the midline (as in the axis), leaving only a narrow slit between them. As a result, these processes form the floor of a broad sub-triangular recess that is defined anteriorly by the posterior margin of the neural spine (Fig. 5C), as also occurs in *Adeopapposaurus* (R. Martínez, pers. comm., July 2018) and *Leyesaurus* (C. Apaldetti, pers. comm., August 2018). A small post-spinal fossa is present at the base of the neural spine in Cv3 (but this area is broken in Cv4 and Cv5). The lateral margin of the postzygapophysis forms a sharp ridge that continues anteriorly onto the lateral surface of the neural arch ventral to the neural spine, but it does not make contact with the ridge extending posteriorly from the prezygapophysis (see above): these ridges lie in equivalent positions to portions of the epipophyseal-prezygapophyseal lamina (EPRL), but they do not fuse to form a true EPRL (Figs 4A,B, 5A). Similar features are also present in *Adeopapposaurus* and *Leyesaurus* (Martínez 2009; Apaldetti *et al*. 2011).

The neural spine is an elongate, transversely compressed plate that extends for most of the length of the neural arch (Figs 4A–C, 5A). Its dorsal margin is slightly convex in Cv4 and Cv5 (but broken in Cv3) and it does not exhibit the anteriorly concave/posteriorly convex morphology present in *Leyesaurus* (Apaldetti *et al*. 2011). In Cv3–5 of *M. carinatus*, the anterior margin of the neural spine extends anterior to the bases of the prezygapophyses to slightly overhang the IPRL, forming a distinct hook-like process (Figs 4C, 5A). This feature is not present in the anterior cervicals of *Adeopapposaurus* or *Leyesaurus* (Martínez 2009; Apaldetti *et al*. 2011) and is considered to be an autapomorphy of *M. carinatus*. The posterior neural spine margin extends to the junction between the postzygapophyses and overhangs it in Cv3 and Cv4 (but is broken in Cv5).

Pairs of elongate, thin, cylindrical cervical ribs are associated with Cv3–5. Although none are complete, they extend posteriorly beyond the margins of the centrum to overlap the following vertebra: the almost complete ribs of Cv3 overlap Cv4 for approximately 25% of its length (Fig. 4A–C). In Cv3, the anterior (articular) end of the rib is slightly expanded dorsoventrally relative to the shaft,

but it is not divided into distinct processes. From Cv4 onwards, however, the anterior ends of the ribs are differentiated into a tuberculum and capitulum. The tuberculum has a rounded, blunt-ending, sub-triangular outline and is subequal in length to the capitulum, which is square in outline. These two processes are separated from each other by an angle of approximately 90° and are connected via a thin plate of bone whose posteroventral corner gives rise to the rib shaft. The shaft has a sub-circular cross-section, with a maximum diameter of 3–4 mm. The minimum length of the most complete cervical rib associated with the anterior cervicals is 151 mm (the left rib of Cv3).

Middle cervicals (Cv6–Cv8)–Cv6–8 are largely complete and have suffered less deformation than the anterior cervicals (Figs 6, 7; Supplementary Model 2). Nevertheless, some areas remain obscured due to the presence of matrix and of the other vertebrae. Cv6 lacks the anterior end of the centrum, the tips of the prezygapophyses and the posterior margin of the neural spine; Cv7 and Cv8 are essentially complete, with only minor damage to the margins of their neural spines. A partial right cervical rib is in articulation with Cv6; small portions of the rib heads of Cv7 are present; and substantially complete left and right ribs lie alongside Cv8.

In many respects Cv6–8 are larger, more robust versions of Cv4 and Cv5. However, in lateral view, each of the middle cervicals exhibits a clear offset between the anterior and posterior articular surfaces, with the anterior surface positioned dorsally relative to the posterior surface, giving the ventral margin of the centrum an upwardly curved appearance (Figs 6A,B, 7A). The centra remain elongate and low, but there is a trend toward anteroposterior shortening of the cervicals posteriorly, with centrum length/height ratios of 5.96 (Cv7) and 4.72 (Cv8), which still exceed those of other massospondylids (see above). Cv6–8 retain the neurocentral depressions described in the anterior cervicals (see above) and, as in the earlier vertebrae, these depressions reach their maximum dorsoventral extents at a point approximately halfway along the centrum (Figs 6A,B, 7A). In the middle cervicals the more prominent overhang of the neural arch over the centrum lateral surface accentuates this feature. Posteriorly, the depression is more extensive than in the anterior cervicals and continues almost to the end of the centrum. The lateral surfaces of the centrum ventral to the neurocentral depression are longitudinally concave, dorsoventrally convex and lack evidence of pneumatic foramina. The lateral surfaces are separated from the ventral surface by distinct breaks in slope, which form stout, rounded ridges, and that produce a sub-rectangular cross-section. As in Cv5, the broken cross-section of Cv6 does not reveal any internal pneumatic spaces. Small, elliptical parapophyses, with their long axes oriented anteroposteriorly, project from the anteroventrolateral corners of the centrum in Cv7 and Cv8 but are difficult to observe due to the presence of matrix and of the adjacent cervical ribs (these areas are broken or obscured in Cv6).

In ventral view, the centra of Cv6–8 are essentially identical to those of Cv3–5, as they are mediolaterally expanded anteriorly and posteriorly, and constricted centrally, to produce the dumbbell-shaped outlines also seen in the latter (Figs 6C, 7B). Cv6–8 all bear prominent midline keels, which are restricted to the anterior two-thirds of the centrum; *Adeopapposaurus*, *Leyesaurus* and *Lufengosaurus* also bear midline keels (Young 1941; Martínez 2009; Apaldetti *et al*. 2011), although that of Cv7 in *Leyesaurus* extends for the entire length of the centrum (Apaldetti *et al*. 2011). In *M. carinatus*, the keel divides the ventral surface into two shallowly concave, longitudinally extending sulci (Figs 6C, 7B). The keel is strongest anteriorly but reduces in prominence posteriorly until it merges into the ventral surface. Posterior to this point, the ventral surface of the centrum is smooth and slightly convex mediolaterally. The posterior articular surface of Cv8 is partially visible and is shallowly concave.

In lateral view, the prezygapophyses project horizontally, possess mediolaterally facing articular surfaces, terminate in bluntly rounded apices and extend well beyond the anterior margin of the centrum, though they are slightly shorter in Cv8 than in Cv6 or Cv7 (Figs 6A,B, 7A). For Cv6 and Cv7 this is similar to the condition in *Leyesaurus* (Apaldetti *et al*. 2011: although more posterior cervicals are not available for comparison), but contrasts with that present in *Adeopapposaurus*, where the prezygapophyses are much shorter (in Cv6–8) and, in the case of Cv8, are anterodorsally inclined (Martínez 2009). In *M. carinatus* the prezygapophyses retain a sub-triangular cross-section and diverge from each other an angle of approximately 30° in dorsal view (Figs 6D, 7C). In addition, a prominent IPRL is present on all three middle cervicals, connecting the bases of the prezygapophyses (Figs 6D, 7C), as also occurs in *Leyesaurus* (Apaldetti *et al*. 2011) and *Adepapposaurus* (R. Martínez, pers. comm., July 2018). In all three middle cervicals, a very small prespinal fossa is present immediately ventral to the neural spine, between the bases of the prezygapophyses. The ridge extending along the lateral margin of the prezygapophyses extends posteriorly to merge with the similar ridge extending anteriorly from the lateral margin of the postzygapophyses, forming an EPRL that divides the lateral surface of the neural arch into dorsal and ventral portions (Figs 6A,B, 7A), as also appears to be present in *Adeopapposaurus* and *Leyesaurus* (Martínez 2009; Apaldetti *et al*. 2011).

As in the anterior cervicals, the postzygapophyses project horizontally in lateral view for a short distance beyond the end of the centrum (Figs 6A,B, 7A). Prominent, distinct epipophyses are present on Cv6 (also in *Leyesaurus*: Apaldetti *et al*. 2011), but these are reduced in size in Cv7, forming low rounded swellings (Fig. 6A). In Cv8, they are absent and replaced by the development of a low ridge, which forms an incipient spinopostzygapophyseal lamina (SPOL: Fig. 7A). Due to the presence of the epipophysis, the postzygapophyses of Cv6 have sub-triangular transverse cross-sections, whereas those of Cv7 and Cv7 and Cv8 have flatter, crescentic cross-sections. In all three vertebrae, their articular facets are oriented mainly ventrally and slightly laterally. In dorsal view, the postzygapophyses are more clearly separated from each other along the midline than in the preceding cervicals, diverg-

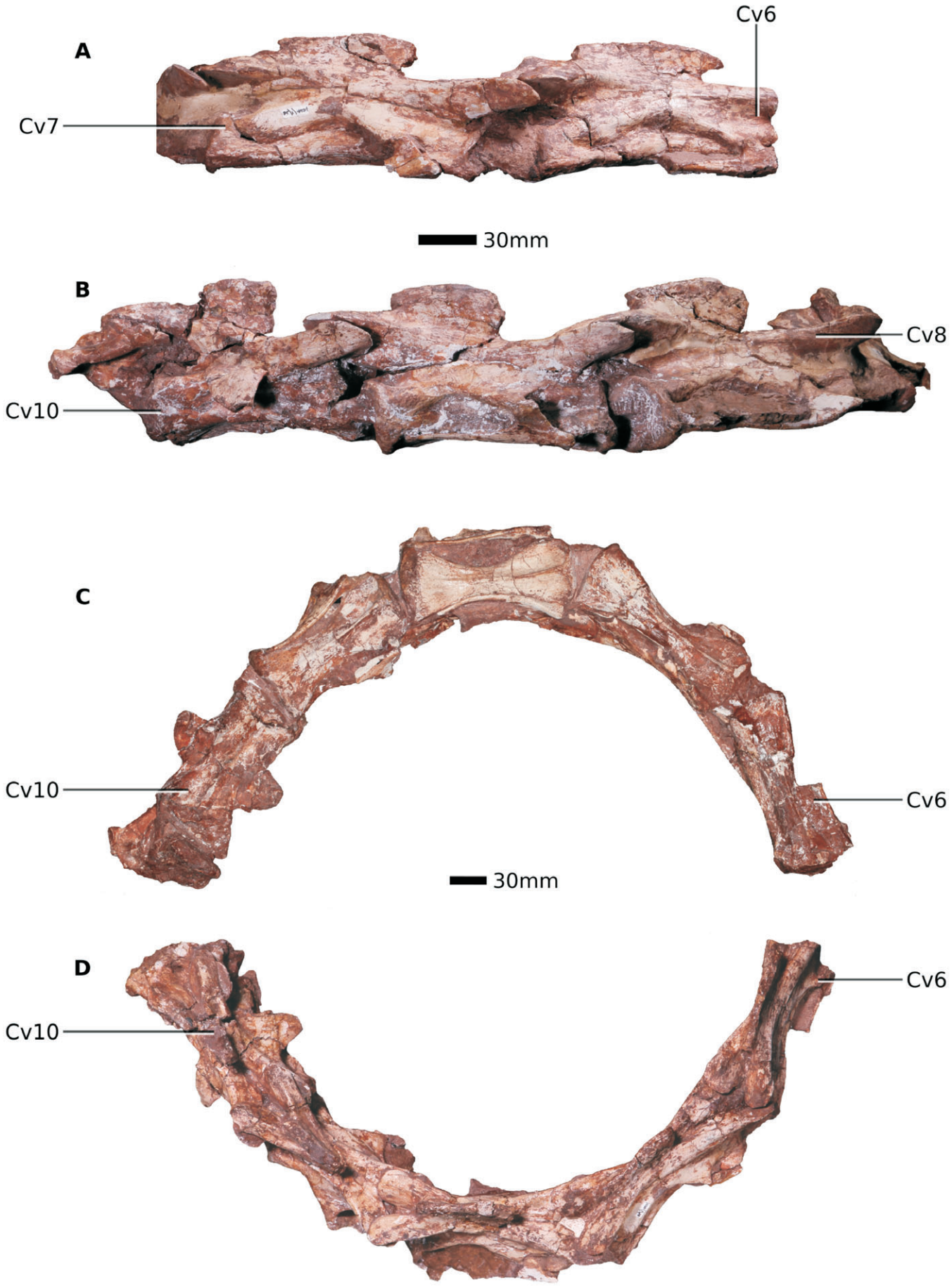


Figure 6. Posterior cervical vertebrae (Cv6–10) and anterior dorsal (D1, in part) of *Massospondylus carinatus* (BP/1/4934). **A**, right lateral view of Cv6–8; **B**, right lateral view of Cv8–10 (and broken centrum of D1); **C**, Cv6–D1 in ventral view; **D**, Cv6–D1 in dorsal view. Anterior is to the right in all images. Scale bars = 30 mm.

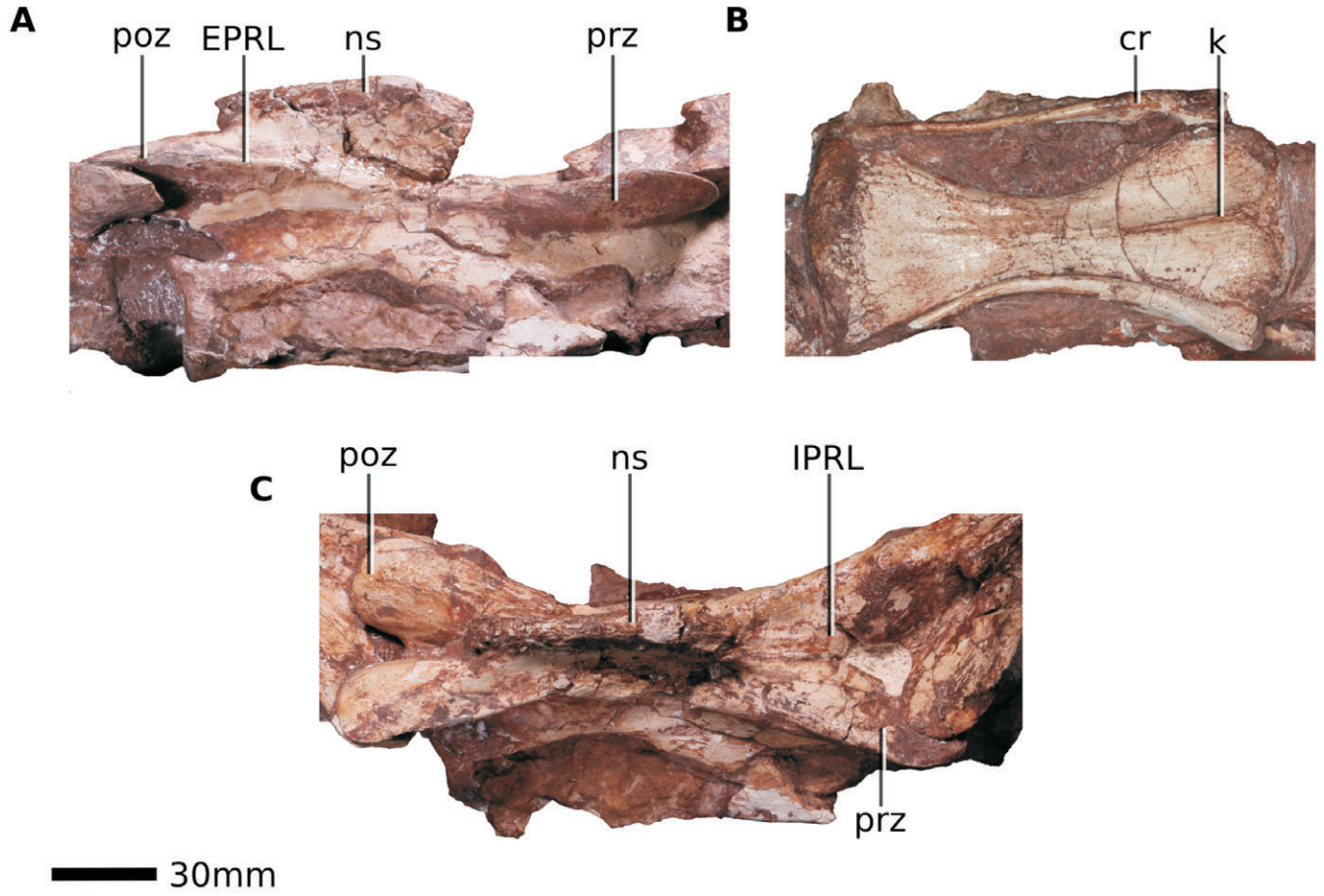


Figure 7. Cervical vertebra 8 (Cv8) of *Massospondylus carinatus* (BP/1/4934) in right lateral (**A**), ventral (**B**) and dorsal views (**C**). Anterior is to the right in all images. Scale bar = 30 mm.

ing at an angle of approximately 45°, with a 'V'-shaped notch opening between them posteriorly (Figs 6D, 7C). The development of this notch separates the medial margins of the postzygapophyses and thereby removes the floor of the sub-triangular recess that is present posterior to the neural spine in Cv3 and Cv4 (see above). A shallow, sub-elliptical postspinal fossa is present on the posterior surface of the neural spine in Cv6, and this fossa increases in size in Cv7 and Cv8.

In lateral view, the wing-like sheet supporting the diapophysis becomes more prominent in Cv6 though to Cv8 (Figs 6A,B, 7A). In Cv6 the diapophysis is a short, stalk-like process with an elliptical longitudinal cross-section that projects anteroventrolaterally from the neural arch. As in Cv3–5, but more clearly expressed in Cv6–8, the diapophysis is posteriorly continuous with the ventral margin of the neural arch that overhangs the lateral surface of the centrum. In Cv6–8, this strongly expanded ventral margin forms a prominent ridge-like structure that is in an equivalent position to the posterior centrodiapophyseal lamina (PCDL) and meets the posterior margin of the diapophysis (same comment also applies to Cv3–5). However, this ridge is also essentially the neural arch boundary. A short ridge also extends anteriorly from the diapophysis in an equivalent position to the prezygodiapophyseal lamina (PRDL) of the posterior cervicals, although it does not extend as far anteriorly as the base of the prezygapophysis in Cv6–8.

The neural spines of Cv6–8 are better preserved than those of Cv3–5. They are mediolaterally compressed, thin, low, elongate sheets, but they become slightly expanded mediolaterally along the sequence, so that the neural spine of Cv8 is considerably more robust that those of the anterior cervicals. The anterodorsal tips of the neural spines in Cv6 and Cv7 overhang the IRPL, forming a hook-like process (this area is broken in Cv8: Fig. 6A), which is absent in *Adeopapposaurus* (Martínez 2009), but present in incipient form in *Leyesaurus* (Apaldetti *et al*. 2011). In all three middle cervicals of *M. carinatus* a similar but much smaller process arises from the posterior margin of the neural spine. The dorsal margin of the neural spine is smoothly convex in lateral view.

The heads of the cervical ribs are arrow-shaped in lateral view, with a sub-triangular, anteriorly projecting capitulum and a sub-rectangular tuberculum. These processes are connected by a sheet of bone and not separated by a distinct notch. Prior to preparation, the ribs of Cv8 were complete (reaching 190 mm in length) and extended well beyond the end of the centrum posteriorly, to overlap the centrum of the next vertebra and articulate with the anterior process of the next rib in the series. The rib shafts are cylindrical in cross-section and gently curved along most of their length, though more the extreme distal curvature might be due to deformation.

Posterior cervicals (Cv9 and Cv10) – Cv9 and Cv10 are relatively complete but have each suffered some superficial damage to their neural arch processes and the lateral surfaces of Cv9 are partially obscured by matrix (Fig. 6;

Supplementary Model 2). The anterior-most part of D1 is preserved in articulation with the posterior articular surface of Cv10. Cv 9 and Cv10 differ substantially in morphology from the preceding cervicals and represent the cervicodorsal transition.

In overall shape, Cv9 is anteroposteriorly shorter and relatively higher than the preceding vertebrae (Fig. 6B), with a centrum length/anterior height ratio of 3.62, which is more elongate of that for *Adeopapposaurus* where this ratio is ~2.2 (Martínez 2009). The centrum is amphicoelous in *M. carinatus*: portions of both the anterior and posterior articular surfaces are visible and each is gently concave and surrounded by a raised rim of bone. The lateral surfaces of the centrum are longitudinally concave, and there is no evidence for pneumatic structures, but these areas are partially obscured by matrix and the overhanging neural arch (Fig. 6B). As a result, it is not possible to determine if the neurocentral depression seen in the previous cervicals is present or absent. The lateral surfaces of the centrum are separated from the ventral surface by a distinct break-in-slope. A stout, elliptical parapophysis with a concave articular surface is present and situated on the anteroventrolateral corner of the centrum, as also occurs in *Adeopapposaurus* (Martínez 2009). In ventral view, the centrum is similar to that of the preceding cervicals in possessing a dumbbell-shaped outline, a midline keel that is prominent anteriorly and that fades out at a point approximately two-thirds of the way along the centrum, and longitudinal sulci lying alongside the keel anteriorly (Fig. 6C). The centrum of Cv10 is very similar in morphology to that of Cv9, although it is slightly more elongate, with a with a centrum length/anterior height ratio of 4.14. A deep depression invades the lateral surface of the centrum below the transverse process, in a position equivalent to the centrodiapophyseal fossa (CDF). Cv10 retains the parapophysis on the centrum, which is one of the criteria supporting the identification of this element as a posterior cervical, rather than an anterior dorsal.

The prezygapophyses of Cv9 and Cv10 are relatively short (Fig. 6B): in Cv9 and Cv10 they project for only 20 mm and 14 mm, respectively, beyond the end of the centrum (*vs* 32 mm in Cv7). In both Cv9 and Cv10, and similar to the condition present in *Adeopapposaurus* (Martínez 2009), they diverge at an angle of approximately 60° and are sub-triangular in cross-section, with flat articular surfaces that face mainly dorsally and slightly medially. An extensive IPRL is present between the bases of the prezygapophyses (as in all preceding cervicals) and a short, deep prespinal fossa invaginates this lamina and the base of the neural spine. In Cv9, very short buttresses arise from the dorsal surfaces of the prezygapophyses, forming stout spinoprezygapophyseal laminae (SPRL) (but this area is damaged in Cv10). A prominent EPRL traverses the lateral surface of the neural arch from the lateral surfaces of the prezygapophyses to the postzygapophyses in both Cv9 and Cv10 (also present in *Adeopapposaurus*: Martínez 2009).

In dorsal view, the postzygapophyses of Cv9 and Cv10 diverge at approximately 45°, but they are more strongly separated from each other than in the preceding cervicals, due to a deeper notch between them (Fig. 6D). As in the preceding cervicals the postzygapophyses do not extend far beyond the end of the centrum. The postzygapophyses have a crescentic cross-section and lack an epipophysis. Both vertebrae possess distinct SPOLs, but these are most strongly developed in Cv10. A deep, dorsoventally elongate postspinal fossa is present in both posterior cervicals. Cv9 is the only cervical in which the posteroventral margin of the neural arch is visible, and there is no evidence for the presence of a hyposphene.

The neural spine of Cv9 is low and plate-like but it is mediolaterally expanded in comparison to those of the preceding vertebrae and is more robustly built (Fig. 6B). It is also relatively shorter anteroposteriorly and taller dorsoventrally than those in Cv3–8. The anterior and posterior margins of the neural spine are broken so it cannot be determined if the anterior and posterior extensions present in Cv6 and Cv7 were present or not. The neural arch base substantially overhangs the lateral surface of centrum and the diapophysis is supported by a large, triangular, wing-like expansion. The diapophysis is linked to the centrum by a prominent PCDL and to the ventral surface of the prezygapophysis by a PRDL.

In lateral view, the neural spine of Cv10 is much shorter anteroposteriorly than that of Cv9 and is also dorsoventrally taller, so it is more similar in morphology to those of the dorsal vertebrae. The summit of the neural spine is damaged, but in dorsal view it is expanded transversely along its posterior margin, to produce a teardrop-shaped transverse cross-section. Although the anterior margin of the spine is slightly damaged, it appears to be straight, so probably lacked the anterior process seen in some of the earlier cervicals. The neural spine summit is abraded but is flat to slightly concave.

In Cv10, the wing-like expansion of the neural arch is modified into a triangular transverse process that is much longer anteroposteriorly and more extensive laterally than in any of the preceding cervicals, as also occurs in Cv10 of *Adeopapposaurus* (Martínez 2009). The anterior margin of this process extends towards the prezygapophysis, forming the PRDL. The posterior margin merges into the side of the centrum in a position equivalent to the PCDL. In anterior view, the transverse process is oriented slightly lateroventrally, but this may have been affected by deformation. The transverse processes are flat sheets that expand slightly towards their tips to form the diapophyseal articular surfaces.

Cervical ribs are present on both sides of Cv9, but each is broken posteriorly, so the full length of the shaft is unknown. In lateral view, the proximal end is identical in morphology to those of Cv7 and Cv8. In medial view, there is a shallow depression that that covers the proximal surface, formed by the presence of a shallow shelf arising from the medial surface of the capitulum, which merges with the base of the shaft as it arises from the rib head. The rib shafts have a cylindrical cross-section and taper posteriorly, curving laterally as they do so. The rib of Cv10 is a more robust version of the ribs seen in Cv7–9 and

forms a second line of evidence supporting the identification of this vertebra as a cervical, rather than a dorsal. The posterior extent of the rib is unknown: however, the shaft tapers in width within a short distance of the proximal end and it seems likely that it would have been very short and may not have reached the level of the next centrum (D1). In lateral view, the rib head is identical to those of the other posterior cervicals.

Dorsal vertebrae

There are 14 dorsal vertebrae in *M. carinatus*, as in *Lufengosaurus* (IVPP V15) and *Sarahsaurus* (Rowe *et al*. 2011), but in contrast to *Adeopapposaurus* where only 13 are present (Martínez 2009). The anterior dorsals are poorly preserved, extensively crushed and cracked, and are slightly disarticulated from each other (Fig. 8). Their centra are either obscured or only partially exposed and they are visible primarily in dorsal view, although partial ventral views are available for D1–8. The neural arches of D1–8 are generally exposed, but none are complete. From D4–D7, the axial column has been rotated so the vertebrae are visible in left lateral and dorsal views. D5–D13 are preserved in articulation, which obscures many details of their anterior and posterior surfaces (Fig. 9). D14 is not articulated with the other dorsals. D8–D13 are largely visible in left lateral view and D9–D12 are partially visible in right lateral view; D14 is visible in anterior and partial posterior views. D5–D14 are all well preserved, though from D6–13 the left transverse processes are missing. The neurocentral sutures are closed in all dorsals. The dorsal series has been subdivided into anterior (D1–D4), middle (D5–D8) and posterior (D9–D14) sections on the basis of changes in neural spine morphology and the position of the parapophysis with respect to the neurocentral junction. Measurements of the dorsal vertebrae are provided in Table 2.

Anterior dorsals (D1–D4) – The centra of D1–D4 are hidden almost entirely by matrix or the presence of other overlying elements. D1 is badly damaged and divided between two blocks: the prezygapophyses and anteriormost part of the centrum are articulated with the posterior cervicals, while the remainder of the neural arch is visible in dorsal view on the anterior thoracic block (Fig. 8A,B; Supplementary Model 3). The centrum of D1 is incomplete, and it also lacks most of the right side of the neural arch as well as the neural spine. D2 lacks the neural spine, right postzygapophysis and right transverse process; the left prezygapophysis, transverse process and neural spine of D3 are missing; D4 lacks the neural spine.

The partially exposed centra of D1–D4 provide little useful anatomical information, but some observations are possible (Fig. 8A–D). In D1, the anterior articular surface is flat to very gently convex. A small part of the left side of the centrum of D4 is visible, as is its ventral surface, revealing that the lateral surface of the centrum is saddle-shaped and that the lateral surfaces merge ventrally without forming a distinctly divided ventral surface. D4 shows no evidence for a midline keel or groove. Laterally, the diapophysis of D4 is supported by a paradiapophyseal lamina (PPDL) anteroventrally and a stouter PCDL posteroventrally (the latter lamina is also visible in D3). These two laminae frame a very narrow, shallow, blind-ending triangular CDF beneath the diapophysis, as is common among all early sauropodomorphs including *Adeopapposaurus*, *Coloradisaurus*, *Ignavusaurus* and *Lufengosaurus* (Young 1941; Martínez 2009; Knoll 2010; Apaldetti *et al*. 2011, 2013). The parapophysis is large and situated on the neurocentral junction with its ventral part on the centrum and dorsal part on the arch. It has a sub-elliptical outline with its long axis directed dorsally and slightly posteriorly, and has a concave articular surface surrounded by a distinct rim of bone.

The prezygapophyses of the anterior dorsals have a stout, sub-triangular outline and are less elongate than those of the cervicals. They are sub-triangular in transverse cross-section and their ventral margins are supported by a stout PRDL. In D4, the ventral margin of the prezygapophysis forms a prezygoparapophyseal lamina (PRPL) that contacts with the anterior margin of the parapophysis at its midheight; the PRPL, PRDL and PPDL frame a deep, triangular prezygapophyseal paradiapophyseal fossa (PRPADF), which is absent in *Coloradisaurus* (Apaldetti *et al*. 2013), but present in *Ignavusaurus* (Knoll 2010) and *Lufengosaurus* (IVPP V15). In dorsal view, the anterior margins of the prezygapophyses are broad and rounded in *M. carinatus* and their articular facets are

Table 2. Measurements of dorsal vertebrae in BP/1/4934. All measurements are in mm. Those marked with an asterisk are minima due to breakage. Some measurements were not possible due to either extensive breakage or the presence of matrix/overlapping elements.

	CL	ACH	ACW	PCH	PCW	NAL	NSL	NSH	VH	CL/ACH
D1	–	52	–	–	–	–	–	–	–	–
D2	–	–	–	–	–	98*	–	–	–	–
D3	–	–	–	–	–	92*	–	–	–	–
D4	73	–	–	–	–	93	–	–	–	–
D5	–	–	–	–	–	83	49	44	–	–
D6	74	–	–	–	–	95	53	55	–	–
D7	74	60	–	55*	–	–	–	–	–	1.23
D8	–	–	–	–	–	–	60	49	–	–
D9	77	59*	–	59	–	106	61	49	126*	1.31*
D10	76	58*	–	64	–	107	62	51	147	1.31*
D11	79	66	–	70	–	109	65	52	156	1.13
D12	82	74	–	76	–	111	61*	55	166	1.11
D13	78	80	–	81	41	105*	52	56	182	0.98
D14	–	72	73	–	–	–	38	57	186	–

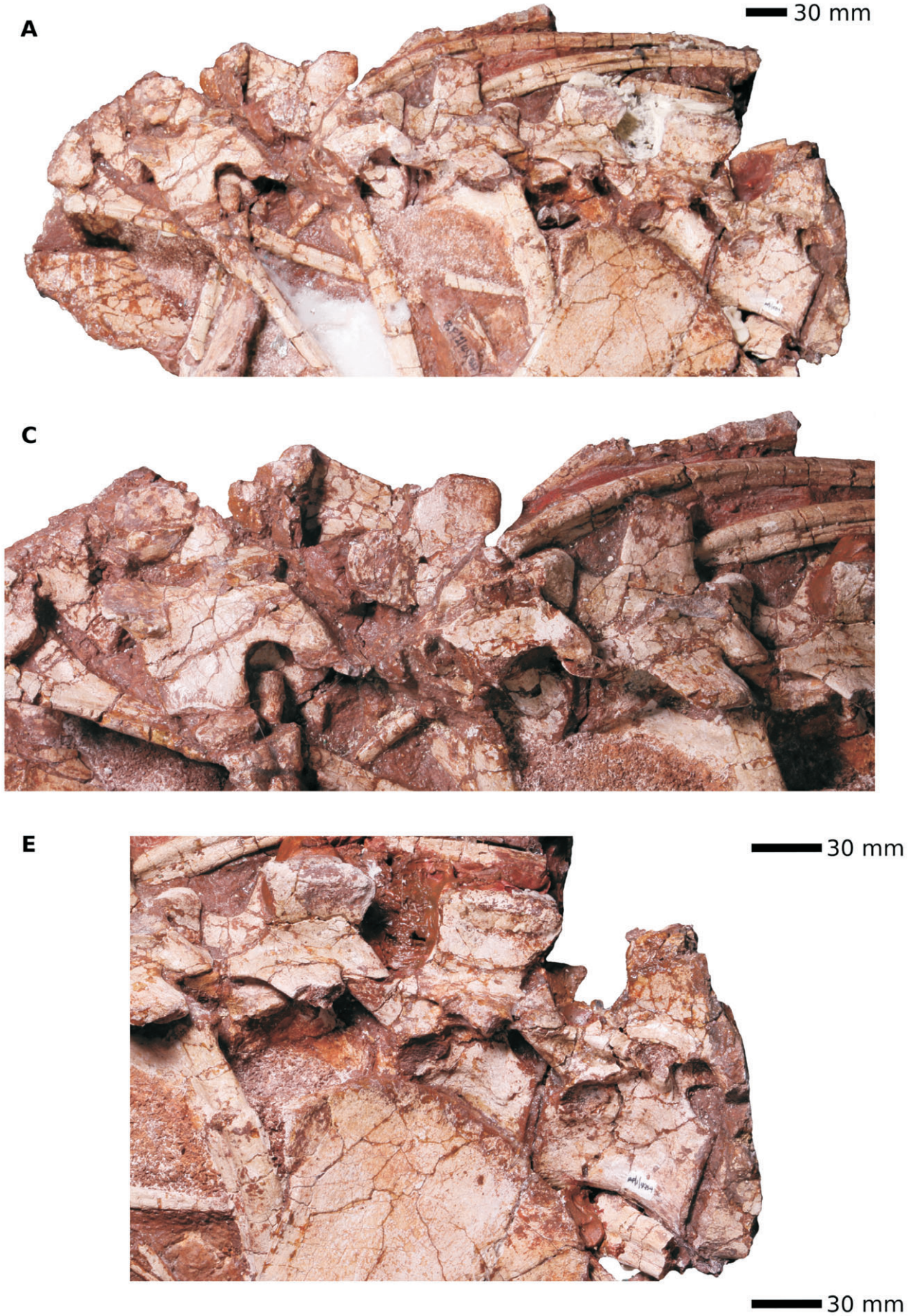


Figure 8. Anterior and middle dorsal vertebrae (D1, in part, to D8, in part) of *Massospondylus carinatus* (BP/1/4934). **A** (photograph) and **B** (line drawing) in dorsal and left lateral views; **C** (photograph) and **D** (line drawing), close-up on neural arches of D2 and D3 in dorsal view; **E** (photograph) and **F** (line drawing), close up on D5–D7 in lateral view. Anterior is to the left in all images. Scale bars = 30 mm. (Continued on p. 131.)

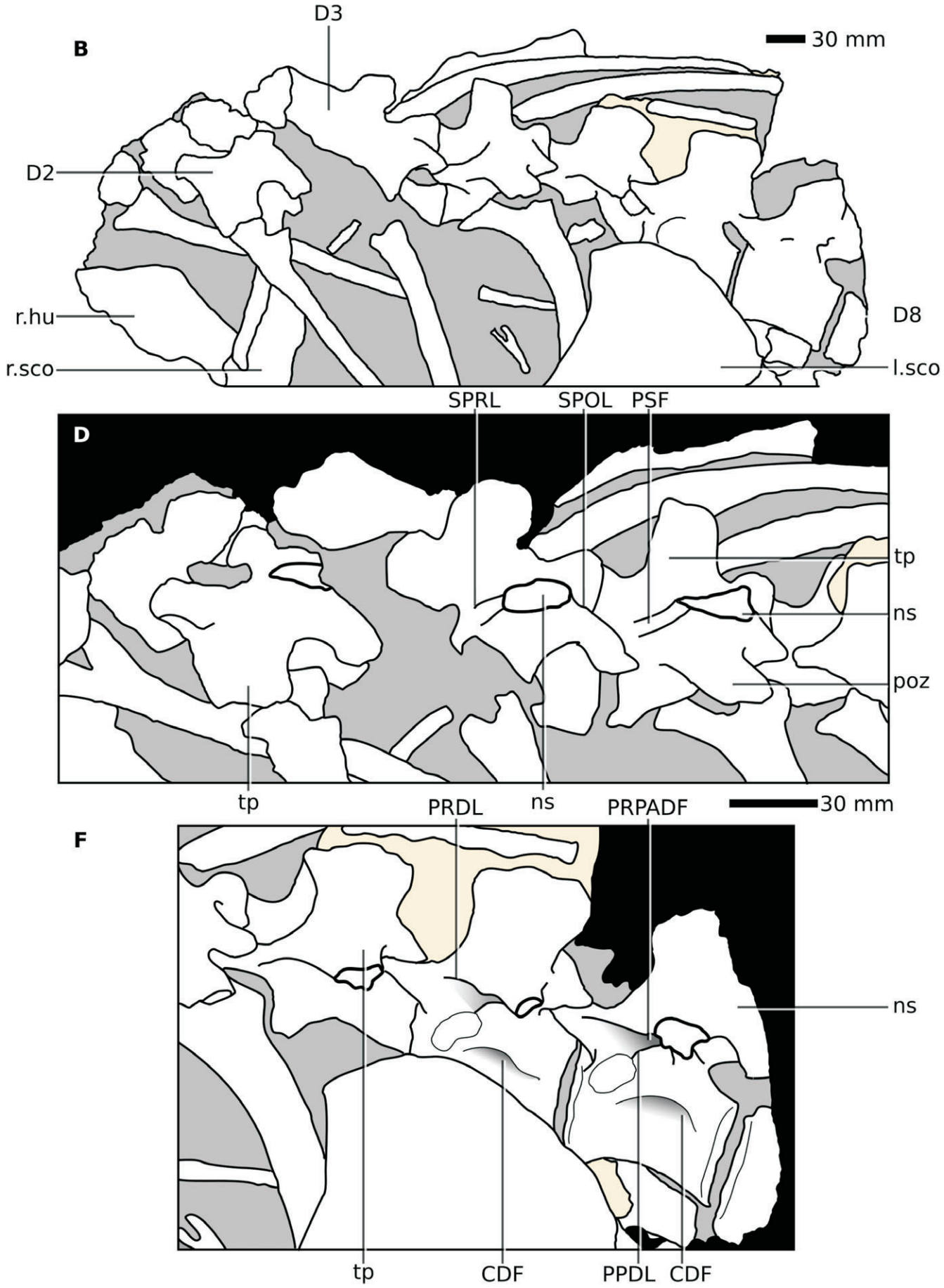


Figure 8 (continued).

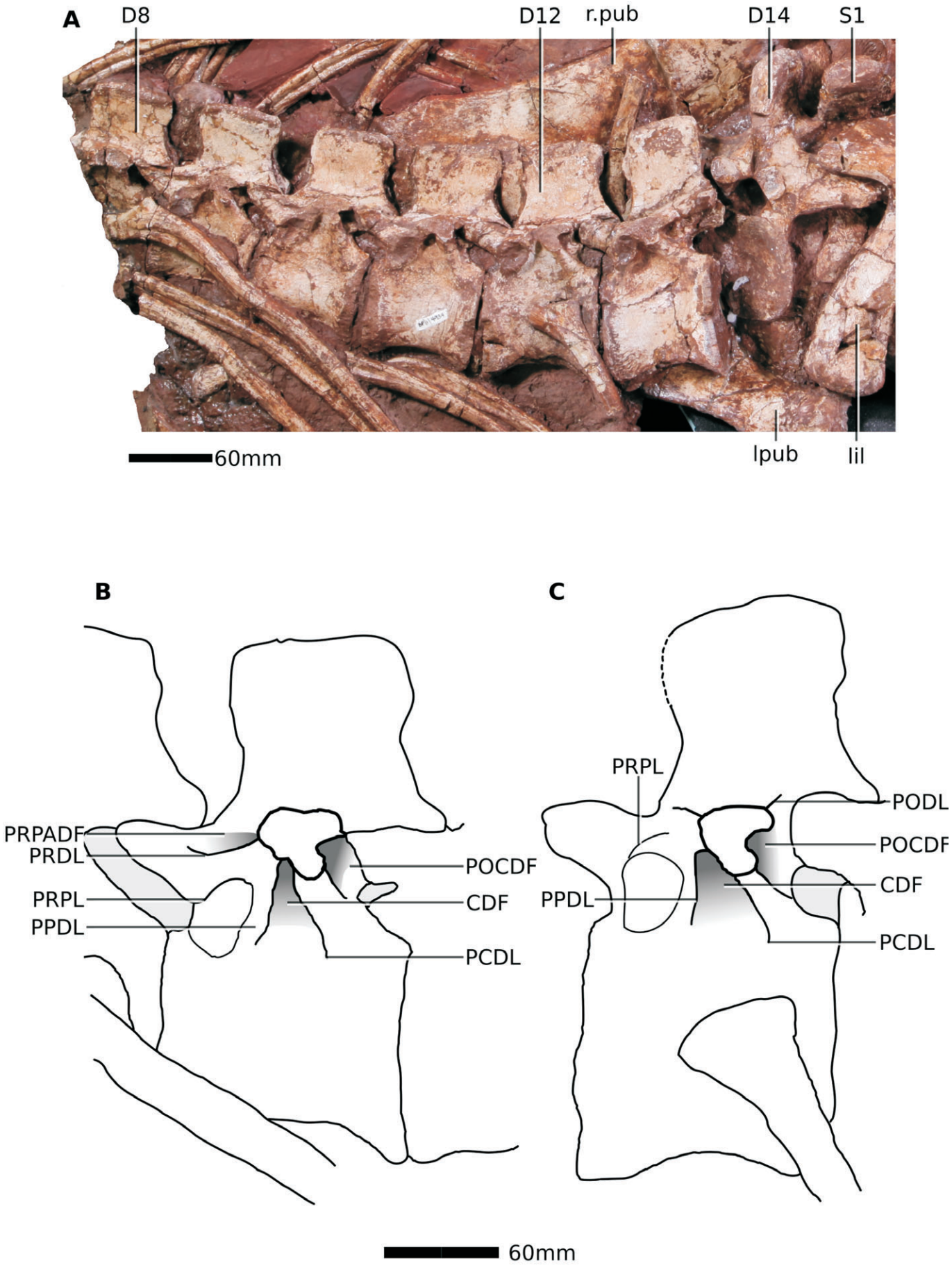


Figure 9. Middle and posterior dorsal vertebrae (D8, in part, to D14) of *Massospondylus carinatus* (BP/1/4934). **A**, left lateral view; **B**, line drawing of D10 in left lateral view; **C**, line drawing of D12 in left lateral view. Anterior is to the left in all images. Scale bars = 30 mm.

sub-elliptical in outline and face mainly dorsally, but also slightly medially. In addition, the prezygapophyses of D2 extend almost parallel to each other, rather than diverging in dorsal view, whereas those of D4 diverge at an angle of approximately 30°. Although obscured by the postzygapophyses of Cv10, the IPRL is either greatly reduced or absent in D1 and is absent from D2 onwards. The EPRL that was present in the posterior cervicals is not present in D2 or any other dorsals (it is also absent from the dorsals of *Adeopapposaurus*, *Coloradisaurus*, *Ignavusaurus* and *Lufengosaurus*: Young 1941; Martínez 2009; Knoll 2010; Apaldetti *et al*. 2013). A small prespinal fossa is present in D1 and this becomes deeper in D2–D4.

The postzygapophyses of D2–D4 are short, stout, have a triangular transverse cross-section and articular surfaces that were oriented ventrolaterally. In D2, the dorsal surface of the postzygapophysis supports a broad, rounded SPOL that merges into the base of the broken neural spine, but SPOLs are effectively absent from D3 and D4, which have smoothly rounded dorsal margins. This contrasts with *Coloradisaurus* in which SPOLs are present on the latter vertebrae (Apaldetti *et al*. 2013). In *M. carinatus*, the postzygapophyses of D3 and D4 diverge from each other at an angle of around 30°, are separated by a 'V'-shaped groove and frame an elongate postspinal fossa. The ventral margin of the postzygapophysis is connected to the posterior margin of the transverse process via a postzygodiapophyseal lamina (PODL).

In D2–D4, the broken bases of the neural spines indicate that they were anteroposteriorly short, approximately twice as long as wide, and that the base of the spine had a trapezoidal transverse cross-section that was narrow anteriorly and widest posteriorly. In dorsal view, the transverse processes of D2 and D3 are oriented laterally and slightly posteriorly. In D2–D4 they are sub-rectangular plates with subparallel, straight anterior and posterior margins, a slightly concave lateral margin and a smoothly convex dorsal surface. In D4, the transverse process has a teardrop-shaped cross-section in lateral view. The transverse processes project laterally and slightly posteriorly, and in the case of D2 and D3 appear to have been angled slightly ventrally, whereas in D4 it is angled slightly dorsally. However, these orientations could be the result of minor deformation in all cases.

Middle dorsals (D5–D8) – D5–D8 are all visible in left lateral view and other views of each neural arch are also available (Fig. 8A,E,F; Supplementary Model 3). D5–D7 are well preserved, though parts of the lateral surfaces of D5 and D6 are obscured by the scapula. The left transverse processes are broken on all four vertebrae and the neural spine of D7 is incomplete posteriorly. D8 is broken, with its anterior-most part (the anterior centrum and a fragment of left prezygapophysis) articulated with D7 in the anterior thoracic block, while the rest of the vertebra is in the posterior thoracic block.

The middle dorsal centra are relatively elongate and tall with length/anterior height ratios of ~1.5 (see Table 2), which are similar to the ratios reported in *Adeopapposaurus* (Martínez 2009) and *Seitaad* (Sertich & Loewen 2010), but more elongate than those in *Coloradisaurus* (0.96–1.05: Apaldetti *et al*. 2013) or *Lufengosaurus* (~1.1: IVPP V15), and shorter than those of the unusually elongate dorsal centra of *Ignavusaurus* (~1.7–2.1: Knoll 2010). In *M. carinatus*, in lateral view, the lateral surfaces are anteroposteriorly and dorsoventally concave, the anterior and posterior centrum margins are both straight and its ventral margin is gently concave. Pneumatic and nutrient foramina are absent. The anterior, posterior and ventral surfaces of the centrum are largely obscured in D5–D8, but D7 suggests that the ventral surface was not offset from the lateral surfaces by ridges or changes or slope, but by merging of the lateral surfaces to form a broad rounded ventral margin that lacks a keel. In D7, short, anteroposteriorly extending striations are present around the anterior and posterior margins of the centrum. The parapophysis is positioned on the neurocentral junction and partially situated on both the centrum and the neural arch. It is best seen in D6 and D7, in which it is a large, concave, sub-circular facet, rimmed by a sharp ridge of bone. In D5–D7 it is situated slightly posterior to the anterodorsolateral corner of the centrum and at the ventrolateral corner of the neural arch (this region is broken in D8).

In lateral view, the neural arch extends for almost the full length of the centrum, with the exception of the anterior few millimetres. The prezygapophyses project dorsally from the neural arch at an angle of approximately 45°, have almost flat articular surfaces that face mainly dorsally, and do not project far beyond the anterior margin of the centrum. The dorsal margin of the prezygapophysis gives rise to a well-defined PRDL that is oriented horizontally as it extends posteriorly. The ventral margin of the prezygapophysis bears a low, rounded ridge that connects with the anterodorsal margin of the parapophysis ventrally, forming a PRPL. The dorsal surface of the process also gives rise to a short, stout SPRL that frames a small prespinal fossa in D5 and D6 (the fossa is not visible in D7 and this area is damaged in D8). The prezygapophyses have stout, sub-triangular transverse cross-sections. Due to the preservation of the specimen it is not possible to determine the degree of divergence between the processes, with the exception of D5, where they diverge at around 30°. The IPRL is absent, at least in D5 and D6.

The left transverse process of D5 and those on the right of D5 and D6 are reasonably complete, but the rest are broken in D6–D8. That of D5 indicates that in dorsal view the process was broader than long, projected laterally and slightly posteriorly, while in lateral view it projected almost horizontally. In dorsal view, the anterior margin of the process is slightly curved where it meets the prezygapophysis, but is otherwise straight, whereas its posterior margin is very slightly concave. The dorsal surface of the process is anteroposteriorly concave and the broken surfaces in D5–D8 reveal sub-triangular cross-sections, with the apex of this triangle pointing ventrally. A short, thin, but sharp PPDL connects the underside of the process with the posterodorsal corner of the parapophysis and together with the PRDL and PRPL frames an inverted triangular PRPADF. The PRPADF is deep in D5, invagi-

nating the lateral surface of the neural arch, but becomes a shallower, but still distinct, sulcus in D6 and D7 (this region not preserved in D8). A similar PRPADF with associated laminae is present in the middle dorsals of *Adeopapposaurus* (Martínez 2009), *Ignavusaurus* (Knoll 2010), *Lufengosaurus* (IVPP V15), *Sarahsaurus* (Rowe *et al*. 2011) and *Seitaad* (at least in D8: Sertich & Loewen 2010), but the PRDL is absent from all of the middle dorsals of *Coloradisaurus* so the PRPADF is correspondingly absent (Apaldetti *et al*. 2013). In *M. carinatus*, the ventral apex of the transverse process is continuous with a strong, rounded PCDL that merges with the posterodorsal part of the centrum. The PPDL and PCDL frame a triangular CDF, as also seen in *Coloradisaurus* (Apaldetti *et al*. 2013), *Ignavusaurus* (Knoll 2010), *Lufengosaurus* (IVPP V15: Young 1941), *Sarahsaurus* (Rowe *et al*. 2011) and *Seitaad* (Sertich & Loewen 2010), which becomes progressively deeper from D5 through to D8. In *M. carinatus*, a postzygodiapophyseal lamina (PODL) is present in D7 and D8 (and ambiguously so in D6, and possibly earlier in the dorsal column) and extends posteriorly to meet the lateral surface of the postzygapophysis. The PODL and PCDL form the boundaries of a crescentic to sub-triangular postzygapophyseal centrodiapophyseal fossa (POCDF) in *M. carinatus*, as in *Ignavusaurus* (Knoll 2010), *Lufengosaurus* (IVPP V15: Young 1941) and *Sarahsaurus* (Rowe *et al*. 2011), but this fossa is poorly developed or absent in *Coloradisaurus* (Apaldetti *et al*. 2013).

In dorsal view, the postzygapophyses are short, bluntly ended processes, which become more elongate from D5 to D8 (not visible in D7), so that in D8 they extend dorsally for almost half of the length of the neural spine. Their dorsal margins are rounded and form broad, rounded SPOLs that frame the postspinal fossa. Epipophyses are absent. In lateral view, the postzygapophyses do not extend beyond the posterior margin of the centrum. They have a stout sub-triangular cross-section and their articular facets are oriented primarily ventrally. A thin, plate-like hyposphene is present on the posterior midline in D6 and D7, just ventral to the postzygapophyses. Hyposphenes are also present on the middle dorsals of *Adeopapposaurus* (Martínez 2009), *Ignavusaurus* (Knoll 2010) and *Lufengosaurus* (IVPP V15).

In contrast to those of the anterior dorsals, the neural spines of D5–D8 are anteroposteriorly elongate (Fig. 8A,E), with bases that extend for almost the entire length of the neural arch table. Moving posteriorly from D5 to D8 the neural spines become progressively longer and higher. The neural spine has a straight to slightly concave anterior margin, a dorsal margin that is straight to gently convex anteriorly, but with a rounded posterior corner that merges in to the straight and slightly anteriorly inclined posterior margin. As a result, the posterodorsal corner of the neural spine slightly overhangs the postzygapophyses. In D8, a similar, but very small overhang also appears on the anterior margin of the spine. In anterior view, the neural spines form a transversely compressed plate, which is narrower than that in D1–4. In D5 and D6 the spine is slightly wider at its summit than ventrally, whereas in D8 it tapers dorsally. The neural spines lack the hook-like posterodorsal projections that are present in the middle dorsals of *Coloradisaurus* (Apaldetti *et al*. 2013) and *Lufengosaurus* (Young 1941).

Posterior dorsals (D9–D14) – In most respects, the posterior dorsals are almost identical in morphology to those of D5–D8, although they are much better preserved (Fig. 9). All of the centra appear to be complete and most of the neural arch processes are present, with the exceptions of slight damage to the posterior neural spine and postzygapophyses of D13 and the anterior neural spine and prezygapophyses in D14.

The centra of D9–D14 are very similar to those of D7 and D8, differing primarily in the absence of the parapophysis, which has migrated dorsally to lie fully on the neural arch. In addition, the posterior dorsal centra are relatively shorter and higher than those of more middle dorsals, with the centra eventually becoming slightly higher than long. This change occurs progressively, with centrum length/anterior height ratios declining through the sequence from a maximum of 1.31 (D9) to 0.98 (D13) (see Table 2). D11–D13 provide clearer views of the ventral surface of the centrum than the anterior dorsals, confirming that there is no distinct ventral surface, but that the lateral surfaces merge smoothly with each other. There is no evidence of a keel or ventral midline groove. Disarticulation between D13 and D14 provides the only clear views of the posterior and anterior articular surfaces. In D14, the anterior articular surface has a rounded outline that is subequal in width and height and a flat to very gently concave surface. The posterior surface of D13 is elliptical in outline, taller than it is wide and gently concave, whereas that of D14 is almost circular in outline.

With respect to the neural arches, D9–D14 retain many of the same structures as seen in the middle dorsals, but various minor changes in the shape, size and orientation of these structures occur along the sequence (Fig. 9; Supplementary Model 4). In D9–11, the parapophysis is positioned on the ventrolateral corner of the neural arch and its posterodorsal corner is linked to the anteroventral surface of the transverse process by a stout PPDL. In D12 and D13, the parapophysis migrates further dorsally and slightly posteriorly to approach the diapophysis, obliterating the PPDL and becoming more laterally prominent. In D13, these two facets are immediately adjacent, though not conjoined. In conjunction with this dorsal migration, a new lamina, the anterior centroparapophyseal lamina (ACPL) appears in D12 and D13, extending ventrally and slightly anteriorly from the anteroventral margin of the parapophysis towards the centrum, as also occurs in *Lufengosaurus* (IVPP V15). In D12 of *M. carinatus* the ACPL is a very short, but in D13 it is forms a clearer, ridge-like feature. A separate parapophyseal facet cannot be identified on D14 and it is inferred to have merged with the diapophysis. D13 and D14 provide the only direct views of the neural canal in the entire dorsal series; the posterior opening in D13 is elliptical with its long axis oriented dorsoventrally, whereas the anterior opening in D14 is sub-circular in outline. In D10–13 of *M. carinatus*, the neural arches are subequal in height to, or only very slightly taller than, their corresponding centra, as also

occurs in *Lufengosaurus* (Young 1941), but differing from the conditions in *Adeopapposaurus* and *Ignavusaurus* where the neural arches are ~40% and ~80% taller than their centra, respectively (Martínez 2009; Knoll 2010).

The shape, size and orientation of the prezygapophyses and the presence of SPRL remains constant throughout the posterior dorsal series, but the PRDL and PRPL reduce in prominence from D9–D11 and are absent from D12 onwards. This reduction, and the coincident loss of the PPDL leads to shallowing of the PRPADF in D9–D11 and its loss in D12 onward, which also occurs in *Ignavusaurus* and *Lufengosaurus* (though from more anterior positions in the dorsal series, potentially D8: see Knoll [2010] and IVPP V15, respectively) and *Sarahsaurus* (Rowe *et al*. 2011). The prespinal fossa is dorsoventrally elongate and slit-like in D13 and D14.

Due to breakage, it is not possible to infer any changes in the shapes and orientations of the transverse processes in D9–D13, but it is clear that they were supported by a strong PCDL posteriorly, which becomes more robust moving posteriorly through the series. As a result, a deep, triangular CDF is present throughout the column (also in *Adeopapposaurus*, *Ignavusaurus*, *Seitaad* and *Sarahsaurus*: Martínez 2009; Knoll 2010; Sertich & Loewen 2010; Rowe *et al*. 2011), though in D9–11 this is framed anteriorly by the posterior margin of the parapophysis ventrally and the PPDL dorsally, whereas in D12 and D13 the anterior border of the fossa consists of the parapopophysis dorsally and the ACPL ventrally, as also occurs in *Lufengosaurus* (IVPP V15). Complete transverse processes are present in D14 and these extend horizontally in anterior view and have a strongly convex dorsal surface, whose anterior margin curves ventrally to meet the ventral part of the neural arch. The posterior margins are straight. Judging from the form of the transverse processes and the size of the anterior process of ilium, which is short and already largely occupied by a rib from a dorsosacral (i.e. sacral 1), D14 was the last free vertebra anterior to the sacrum. The diapophyseal laminae in *Coloradisaurus* are reduced in comparison to *M. carinatus* (see Apaldetti *et al*. 2013): consequently, the former lacks many of the associated fossae observed in the latter (or they are reduced in size), including both the CDF and POCDF, which are normally prominent in sauropodomorphs.

The postzygapophyses remain similar in size, shape and orientation throughout most of the posterior dorsals (D9–D13), with the retention of a prominent PODL, and the presence of a deep, sub-crescentic POCDF in D9–D13, as also occurs in *Ignavusaurus*, *Lufengosaurus* and *Sarahsaurus* (Young 1941; Knoll 2010; Rowe *et al*. 2011). An elongate, deeply incised postspinal fossa is present in *M. carinatus* until at least D12 (this area is damaged or obscured in D13 and D14), which is framed by dorsally extensive SPOLs. A thin, plate-like hyposphene is present in D9–13, which extends slightly posterior to the posterior margin of the centrum. In D14, the postzygapophyses are situated more dorsally on the neural arch than in D1–13, lying at a level much higher than the prezygapophyses in lateral view. They are also more widely divergent from the midline than in the preceding dorsals, with both of these differences presumably reflecting its articulation with the first sacral vertebra.

The neural spines of D9–D12 are very similar to those of D8, with the only substantive difference relating to a trend towards increasing neural spine height along the series from D9–D14 (Fig. 9). In D5–D12 all of the neural spines dorsal margins are all longer than the spine is tall (as measured from the point it merges into the rest of the neural arch). In D13 the neural spine is taller than long but is otherwise similar to those in D9–12. All of the neural spines in D9–D13 are mediolaterally compressed and plate-like. However, D14 has a differently shaped neural spine that is more than twice as tall as it is long and that projects slightly posterodorsally. It is also mediolaterally expanded towards its summit, so that the spine is widest dorsally, giving it a sub-rectangular cross-section that is intermediate in morphology between those present in the other dorsals and those of the sacral vertebrae.

Dorsal ribs – Numerous dorsal rib sections are scattered through the two thoracic blocks. Some of these are very elongate and many ribs can be traced through the blocks to their full lengths, with some missing only their distal-most positions, whereas others are represented by short sections of shaft or their proximal ends only. All of the ribs are similar in overall morphology, differing primarily in length and robustness along the vertebral column. The proximal end is divided into a distinct capitulum and tuberculum, which meet in a small proximal plate that then extends to form the rib shaft. A few of the ribs are still in articulation with their respective vertebrae, but the majority are at least partially displaced (Supplementary Models 3–4).

In the anterior-most dorsals (D1, D2, ?D3), the capitulum and tuberculum diverge from each other at an angle of approximately 45° in anterior view, leaving only a narrow gap between their bases. The tuberculum is the longer of the two processes, but it is only slightly longer than the capitulum. Both processes have a sub-elliptical cross-section, end in a flat or gently convex articular surface, and are subequal in mediolateral diameter. Ventrally the two processes fuse to form a small proximal plate, whose anterior surface is gently convex mediolaterally and whose posterior surface is shallowly excavated to form a short concavity around the junction between the two processes. The proximal plate narrows mediolaterally and anteroposteriorly to form the rib shaft, which is long, bowed laterally and ends in a slightly convex ventral terminus. The rib shafts are straight or very gently curved in lateral view, with subparallel sides, and do not taper appreciably towards their distal ends. The rib shafts have a 'D'-shaped cross-section proximally, with smooth transversely convex anterior surfaces and a flat to gently concave posterior surface. The posterior surfaces of all ribs bear a wide shallow groove that extends ventrally from a point just below the capitulum: this groove extends for most of the length of the shaft.

With only minor exceptions the ribs of the middle and posterior dorsals are effectively identical to those of the anterior dorsals. In middle dorsals (e.g. the rib for D4), the capitulum and tuberculum are separated by an angle of

around 60° in anterior view and linked by a concave web of bone. The tuberculum is approximately three times the length of the capitulum, but slightly smaller in diameter. More posterior ribs (from D8 onwards) taper a little more in their distal parts than the anterior dorsal ribs, ending in slender pointed tips. The longest complete rib in the specimen is that for D4 (left), which reaches 460 mm in total length (from the capitulum to the base of the shaft). However, it is likely that some of the middle dorsal ribs exceeded this, as another partial shaft lacking the proximal end reaches a minimum length of 400 mm.

Gastralia

Only the posterior portion of the gastral basket is preserved and consists of the posterior-most nine pairs of gastralia (Fig. 10). It is preserved approximately in life position, although the dorsoventral compression of the specimen has displaced the posterior-most gastralia from the distal ends of the pubes and interspersed the head and proximal shafts of at least three dorsal ribs within the gastral series. Each gastralium consists of a medial and a lateral gastral element, which articulate via a long, mediolaterally extending lap joint and are arranged so that the posterior surface of the medial end of the lateral segment overlaps the anterior surface of the lateral end of the medial segment.

The overall length of the gastralia changes markedly in the posterior-most two elements in the series: the penultimate gastralium is approximately 50% of the length of the preceding element and the posterior-most gastralium is slightly less than 50% of the length of the penultimate element (Fig. 10). The reduction in length is most pronounced in the lateral gastral segment – the medial segment of the penultimate gastralium is subequal in length to the preceding two medial segments. The posterior-most gastralium is very small (approximately 25% the length of the longest gastralia), with the lateral and gastral segments equal in length.

As preserved, the lateral gastral segments are nearly touching one another, but lack any indication (e.g. flattened anterior and posterior surfaces) that they were imbricated in life (Fig. 10). In general, the lateral segments of the anterior-most eight preserved gastralia have oval cross-sections with similar diameters. The posterior-most lateral segment is only 36% of the diameter of these more anterior segments. The medial and lateral ends of all lateral gastral segments taper gradually, with the medial end reaching a slightly sharper point. The shafts of the lateral segments are generally anteriorly convex, but the penultimate element and the preceding lateral segment have a short portion of the lateral end which is recurved, describing a low-amplitude sinusoidal curve in ventral view.

The medial gastral segments taper gradually as they extend laterally and are approximately one-third the length of the lateral segments in the two best-preserved gastralia (the third and fourth from the pubis) (Fig. 10). In the medial segment of the penultimate gastralium, the medial end forms a small, expanded, club-like structure, which articulates in a zipper-like fashion with the contralateral element. The presence of this articulation cannot be confirmed in more anterior gastralia due to poor preservation; however, the midline does appear to feature an anterior/posterior arrangement of contralateral medial ends forming a single, alternating midline articulation, as is typical of other sauropodomorphs and theropods.

Two possible pathologies are present. A rugose ridge is present on the posterior surface of the middle of the

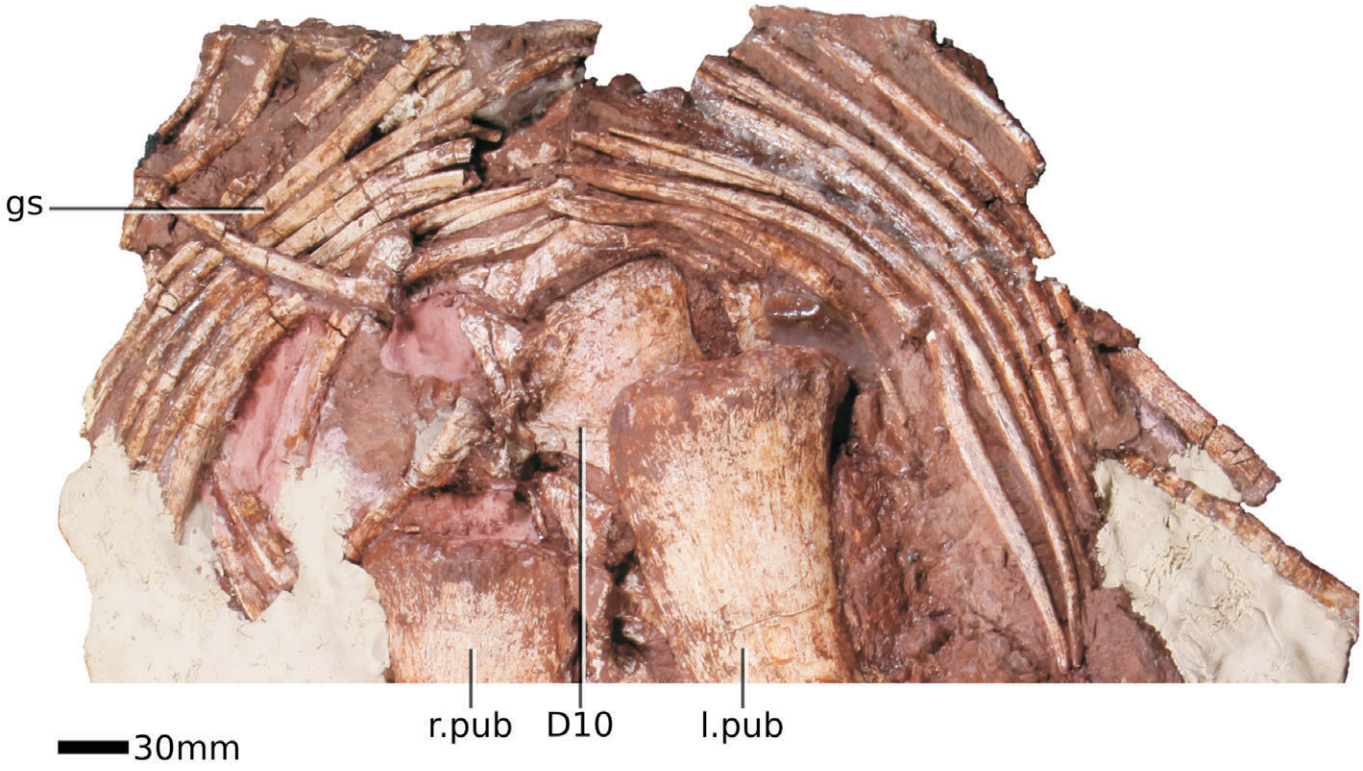


Figure 10. Gastral basket of *Massospondylus carinatus* (BP/1/4934). Anterior is to the top of the image. Scale bars = 30 mm.

lateral segment of the third (from pubis) left gastralium. On the contralateral element, in approximately the same position, the shaft of the gastralium expands abruptly. The remaining portion of the right lateral segment lateral to this expansion appears to be disconnected, suggesting perhaps that the element was broken and healed without bony connection. The similar position of these features is intriguing, however, especially given that the gastralia posterior to this position have an abrupt change in size and lateral segment length. It is possible that these 'pathologies' actually mark an important attachment site for soft tissue.

Sacrum

There are three sacral vertebrae (Fig. 11), consisting of one dorsosacral (sacral [S] 1) and two primordial sacral vertebrae (S2 and S3). Small sections of the neural spines are visible in the specimen's usual display orientation, but the reverse side of this block exposes all three sacral centra and their associated sacral ribs. It is not possible to determine if the sacral centra were fully co-ossified, due to preparation damage. Junctions between most of the sacral ribs and their respective vertebrae are partially traceable as are those between adjacent ribs, suggesting that the sacrum of this individual was not yet fully fused. Measurements of the sacral vertebrae are provided in Table 3.

The anterior articular surface of S1 is broader than tall and has an elliptical outline with its long axis oriented transversely. It is flat to very gently concave. The posterior articular surface of S3 has a similar morphology but is narrower and shorter. The lateral surfaces of the centra merge into the ventral surfaces around a subtle break in slope and they are not strongly offset from each other. Pneumatic foramina are absent. In ventral view, the centra are all mediolaterally expanded at their articular margins, whereas the central part is constricted to produce an hourglass-shaped outline (Fig. 11). The anterior margins of each centrum are broader than their posterior margins and the centra decrease in overall width from S1 to S3, though they maintain similar lengths. The ventral surfaces are anteroposteriorly concave and mediolaterally convex ('saddle-shaped'). S1 and S2 bear faint midline grooves that extend along the anterior two-thirds of the ventral surface; this groove is absent in S3.

S1 has sacral ribs that contacted the medial surface of the ilium in the region of the preacetabular process (Fig. 11). In dorsal or ventral view, they have elongate, dumbbell-shaped outlines, consisting of medial and lateral expansions that are connected via a stout, constricted shaft. They appear to have projected from the centrum almost horizontally and slightly posteriorly in ventral view. Medially, the rib contacts the anterior half of the centrum's lateral surface. The lateral expansion is asymmetrical with respect to the shaft and extends farther posteriorly than anteriorly. The posterior part contacts the anterior margin of S2's sacral rib, as also occurs in *Adeopapposaurus* (Martinez 2009) and *Sarahsaurus* (Rowe *et al*. 2011). As the sacral ribs are simple in morphology, project mainly laterally, and articulate with the preacetabular process of the ilium, this is regarded as a dorsosacral, as in *Adeopapposaurus* (Martínez 2009), *Ignavusaurus* (Knoll 2010) and *Lufengosaurus* (IVPP V15).

The sacral rib of S2 has a more complex morphology in ventral view and the medial and lateral expansions have increased in size, reducing the length of the shaft between them (Fig. 11). The medial expansion articulates with the anterior two-thirds of the S2 centrum and also contacts the posterior-most corner of S1. The lateral expansion is elongate, forming the central part of the sacricostal yoke and contacting the medial surface of the main body of the ilium. The lateral expansion is almost twice the length of the medial expansion. The short, twisted shaft that connects these two processes forms the posterior margin of the medial expansion (so that all of this process extends anteriorly from this point), but merges with the lateral expansion at a point around two-thirds of its length from the anterior end. The anterior part of the lateral expansion is mediolaterally broad and strap-like, leaving only a shallow notch between it and the medial expansion. As a result, the foramen between sacral ribs 1 and 2 has an irregular sub-triangular outline that is broadest anteriorly (adjacent to the centrum of S1) and tapers posteriorly. The posterior flange of the lateral expansion has a triangular outline that flares posteriorly to meet the anterior margin of the third sacral rib, forming a complete sacricostal yoke, as in *Sarahsaurus* (Rowe *et al*. 2011) (it is not clear if a complete sacricostal yoke was present in *Adeopapposaurus*: Martínez 2009). The morphology of sacral 2 suggests that it represents primordial sacral 1, as in *Adeopapposaurus* (Martínez 2009), *Ignavusaurus* (2010) and *Lufengosaurus* (IVPP V15: Young 1941).

S3 bears a complex sacral rib that is visible in both ventral and posterior views. Medially, the rib attaches to the entire lateral surface of S3 and it also extends onto the posterior-most part of S2 (Fig. 11). The medial expansion forms a low, stout, triangular buttress, which gives rise to a thick shaft at a point approximately one-quarter of the distance from its anterior end. Laterally, this shaft expands into a large sheet-like process. Anterior to the shaft this sheet forms a small, triangular projection that articulates with the second sacral rib. Posterior to the shaft, it expands laterally, dorsally and posteriorly to form an extensive contact with the posterior part of the medial iliac blade. This posterior sheet is oriented obliquely with respect to

Table 3. Measurements of sacral vertebrae and ribs in BP/1/4934. All measurements are in mm. Some measurements were not possible due to either extensive breakage or the presence of matrix/overlapping elements.

	CL	ACH	ACW	PCH	PCW	NSL	MPL	LPL	SRL
S1	79	55*	83	–	79	52	40(r)	37*(l)	45
S2	80	–	74	–	70	74	54(r)	88(r)	84
S3	77	–	65	50*	72	57	84(l)	89(r)	119

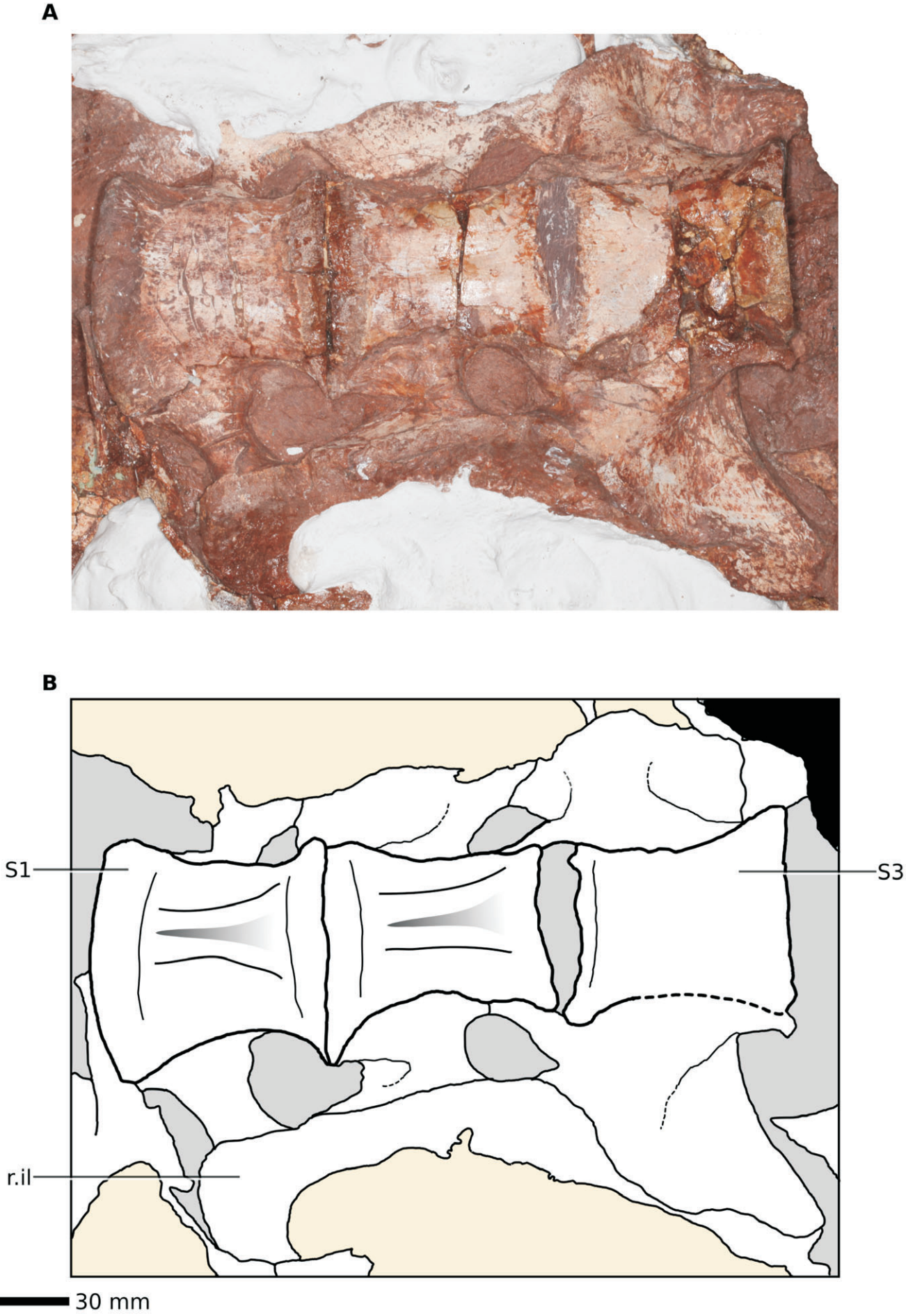


Figure 11. Sacrum of *Massospondylus carinatus* (BP/1/4934) in ventral view. Scale bars = 30 mm.

the rest of the sacricostal yoke and is mediolaterally broadest posteriorly, giving S3 a butterfly-shaped outline in posterior view. In lateral view, the margin of this rib describes a flattened, reversed 'S'-shaped curve. The foramen formed between the S2 and S3 sacral ribs has an inverted teardrop-shaped outline that is broadest anteriorly and tapers posterolaterally. The complex shape of this rib is characteristic of the morphology seen in primordial sacral 2, as is also the case in *Adeopapposaurus* (Martínez 2009), *Ignavusaurus* (Knoll 2010) and *Lufengosaurus* (IVPP V15: Young 1941). In *M. carinatus*, the postzygapophyses of S3 are rectangular in lateral view and have thin, plate-like cross-sections. They extend posteriorly and subparallel to each other for a short distance beyond the centrum.

In lateral view, all three sacral neural spines have straight anterior and posterior margins, gently convex dorsal margins, are canted posteriorly and are of similar height. The neural spine of S1 is taller than it is long and is the anteroposteriorly narrowest of the three. That of S2 is approximately as tall as it is long, forming a thick, robust plate. S3 has a neural spine that is taller than long and anteroposteriorly narrower that of S2, although this has been accentuated by breakage. All three spines are transversely narrower at the base and swell mediolaterally towards their summits to form slightly bulbous spine tables. In dorsal view, S1 and S3 have spine tables with an elongate elliptical outline, whereas that of S2 is more ovate, being broader anteriorly and narrowing posteriorly. The lateral surfaces of the spines are flat and bear no ornament or laminae.



Figure 12. Anterior caudal vertebra (Cd1?) of *Massospondylus carinatus* (BP/1/4934) in anterior view. Scale bar = 20 mm.

Caudal vertebrae

Only five caudal vertebrae are preserved – one in isolation behind the sacrum and another four in articulation (Figs 12, 13; Supplementary Model 4). It is not possible to determine exactly where they lie in the caudal series, but all pertain to the proximal part of the tail and are numbered as Cd1–5 for convenience, although they may not form a continuous series or have started from the Cd1 position. No neurocentral sutures are visible in any of the vertebrae. Distinct vertebral laminae are absent. The heights of the neural spines decrease slightly along the articulated series. In general, the caudal vertebrae are very similar to those of *Adeopapposaurus* (Martínez 2009), *Ignavusaurus* (Knoll 2010) and *Lufengosaurus* (Young 1941). Measurements of the caudal vertebrae are provided in Table 4.

Cd1 – In anterior view, the articular surface is almost sub-circular in outline, but has a straight dorsal margin, and is deeply concave (Fig. 12). The lateral surfaces of the centrum are anteroposteriorly concave and dorsoventrally convex and are separated by smooth, but distinct breaks-of-slope from the ventral surface. The ventral surface is mediolaterally convex and its midline bears a low, rounded swelling. The posterior articular surface of the centrum is taller than wide in anterior view, has a sub-elliptical outline with the long axis of this ellipse extending dorsoventrally, rounded margins, and is gently amphicoelous with the central concavity surrounded on all sides by a thick, raised rim. No obvious chevron facets are present at the base of either the anterior or posterior articular surface, so it is possible that this is genuinely Cd1. The neural canal is infilled and obscured by matrix posteriorly, but the anterior opening is elliptical in outline, with its long axis oriented transversely.

Table 4. Measurements of caudal vertebrae in BP/1/4934. All measurements are in mm. Some measurements were not possible due to either extensive breakage or the presence of matrix/overlapping elements. Heights of the anterior and posterior articular surfaces exclude chevron facets. Note that the designations for Cd1–5 do not necessarily match their anatomical positions within the tail (see text for details).

	CL	ACH	ACW	PCH	PCW	NSL	NSH	VH
Cd1	50	75	63	80	64	–	–	175*
Cd2	54	70	41	76	–	37	85	194
Cd3	65	64	–	60	–	40	80	179
Cd4	65	–	–	54	–	35	80	165
Cd5	65	55	–	47	37	29	78	162

In anterior view, the base of the left caudal rib attaches to the centrum in its ventral part and the neural arch dorsally. The rib arises from the posterolateral part of the vertebra, just behind vertebral midlength. In anterior view, the base of the spine has a broad contact with the centrum: this basal region is laterally expanded ventrally, which is the area that supports the rib shaft, and tapers dorsally to a slender triangular process (which contacts the neural arch). The rib shaft arcs slightly dorsally from its base and then extends horizontally. The dorsal surface of the shaft is flat, but the ventral surface bears a prominent swelling, which gives the rib a sub-triangular longitudinal cross-section. The right caudal rib is broken.

The prezygapophyses are well-preserved, sub-triangular processes that have their articular facets facing medially and that are oriented almost vertically (Fig. 12). A narrow prespinal fossa is present at the base of the neural spine. The tips of the postzygapophyses and the posterior and dorsal margins of the neural spine have been sheared off, and the area has been crushed slightly. Little can be said about the morphology of the postzygapophyses other than they have a triangular transverse cross-section. The neural spine also has an elongate triangular cross-section. It is a transversely compressed, elongate, strap-like process that extends dorsally and slightly posteriorly in lateral view.

Cd2–5 – Cd2–Cd5 are generally well preserved and are almost complete (Fig. 13). Cd2 and Cd3 lack the right caudal rib, Cd2 lacks the right prezygapophysis, the anterior margins of the centra are damaged on the right sides of Cd3 and Cd4, and the postzygapophyses are sheared off in Cd5. The close apposition of the vertebrae and the presence of matrix on the neural arches obscures some features.

In Cd2, the anterior articular surface is taller than wide, has a sub-elliptical outline (with a straight dorsal margin) and is deeply amphicoelous, with the central concavity surrounded by a well-defined bony rim. Although they cannot be seen in anterior view the proportions of Cd3–Cd5 appear to be similar. A small, sub-triangular chevron facet is present at the base of the anterior surface in Cd2–5. In lateral view, the centra of Cd2 and Cd3 are taller than long, but in Cd4 and Cd5 the vertebrae are approximately as long as they are tall (Fig. 13). In Cd2–Cd5, the centra have straight anterior and posterior margins. In Cd2 and Cd3, the ventral margin is gently convex ventral margin, but this becomes more strongly convex in Cd4 and Cd5. In all of these caudals, the lateral surfaces of the centra are gently concave anteroposteriorly and flat to gently convex dorsoventrally. The posterior articular surface of Cd5 centrum is shallowly amphicoelous and is taller than wide with a sub-elliptical outline. Ventral to this, the posteroventral corners of the centra in Cd3–Cd5 bear a large, sub-crescentic chevron facet (this area is damaged in Cd2). The ventral surfaces of the vertebrae are poorly exposed, but they appear to lack keels or midline grooves. The neural canal, as seen in Cd2 and Cd5, was small and sub-circular in outline.

The base of the caudal rib on Cd2 is situated on the neurocentral boundary, but in Cd3–Cd5 it appears that

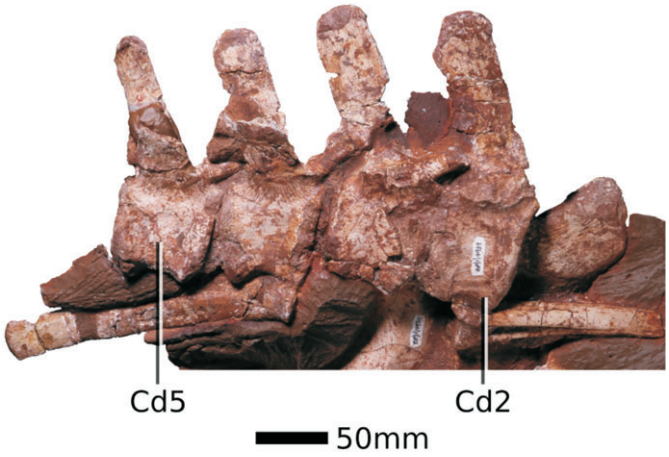


Figure 13. Anterior caudal vertebrae (Cd2–5?) of *Massospondylus carinatus* (BP/1/4934) in right lateral view. Scale bar = 50 mm.

the rib has migrated dorsally to lie fully on the arch. In anterior view, the left caudal ribs extend almost strictly horizontally, whereas the preserved right ribs form an angle of approximately 50° with the horizontal, though the latter probably represents deformation. The ribs have smoothly convex dorsal and ventral surfaces and a dorsoventrally compressed elliptical cross-section (thereby lacking the ventral swelling present on the rib of Cd1). Where preserved, the distal parts of the ribs are gently convex. The anterior and posterior margins of the ribs are subparallel and do not diverge markedly, giving them a sub-rectangular outline in dorsal view.

The prezygapophyses of Cd2–Cd5 have sub-triangular transverse cross-sections, extend for only a short distance beyond the anterior margin of the centrum and possess flat, sub-ovate articular facets that face dorsomedially at an angle of approximately 45° to the horizontal. In lateral view, the prezygapophyses of Cd2–Cd4 extend anterodorsally at an angle of approximately 45° to the horizontal; this angle is reduced to around 30° in Cd5. A small prespinal fossa is positioned at the confluence of the prezygapophyses in Cd2 (the presence/absence of this fossa cannot be established in Cd3–Cd5).

The postzygapophyses are situated at the base of the neural spine and form small, subtriangular processes that are separated by a deep cleft, which probably represents a postspinal fossa. The articular surfaces have an oval outline and are angled to face ventrolaterally at an angle of around 60° to the horizontal.

The neural arch occupies almost the entire length of the centrum (*contra* Knoll 2010). The neural spines of Cd2–Cd5 are elongate and strap-like, being much taller than they are long. They have subparallel, straight anterior and posterior margins and a gently convex dorsal margin in lateral view. All of the neural spines extend dorsally and slightly posteriorly. In Cd2, the dorsal margin of the spine is subtly thickened transversely relative to the rest of the spine, but in the remaining caudals the spine summit is mediolaterally compressed.

Chevrons – Three chevrons are visible on the displayed side of the specimen, two of which are in close association with the articulated series of four proximal caudal vertebrae and the third with the disarticulated caudal. That

associated with Cd4 is complete; that associated with Cd2 includes a complete proximal end but is missing the distal blade; and that associated with Cd1 lacks the proximal end and consists of a partial blade whose distal end is either missing or obscured by matrix.

In posterior view, the chevrons are broadest dorsally and taper ventrally. The haemal canal forms a deep, narrow 'V'-shaped slot in the proximal end and is bridged dorsally by a complete bar of bone. The canal is set within a slightly larger fossa that extends as a shallow groove for a short distance ventral to the base of the canal on the posterior surface of the blade. The dorsal bridge forms the articular surface: it is subdivided into large anterior and small posterior facets by a well-defined transverse ridge and each articular facet is gently convex. The lateral margins of the articular facet are formed by raised rims of bone.

In lateral view, the margins of the chevron blade are subparallel for their entire length. The lateral surfaces are gently convex anteroposteriorly. The complete chevron shows that the chevrons were straight in lateral view with no appreciable curvature and no distal expansion of any kind (either anteroposteriorly or mediolaterally). The distal margin of the blade is subtly convex.

Pectoral girdle

Clavicle

Both clavicles are present, but they are not in articulation. The left clavicle lies alongside, and is partially overlapped by, the left coracoid, whereas the right clavicle overlies the base of the right scapula (Figs 14–16; Supplementary Model 3). They are thin, elongate elements that taper both laterally and medially and are anteroposteriorly widest in the middle sections. At the midline, the clavicles terminate in a bluntly rounded, slightly expanded point. Laterally, the shaft curves slightly posteriorly. The anteroventral surface of the bone is mildly convex, whereas the opposite surface is flat to very gently concave, giving it a flattened 'D'-shaped cross-section. A clavicle has also been reported in a referred specimen of *M. carinatus*, BP/1/5241 (Yates & Vasconcelos 2005).

Scapulocoracoid

The left and right scapulocoracoids appear to be at least partially fused, with the exception of a short, open suture immediately dorsal to the glenoid fossa (Figs 14–16; Supplementary Model 3). There is no trace of a suture in the dorsal half of the pectoral girdle. Both of the scapulae are broken at midlength, but although the posterior parts of the scapula blades are slightly displaced, and a small section of the posterodorsal corner of the right scapula blade is missing, they are essentially complete. Although parts of both scapulocoracoids are obscured by other elements, plaster or matrix, the duplication of elements makes it possible to assess its entire morphology. For convenience, it is described with the long axis oriented horizontally. Measurements of the scapulocoracoids are provided in Table 5.

The coracoid is very similar to that of other massospondylids, including *Adeopapposaurus* (Martínez 2009), *Coloradisaurus* (Apaldetti *et al*. 2013) and *Lufengosaurus* (Young 1941). It has a sub-crescentic outline in lateral view, with a presumably straight, vertically oriented posterior margin fused to the scapula, dorsal and anterior margins that merge along a smooth continuous convex curve, and a more complex biconcave ventral margin (Figs 14–16). The lateral surface of the bone is flat in its central part, but is gently convex dorsally and ventrally, and more strongly convex in its anterior-most third. A small, circular coracoid foramen is positioned approximately one-third of the distance anteriorly from the junction with the scapula and at the midheight of the coracoid. The anteroventral corner of the coracoid forms a blunt, rounded sternal process, whose lateral surface bears a rugose, low boss (Figs 14, 16A). The sternal process forms the anterior margin of a short dorsally convex emargination on the anterior part of the lateral surface, whose dorsal margin is composed of a sloping crescentic surface that is separated from the rest of the lateral surface by a low, subtle ridge. Posterior to this emargination, the ventral margin of the coracoid extends posterodorsally at an angle of approximately 45° to the horizontal to form the coracoid contribution to the glenoid fossa. The coracoid contributes around 40–45% of the total anteroposterior length of the glenoid. In ventral view, the glenoid articular surface has a shield-shaped outline whose long axis trends posterodorsally/anteroventrally (Figs 15, 16B). The articular surface is gently concave and has raised, rugose margins that extend a short distance laterally to the adjacent surface of the

Table 5. Measurements of pectoral girdle elements in BP/1/4934. All measurements are in mm. Some measurements were not possible due to either extensive breakage or the presence of matrix/overlapping elements.

Element	Measurement	Value (mm)
l scapulocoracoid	Total length	459*
	Total length of glenoid fossa	98
r scapulocoracoid	Total length	467*
	Total length of glenoid fossa	101
l coracoid	Maximum length	107
	Maximum height	137
	Coracoid glenoid length	48
r coracoid	Maximum length	109
	Maximum height	
	Coracoid glenoid length	40
l scapula	Length	352
	Proximal plate maximum height	153
	Proximal plate maximum length	
	Distal expansion maximum height	149
	Minimum shaft height	59
	Scapula glenoid length	50
r scapula	Length	360*
	Minimum shaft height	52
	Scapula glenoid length	51
l sternum	Maximum length (anterposterior)	195
	Maxiumum width (mediolateral)	120* (estimate)
r sternum	Maximum length (anterposterior)	188*
	Maxiumum width (mediolateral)	120* (composite)



Figure 14. Anterior thoracic region of *Massospondylus carinatus* (BP/1/4934) in left lateral view, including the anterior dorsal vertebral column (D1, in part to D8, in part), dorsal ribs, pectoral girdles and complete left forelimb. **A**, photograph; **B**, interpretative line drawing. Scale bar = 50 mm. (Continued on p. 143.)

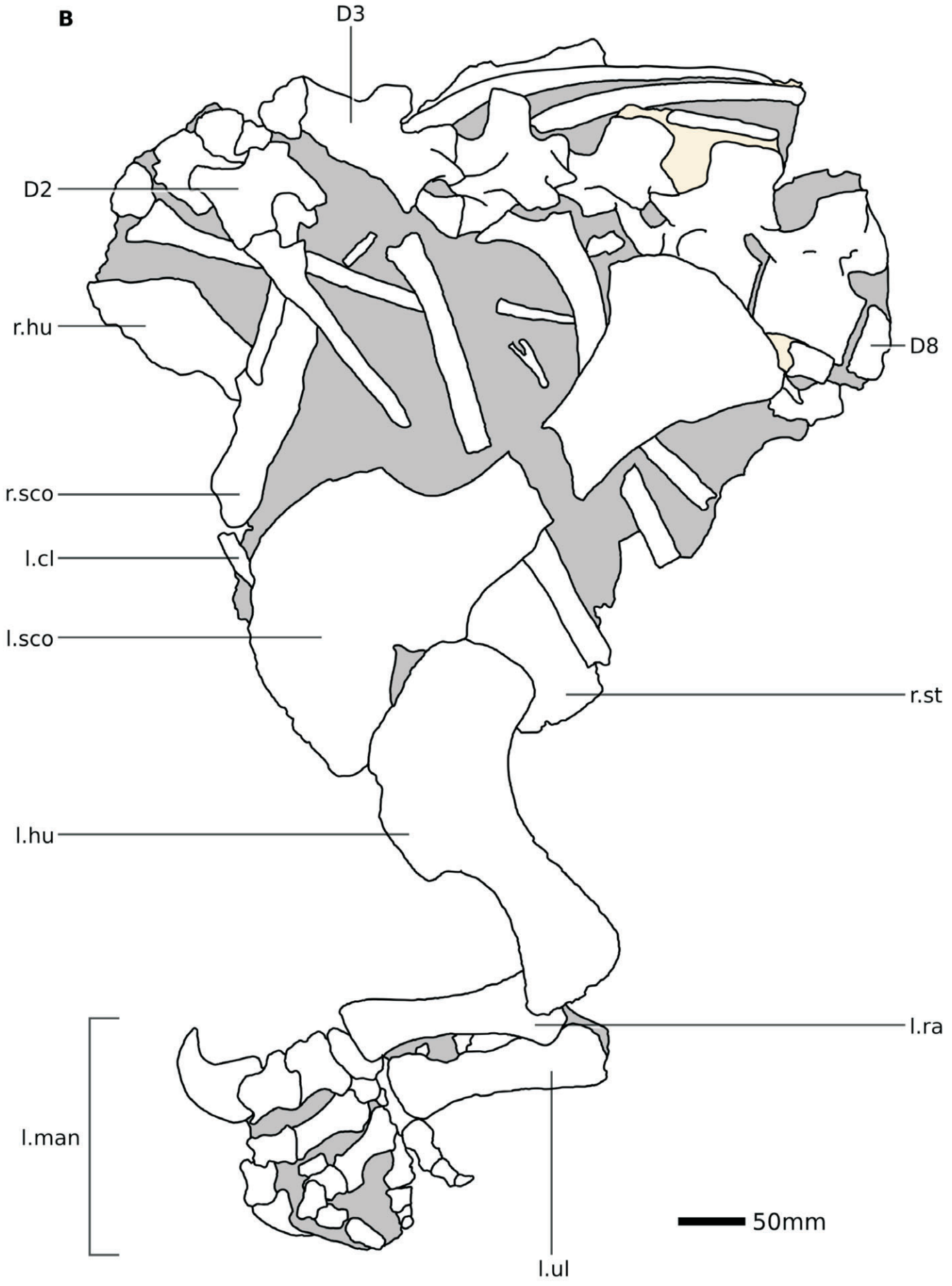


Figure 14 (continued).



Figure 15. Anterior thoracic region of *Massospondylus carinatus* (BP/1/4934) in right lateral view, including the anterior dorsal vertebral column (D1, in part to D8, in part), dorsal ribs, pectoral girdles, complete left forelimb and partial right humerus. **A**, photograph; **B**, interpretative line drawing. Scale bar = 50 mm. (Continued on p. 145.)

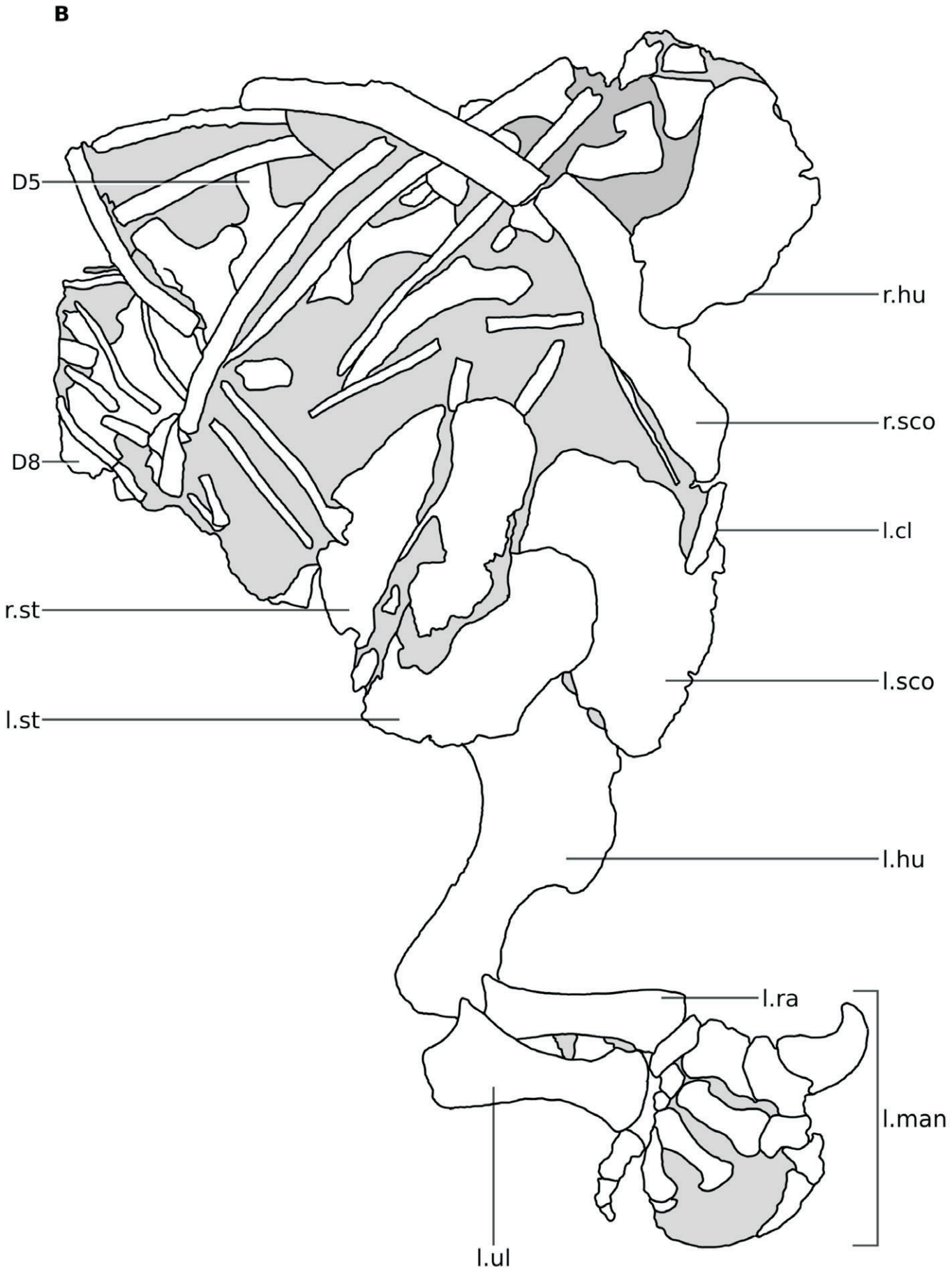


Figure 15 (continued).

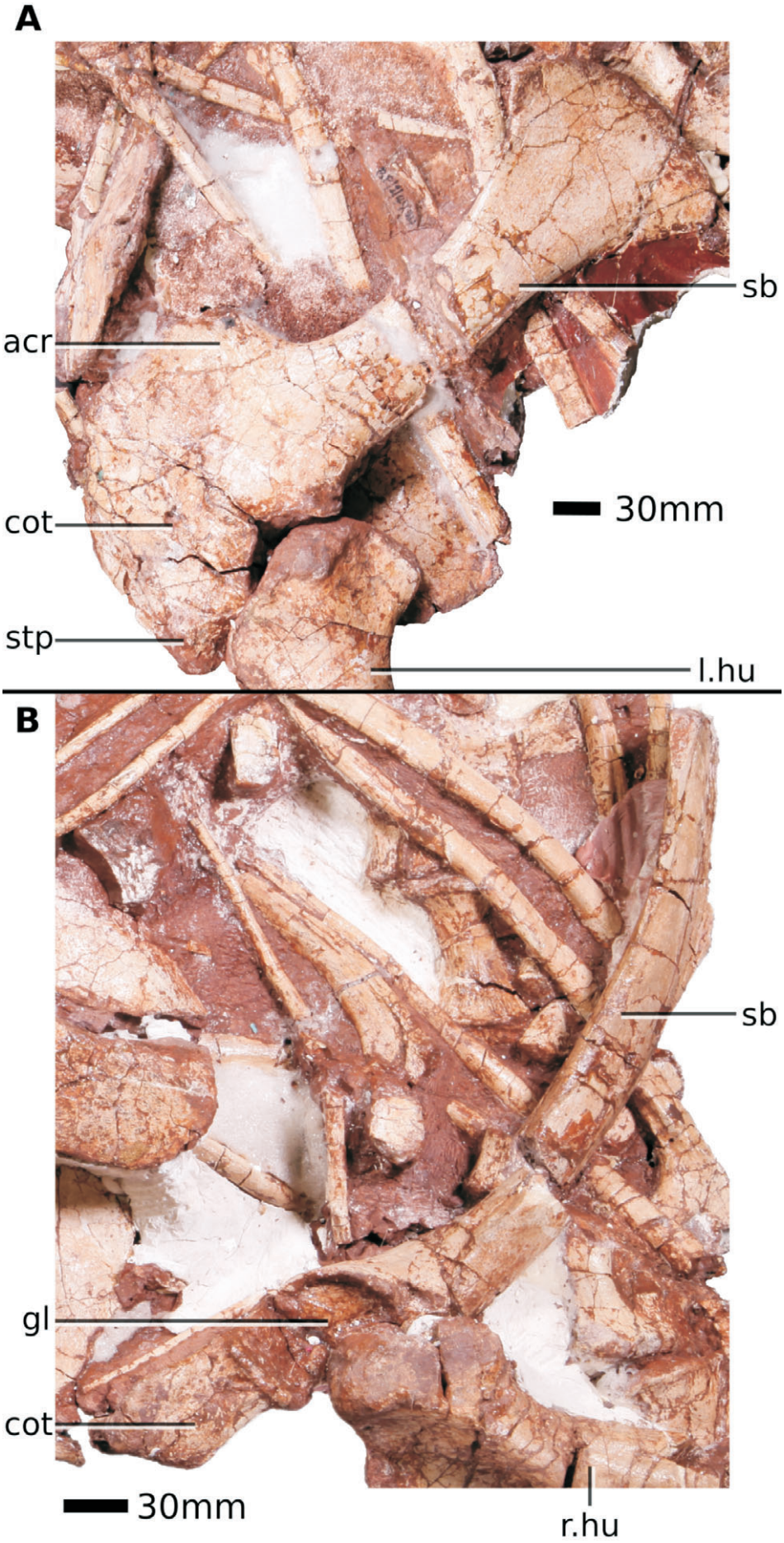


Figure 16. Scapulocoracoids of *Massospondylus carinatus* (BP/1/4934). **A**, left scapulocoracoid in left lateral view; **B**, right scapulocoracoid in ventral view. Scale bar = 30 mm.

coracoid. The posteroventral margin of the coracoid (part of the scapula articulation) is also swollen laterally, forming a low boss that continues on to the scapula. In ventral view, the coracoid is narrow anteriorly, but expands strongly mediolaterally to form a broad surface for the ventral emargination and glenoid. Dorsally, the coracoid decreases in mediolateral width, so that is posterodorsal corner is the thinnest part of the element. Medially, the coracoid surface is dorsoventrally and anteroposteriorly concave (Fig. 15).

The scapula consists of a dorsoventrally expanded proximal plate and a horizontally inclined blade (Figs 14–16). The lateral surface of the proximal plate is dorsoventrally convex in its ventral part: dorsally the proximal plate is much flatter. Its lateral surface is defined posteriorly by a low, rounded and vertically inclined acromial ridge that merges with the base of the scapular blade ventrally and posteriorly (Fig. 16A). The anterior margin of the scapula was presumably straight. The anteroventral margin of the proximal plate forms the scapular contribution to the glenoid fossa and accounts for 55–60% of its total length. In ventral view, the glenoid fossa forms an elongate, 'D'-shaped facet, which is concave and surrounded by a thick, swollen rim (Fig. 16B). The posterodorsal margin of the proximal plate is straight and curves posteriorly in its ventral part to form the dorsal margin of the blade. In *M. carinatus* the scapular length/minimum scapular blade height ratio is ~6.0, which is similar to that of *Coloradisaurus* (~5.9: Apadetti *et al*. 2013), *Lufengosaurus* and *Sarahsaurus* (~6.3 in both cases: Young 1941; Rowe *et al*. 2011), but the scapula of *Adeopapposaurus* is more gracile, with a ratio of ~7.8 (Martínez 2009).

The base of the scapular blade arises from the ventral two-thirds of the proximal plate's posterior margin (Figs 14, 16A). The anterior part of the blade's lateral surface is dorsoventrally convex, but it becomes flat distally. Anteriorly, the blade is dorsoventrally narrow and parallel-sided, but distally it expands both dorsally and ventrally to form a fan-like distal expansion. The proximal and distal expansions are of subequal height. Although expanded both dorsally and ventrally, the distal end is asymmetrical around the blade long axis as the greatest dorsal expansion occurs at a point just anterior to the distal end of the scapula blade, whereas the greatest ventral expansion occurs more posteriorly, the latter forming the posteroventral corner of the blade. As a result, the dorsal margin of the blade bears a low, broad-based subtriangular swelling with a pointed apex, situated anterior to the distal margin, whereas the posteroventral corner of the blade is formed of a narrower-based triangular flange, with a more rounded margin (Figs 14, 16A). The posterior margin of the blade is rugose and forms a gently convex curve linking the dorsal and ventral expansions: the ventral part of this margin is almost dorsoventrally inclined, whereas the dorsal part is more strongly curved anterodorsally, reflecting the asymmetry of the dorsal and ventral margins. By contrast, the distal margin of the scapula is straight to slightly concave in *Coloradisaurus* (Apaldetti *et al*. 2013). Although similar (or more prominent) ventral expansions of the distal scapular blade are present in *Adeopapposaurus*, *Coloradisaurus*, *Ignavusaurus* and *Seitaad* (Martínez 2009; Knoll 2010; Sertich & Loewen 2010; Apadetti *et al*. 2013), the dorsal expansion is absent in these taxa. By contrast, *Lufengosaurus* and *Sarahsaurus* possess the dorsal and ventral expansions of the distal blade, but they differ subtly from the condition in *M. carinatus*, as in both of the former taxa the dorsal expansion is much more prominent that the ventral expansion (Young 1941; Rowe *et al*. 2011), resulting in the distal scapula blade being more strongly asymmetrical in lateral view. As a result, we regard the morphology of the distal scapula in *M. carinatus*, with its small dorsal and large ventral expansions, as a possible autapomorphy, at least with respect to the condition present in other massospondylids.

In *M. carinatus*, the ventral part of the posterior proximal plate bears a broad, rounded ridge in medial view that extends posteriorly along the ventromedial surface of the scapula blade, fading out at a point approximately two-thirds of the distance to the distal end. By contrast, the surface of the blade dorsal to this ridge is shallowly concave, so that the proximal part of the blade has a comma-shaped transverse cross-section, with a thick ventral margin and thin dorsal margin. The distal one-third of the blade is flat and mediolaterally compressed, with an elongate, lenticular cross-section. In dorsal view, the scapulocoracoid bows strongly laterally, reflecting the shape of the rib cage (Figs 15, 16B).

Sternum

Both sterna are almost complete, but the right sternum has been broken in half longitudinally and the two halves have become separated (Figs 15, 17). They are both exposed in anterior (external) view, although the left sternum is partially overlapped by the right. The posterior (internal) surface of the right sternum is obscured, but a small part of the left sternum's ventral surface is visible. They are described as if found in life position, with their long axes canted anterodorsally/posteroventally. In general, they are very similar in overall morphology to the sterna described in *Adeopapposaurus*, *Lufengosaurus*, *Sarahsaurus* and *Seitaad* (Young 1941; Martínez 2009; Sertich & Loewen 2010; Rowe *et al*. 2011). See Table 5 for measurements.

In anterior view, the sternum has a sub-ovate outline that is slightly broader along its ventral margin than dorsally (Figs 15, 17). The ventral margin is concave and is separated from the lateral margin by sharp change in slope, forming a low, pointed triangular flange (seen on the left sternum only, as this region obscured on the right). The lateral margin is concave ventrally, due to the presence of this flange, continues straighter dorsally, but curves medially at an angle of around 120° to form the dorsal margin. The dorsal margin is strongly rounded, but the medial margin is straighter, where it abuts its antimere. As the ventral margins are damaged in both sterna, there are no clear facets for the sternal ribs, although it is possible that the lateral flange might represent an articular surface for one or two ribs. No sternal ribs are preserved.

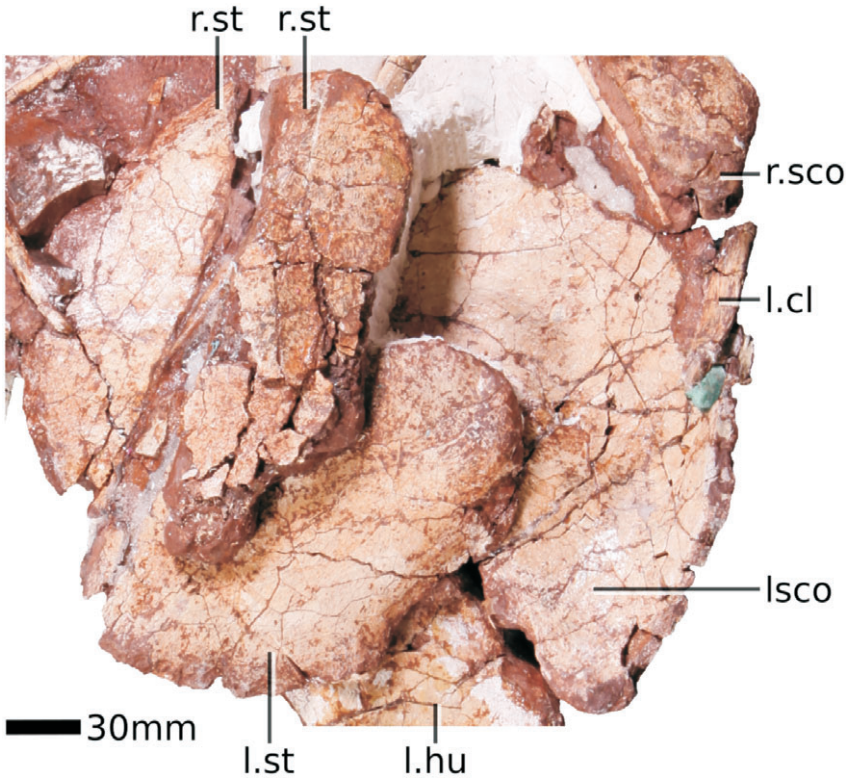


Figure 17. Sternal plates of *Massospondylus carinatus* (BP/1/4934) in anterior (external) views. Scale bar = 30 mm.

The anterior surface of the sternum is gently convex mediolaterally and almost flat dorsoventrally, so is only weakly curved. A low, rounded buttress arises at the laterodorsal corner of the anterior surface and extends for a short distance ventrally before merging with it. This buttress is present on both sterna, so appears to be a genuine feature. The exposed posterior surface indicates that it was shallowly concave, both mediolaterally and dorsoventrally. With the exception of the abovementioned anterodorsal buttress, the sternum maintains an almost constant cross-sectional thickness along its entire length.

Forelimb

Humerus

Both humeri are nearly complete, although large cracks are pervasive and small portions are broken from the medial and lateral surfaces of the left deltopectoral crest and parts of the right humeral shaft are missing (Figs 14, 15, 18; Supplementary Model 5; see Table 6 for measurements). Prior to recent preparation, the right humerus was closely adhered to the thoracic region, but its distal part has now been removed. The fully prepared left humerus was originally preserved in articulation with the glenoid facet of the left scapulocoracoid and the proximal part of the right humerus is similarly articulated with the right pectoral girdle. The left humerus has been mildly distorted, so that it is slightly mediolaterally compressed. The humerus is described as if held vertically, and in this orientation the long axis of the proximal expansion is twisted to lie at an angle of approximately 45° to the long axis of the distal expansion.

Viewed anteriorly, the humerus has a large proximal expansion, which bears the internal tuberosity medially, the humeral head dorsally and the deltopectoral crest laterally (Fig. 18A). The humeral head is positioned dorsal to the internal tuberosity, whose ventral margin in turn lies in the same plane as the dorsal margin of the deltopectoral crest. The internal tuberosity is large and triangular in anterior view, with the apex of the triangle projecting medially and slightly posteriorly, as in *Adeopapposaurus* (Martínez 2009), *Coloradisaurus* (Apaldetti *et al*. 2013), *Lufengosaurus* (Young 1941) and *Seitaad* (Sertich & Loewen 2010). Its dorsal margin is oriented medioventrally, forming an angle of approximately 45° with respect to the humeral head. The anterior surface immediately lateral to the internal tuberosity is mediolaterally convex and is separated from the rest of the anterior humeral surface by a vertically extending intramuscular line, which extends ventrally from the proximal margin of the humerus, at a point halfway between the apex of the internal tuberosity and the humeral head, to merge with the medial margin of the shaft. The posterior surface of the internal tuberosity is flat and separated from the rest of the posterior humeral surface by a vertically extending trough that arises from the medial margin of the humeral head and has a sub-elliptical outline that tapers medially (Fig. 18B). Its proximal surface is gently convex mediolaterally and anteroposteriorly.

In anterior view, the humeral head is strongly convex and overhangs the surface of the proximal humerus slightly, from which it is separated by a low, rugose ridge. In proximal view it is a bulbous, rounded structure that extends much farther posteriorly than anteriorly, so that it overhangs the posterior humeral surface markedly (Fig. 18C). The head has an elliptical outline in proximal view, whose long axis is oriented mediolaterally, and the

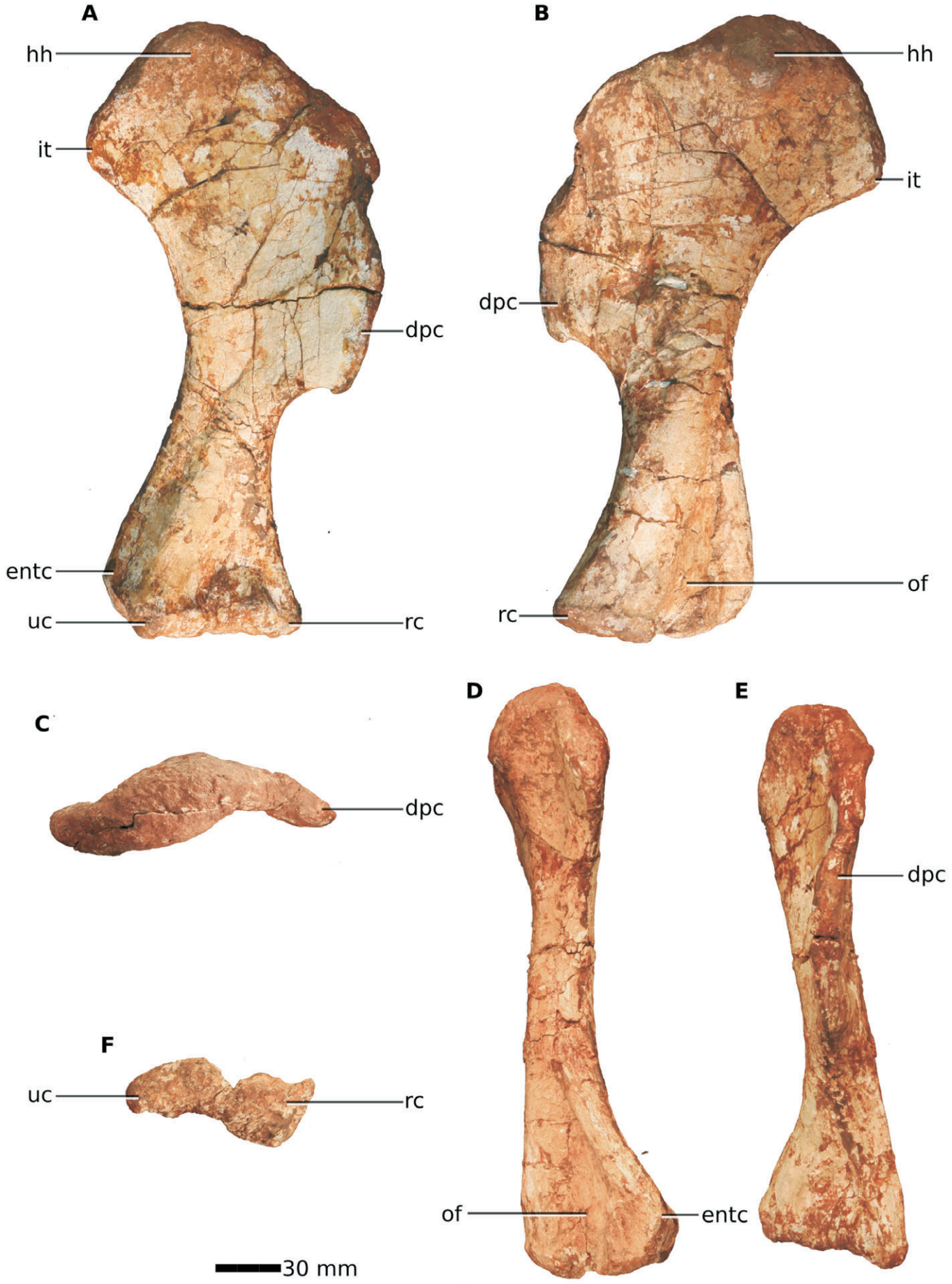


Figure 18. Left humerus of *Massospondylus carinatus* (BP/1/4934) in anterior (**A**), posterior (**B**), proximal (**C**), lateral (**D**), medial (**E**) and distal (**F**) views. Scale bar = 30 mm.

Table 6. Measurements of forelimb elements in BP/1/4934. All measurements are in mm. Those marked with an asterisk are minima due to breakage.

Element	Measurement	Value (mm)
l humerus	Total length	270
	Distance from proximal end to base of dpc	170
	Proximal end, maximum width (including dpc)	152
	Shaft, minimum width	36
	Shaft, circumference	135
	Distal end, maximum width (mediolateral)	87
	Distal end, maximum length (anteroposterior)	36
r humerus	Distal end, maximum width (mediolateral)	35*
	Distal end, maximum length (anteroposterior)	79
l ulna	Total length	164
	Proximal end, maximum length (dorsoventral)	84
	Proximal end, maximum length (mediolateral)	30
	Shaft, minimum width (dorsoventral)	32
	Distal end, maximum length (dorsoventral)	56
	Distal end, maximum length (mediolateral)	18
r ulna	Total length	66
	Proximal end, maximum length (dorsoventral)	84
	Proximal end, maximum length (mediolateral)	36
	Shaft, minimum width (dorsoventral)	32
	Distal end, maximum length (dorsoventral)	58
	Distal end, maximum length (mediolateral)	18
l radius	Total length	144
	Proximal end, maximum length (dorsoventral)	57
	Proximal end, maximum length (mediolateral)	20
	Shaft, minimum width (dorsoventral)	30
	Distal end, maximum length (dorsoventral)	47
	Distal end, maximum length (mediolateral)	22
r radius	Total length	153
	Proximal end, maximum length (dorsoventral)	51
	Proximal end, maximum length (mediolateral)	24
	Shaft, minimum width (dorsoventral)	33
	Distal end, maximum length (dorsoventral)	40*
	Distal end, maximum length (mediolateral)	22

articular surface is strongly convex mediolaterally but weakly convex anteroposteriorly. Posteriorly, the head extends on to the posterior humeral surface and is delimited from it by a distinct ridge of bone, similar to the condition in *Adeopapposaurus* (Martínez 2009), *Lufengosaurus* (Young 1941) and *Sarahsaurus* (Rowe *et al*. 2011), but unlike *Coloradisaurus* in which the humeral head is less prominent (Apaldetti *et al*. 2013). In *M. carinatus*, the ventral margin of the head is confluent with a low, broad intramuscular line, which merges into the posterior humeral surface after a short distance. Most of the humeral surface ventral to this point is strongly convex mediolaterally, with this convexity bounded by a medial trough and a prominent intramuscular line laterally (see below).

The deltopectoral crest is elongate and extends ventrally to a point approximately 60% of the distance from the dorsal margin of the humeral head (Fig. 18A,B), thus differing from the conditions in *Adeopapposaurus*, *Coloradisaurus*, *Lufengosaurus*, *Sarahsaurus* and *Seitaad*, in which the crest descends for approximately c.45–50% of humeral length (Young 1941; Martínez 2009; Sertich & Loewen 2010; Rowe *et al*. 2011; Apaldetti *et al*. 2013), and this feature is regarded as a potential autapomorphy of *M. carinatus*. As it descends ventrally, the dorsal margin of the deltopectoral crest forms an angle of 45° with the humeral head, before turning though approximately 120° to form its lateral margin (Fig. 18A). The dorsal margin of the crest bears a very small dorsal protuberance at a point around halfway along its length, which is more clearly visible in posterior view. The lateral margin of the crest is 'stepped' in both anterior and lateral views (Fig. 18A,D), due to an abrupt break-in-slope that occurs approximately one-third of the distance from its dorsal margin, as also occurs in *Adepapposaurus* (Martínez 2009) and *Lufengosaurus* (Young 1941). In *M. carinatus*, the anterior surface of the humerus between the crest and the intramuscular line defining the internal tuberosity is strongly concave mediolaterally and weakly concave dorsoventrally. The anterior surface of the lateral portion of the crest is dorsoventrally convex, separating it from the main anterior concavity of the proximal end. The anteroventral apex of the deltopectoral crest forms a subtle, hook-like process in anterior view and the ventral margin of the crest forms a convex arc that merges with the lateral margin of the humeral shaft (Fig. 18A). In posterior view, the deltopectoral crest is traversed by two prominent intramuscular lines (Fig. 18B). The medial-most of these arises from the 'step' in the lateral margin and extends ventrally for most of the length of the crest, merging into the surface just above the ventral margin of the crest. The more laterally positioned line is positioned approximately halfway between the medial ridge and the lateral margin of the deltopectoral crest and extends vertically from the ventral margin of the crest, merging into the surface at a level approximately 50% of the height of the crest at this point. The lateral margin of the deltopectoral crest is thickened, which is more evident in posterior view as this swelling forms a distinct ridge. The proximal surface of the crest has a narrow surface that is broadest where it meets the humeral head, but which tapers laterally. Taken together in dorsal view, the proximal surface of the humerus describes a sinusoidal curve (Fig. 18C).

The humeral shaft separates the proximal and distal expansions. It is relatively short, stout and has an ovate transverse cross-section that is broadest posteromedially and narrowest anteromedially just ventral to the deltopectoral crest.

In anterior view, the distal end of the humerus is mediolaterally expanded and is approximately twice the transverse width of the shaft (Fig. 18A). This expansion is gradual and begins only a short distance ventrally from the distal end of the deltopectoral crest. The anterior (flexor) surface bears a proportionally large, deep cuboid fossa. This fossa is triangular in shape with the apex of the triangle pointing proximally and is deepest ventrally. The lateral and medial margins of the cuboid fossa are bordered along their entire lengths by narrow, low ridges of bone that extend ventrally to merge with the distal condyles. The ridge connecting to the medial (ulnar) condyle is broad and rounded, while the lateral ridge is narrower and continuous with the ectepicondyle (see below). A second, elongate triangular fossa, the olecranon fossa, is present on the posterior surface of the distal end

(Fig. 18B). It extends further dorsally than the cuboid fossa but is shallower than the latter and its lateral and medial margins are defined by lower, rounder ridges. The narrower of these ridges merges with the entepicondyle of the ulnar condyle, whereas the broad ridge is continuous with the radial condyle.

The medial (ulnar) and lateral (radial) distal condyles are anteroposteriorly and mediolaterally expanded and are separated anteriorly by a broad 'U'-shaped notch that is continuous with the floor of the cuboid fossa. Posteriorly, they are separated along the posterior margin by a broad, 'V'-shaped notch that is continuous with the floor of the olecranon fossa. The radial condyle bears a small, anterolaterally projecting, triangular ectepicondyle, which is separated from the rest of the condyle by a shallow groove along the anterior surface. The lateral surface of the ectepicondyle bears a proximodistally elongated, shallow fossa that extends for a short distance dorsally. The ulnar condyle bears a larger entepicondyle, which forms a posteromedially projecting protuberance. In distal view, the humerus has a dumbbell-shaped outline (Fig. 18F). The ulnar condyle has a larger surface area than the radial condyle as it projects further anteriorly and has a broad, ovate outline, whereas the radial condyle has a narrower, sub-triangular outline. The articular surface of the ulnar condyle is mediolaterally and anteroposteriorly convex, but that of the radial condyle is slightly concave to flat in both directions.

Radius

The left and right radii are well preserved and complete, but both have been slightly flattened mediolaterally (Figs 14, 15, 19; Supplementary Model 5). The left radius is still articulated within the radial fossa of the ulna, but been displaced slightly displaced distally within that fossa, whereas the right ulna is connected with the distal part of



Figure 19. Left radius and ulna of *Massospondylus carinatus* (BP/1/4934) in lateral (**A**), medial (**B**), proximal (**C**) and distal (**D**) views. Scale bar = 30 mm.

the right humerus. The radius is described with its long axis extending horizontally, in approximate life position. The radius length/humerus length ratio in *M. carinatus* is 0.55, which is proportionally shorter than that of *Adeopapposaurus* (radius length/humerus length ratio of 0.62: Martínez 2009; see Table 6 for measurements).

In lateral view, the proximal end of the radius is dorsoventrally expanded with respect to the shaft; the distal end is also expanded, but to a lesser degree (Fig. 19A). The proximal surface is dorsoventrally concave, forming the humeral cotyle. This is similar to the condition present in *Ignavusaurus* (Knoll 2010) but contrasts with that in *Adeopapposaurus*, where this surface is flatter (Martínez 2009). The lateral and medial margins of this surface are formed by low lips of bone. The cotyle is elliptical in outline with its long axis trending dorsoventrally (Fig. 19B). Ventral to the cotyle is a well-developed process, which is also visible in lateral view, forming a sub-rectangular, posteroventrally projecting tab. The medial surface of this process is convex and articulates within the radial fossa of the ulna. The dorsal margin of the proximal end forms a similar dorsally projecting process, but this is not as well-developed as that projecting ventrally.

Anterior to the humeral cotyle, the radius tapers slightly in lateral view as it extends anteriorly, reaching its minimum height in the midshaft region (Fig. 19A,C). Distal to this point, the radius expands once more ventrally to form the distal expansion. The dorsal and ventral margins of the shaft are both shallowly concave. At midlength, the shaft has a mediolaterally compressed, elliptical cross-section, with its long axis oriented dorsoventrally. The lateral and medial surfaces of the shaft merge smoothly with each other and are not separated by any clear breaks in slope or intramuscular lines.

The distal surface is flat and has a sub-elliptical to 'D'-shaped outline in distal view, with its flatter surface facing laterally and its long axis extending anteroposteriorly (Fig. 19D). This contrasts with the circular outline in *Adeopapposaurus* (Martínez 2009) and the subquadrate outline of *Lufengosaurus* (Young 1941). The plane of the distal surface is not orthogonal to the long axis of the bone, but is orientated at approximately 80°, and the medial margin of the articular surface is defined by a distinct lip of bone. The ventral corner of the medial surface, adjacent to the distal margin of the radius, bears a shallow fossa that articulates with the laterodorsal corner of the distal ulna.

Ulna

Both ulnae are preserved and complete, but each has been slightly flattened. The right ulna is fully prepared, but the left ulna is in articulation with the radius (Figs 14, 15, 19; Supplementary Model 5). The lateral crest (= anterolateral process) of the left ulna is broken at its base. As with the radius, the ulna is described with its long axis extending horizontally, in approximate life position. The ulna length/humerus length ratio of *M. carinatus* (0.60) is lower than those of both *Adeopapposaurus* (0.72: Martínez 2009) and *Lufengosaurus* (0.63–0.68: Young 1941), and this proportionally short ulna of *M. carinatus* is tentatively regarded as an autapomorphy. Measurements are provided in Table 6

In lateral view, the proximal end is markedly expanded dorsoventrally with respect to the shaft (Fig. 19A). This expansion is asymmetrical and particularly pronounced dorsally, to produce the medial crest (= anterior process). The medial crest has a narrow, triangular outline in lateral view and its anterior margin forms an angle of around 45° with respect to the shaft. The posterior margin of the medial crest is dorsoventrally concave and forms the humeral cotyle. Ventral to this sulcus, the posteroventral portion of the proximal margin expands posteriorly to form a low, pyramidal olecranon process. The posterior margin of the process terminates in a bluntly rounded apex and has a rugose texture. A stout ridge, the lateral crest (= anterolateral process) arises from the proximal margin of the ulna, at a point immediately lateral to the olecranon process and extends anteriorly along the lateral surface, merging into it at around midlength, although its distal portion is a very subtle feature. This crest subdivides the lateral surface of the proximal end into two shallow, longitudinal sulci. The dorsal sulcus represents the articular surface for the radius (the radial fossa whereas the ventral sulcus bears a large number of short striations signifying muscle attachment sites. In proximal view, the ulna has an elongated, triangular outline with the apex of the triangle formed by the lateral crest (Fig. 19B). The medial margin of the proximal end is gently concave. The dorso- and ventrolateral margins are more strongly concave. The humeral cotyle is strongly concave dorsoventrally, mildly concave mediolaterally and has a sub-rectangular outline. The medial surface of the proximal end is strongly concave dorsoventrally, with this concavity merging into the dorsal part of the shaft.

In lateral view, the shaft has a weakly concave ventral margin and more strongly concave dorsal margin, so is constricted in its central portion (Figs 19A,C). In dorsal view, the shaft is bowed slightly laterally. At midlength the shaft is dorsoventrally convex laterally, but flatter medially, producing a 'D'-shaped transverse cross-section. The distal end of the ulna is also expanded dorsoventrally, but to a lesser extent than the proximal end. As with the proximal end, the dorsal part of the expansion is more strongly developed than the ventral part. The dorsal margin of the distal end is offset from that of the shaft by a distinct break-in-slope, whereas its ventral margin forms continuous curve with that of the shaft. The distal condyle is bound by a low lip of bone that is more pronounced laterally than medially. The distal articular surface is mediolaterally compressed, has an elongate elliptical outline with its long axis trending dorsoventrally, and its articular surface is convex, evenly rounded and slightly rugose (Fig. 19D). In lateral view, it has a convex margin. A small rugosity, probably representing a muscle attachment site, is present on the medial surface, just ventral to the anterodorsal corner of distal end. The medial and lateral surfaces of the distal end are shallowly concave dorsoventrally.

Manus

For the manus and carpus, we use the following anatomical terminology. The flexor surface of the hand is referred to as the 'palmar' surface. This is variably called the ventral surface (in quadrupedal sauropodomorphs) and would have been medially facing if the hands were held supinated in assumed life position. The extensor surface of the hand is referred to as the 'dorsal' surface, which would have faced laterally in life position. The side of the hand bearing digit I is referred to as 'radial'. This surface is often called the 'medial' surface because of the directional terms used in developmental biology, but it would have faced dorsally in life position. The side towards the digit V is referred to as the 'ulnar' surface and would be been oriented ventrally. Measurements are provided in Table 7.

The left and the right hands are both nearly complete, articulated and well preserved (Fig. 20; Supplementary Model 5). The left hand is missing phalanx IV-3 and a small portion of the proximal end of metacarpal IV. The right hand is still partially covered by matrix, the distal end of the first ungual phalanx is reconstructed with plaster, and it is missing phalanx V-2. As in most basal dinosaurs, digits IV and V are reduced in length and bear weak unguals. The phalangeal formula is 2-3-4-3-2, as in *Adeopapposaurus* (Martínez 2009), but in contrast to that of *Sarahsaurus* (2-3-4-2-2: Rowe *et al*. 2011).

Carpus – The proximal carpals are not preserved, but the left distal carpals 1–3 are preserved in life position and are nearly complete (Fig. 20). The distal carpals of the right hand are not preserved. By contrast, four distal carpals are present in *Adeopapposaurus* (Martínez 2009) and *Lufengosaurus* (Young 1941), but it is unclear if this difference is genuine or whether a small fourth distal carpal might have originally been present in *M. carinatus* and lost during preservation.

Distal carpal 1 is the largest and is transversely wide and proximodistally flattened. Its distal surface articulates with metacarpal (Mc) I in a complex fashion: the dorsal half of the distal surface is in complete articulation with the proximal surface of Mc I, but only the radial side of the palmar half of the distal surface articulates with that metacarpal (Fig. 20). The remaining portion of the palmar half of the distal surface forms a tight articulation with the proximal surface of distal carpal 2. The proximal surface of distal carpal 1 is sub-trapezoidal in proximal view, with a transversely narrower dorsal margin and wider palmar margin. The proximal surface is slightly convex, and this convexity is more pronounced on the radiopalmar corner. Although the entire distal surface cannot be seen, it appears to be shallowly concave, cupping the proximal surface of Mc I. Its radial margin, however, bears a well-developed lip of bone that has a 'C'-shaped outline in radial view, opening distally. The flat palmar surface is sub-ellipsoid in outline with the major axis oriented transversely. This surface bears a small, distinct, sub-circular fossa on its ulnar half. A step-like groove marks the boundary between the palmar surface and the radial surface. This groove excavates the proximoradial margin of the bone and continues distally to underlie the 'C'-shaped feature of the medial margin. The ulnar surface is

Table 7. Measurements of left manus elements in BP/1/4934. All measurements are in mm. Those marked with an asterisk are minima due to breakage. Phalanx IV.3 is missing from the left manus.

Element	Measurement	Value (mm)
Carpal 1	Maximum height (dorsoventral)	50
	Maximum width (dorsopalmar)	29
Carpal 2	Maximum height (dorsoventral)	30
	Maximum width (dorsopalmar)	24
Carpal 3	Maximum height (dorsoventral)	12
	Maximum width (dorsopalmar)	14
Mc I	Maximum length	49
	Proximal end, maximum height	49
	Distal end, maximum height	43
Mc II	Maximum length	70
	Proximal end, maximum height	32*
	Distal end, maximum height	34
Mc III	Maximum length	65
	Proximal end, maximum height	32
	Distal end, maximum height	29
Mc IV	Maximum length	47
	Distal end, maximum height	23
Mc V	Maximum length	38
	Proximal end, maximum height	23
	Distal end, maximum height	17
Ph I.1	Maximum length	46
	Proximal end, maximum height	45
	Distal end, maximum height	31
Ph I.2 (ungual)	Maximum length (curved dorsal margin)	108
	Proximal end, height	52
	Proximal end, width	27
Ph II.1	Maximum length	37
	Proximal end, maximum height	28
	Distal end, maximum height	21
Ph II.2	Maximum length	33
	Proximal end, maximum height	24
	Distal end, maximum height	22
Ph II.3 (ungual)	Maximum length (curved dorsal margin)	68
	Proximal end, height	31
	Proximal end, width	21
Ph III.1	Maximum length	22
	Proximal end, maximum height	25
	Distal end, maximum height	23
Ph III.2	Maximum length	26
	Proximal end, maximum height	19*
	Distal end, maximum height	18
Ph III.3	Maximum length	22
	Proximal end, maximum height	18
	Distal end, maximum height	15
Ph III.4 (ungual)	Maximum length (curved dorsal margin)	34*
	Proximal end, height	16*
	Proximal end, width	16
Ph IV.1	Maximum length	16
	Proximal end, maximum height	19
	Distal end, maximum height	15
Ph IV.2	Maximum length	15
	Proximal end, maximum height	10
	Distal end, maximum height	8*
Ph V.1	Maximum length	20
	Proximal end, maximum height	16
	Distal end, maximum height	13
Ph V.2	Maximum length	11
	Proximal end, maximum height	9
	Distal end, maximum height	7

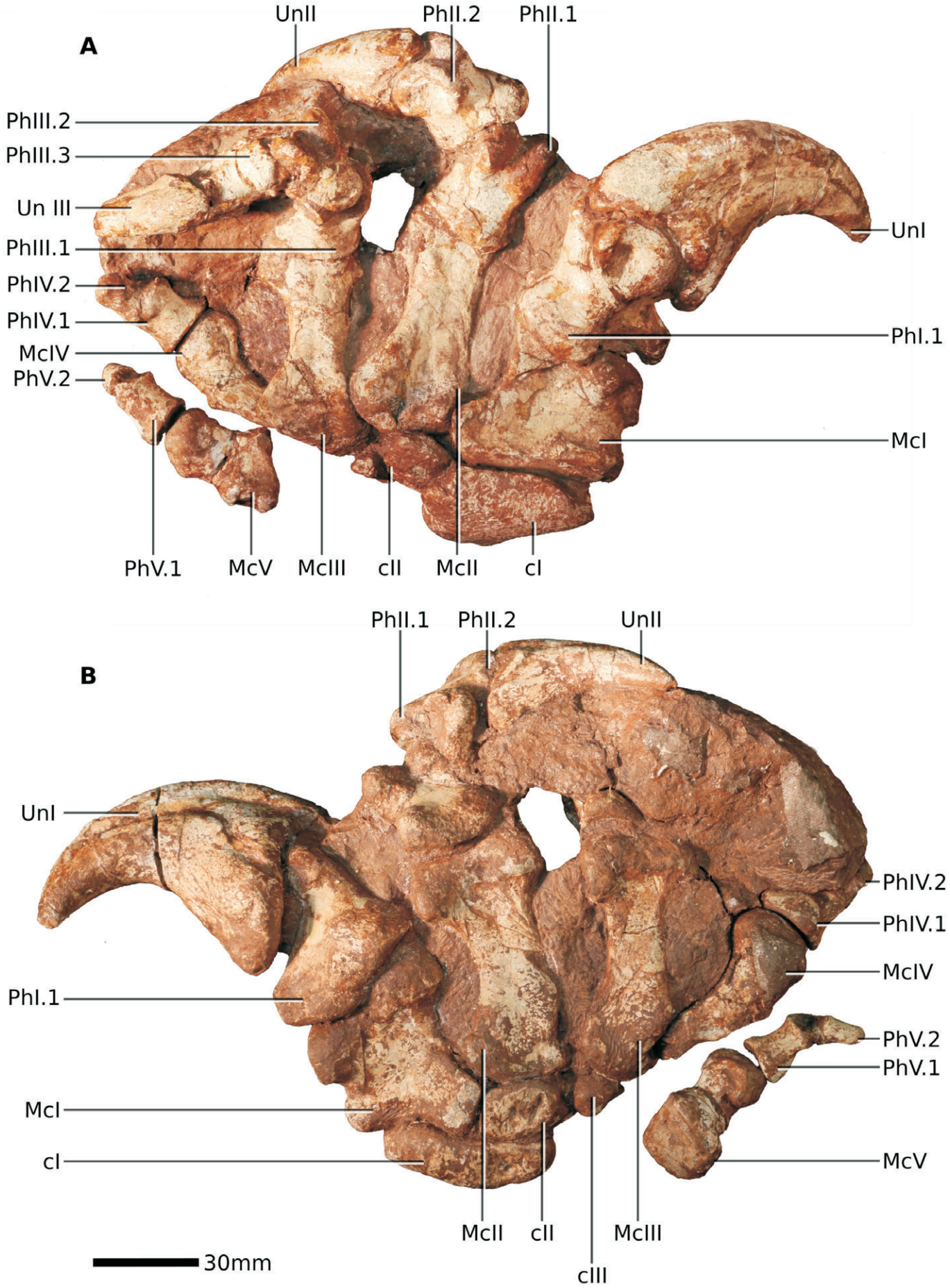


Figure 20. Left manus of *Massospondylus carinatus* (BP/1/4934) in dorsal (**A**) and palmar (**B**) views. Note that anterior is towards the top of the image. Scale bar = 30 mm.

developed as a vertically oriented ridge, formed by the confluence of the tapering ulnar sides of the proximal and distal surfaces.

Distal carpal 2 is considerably smaller than distal carpal 1, with a proximal surface that is less than half of the transverse width of the latter (Fig. 20). Its distal surface articulates exclusively with the proximal surface of Mc II. Its radial surface forms a flat contact with an ulnarly directed flange extending from the base of Mc I. Its proximal surface bears an extensive, flat articulation with the ulnar side of the distal surface of distal carpal I. Only the ulnar half of the proximal surface is visible. This portion is sub-rectangular in outline and very slightly convex. The dorsal surface is a thin, transversely oriented bar of bone with no distinguishing features. The palmar surface, however, is transversely wide, proximodistally extensive, and flat with rounded margins. The palmar surface bears two distinct portions. The radial two-thirds is sub-rectangular, and its palmar surface is at the same level as that of distal carpal 1 and the ulnar flange of Mc I. This surface bears two proximodistally oriented grooves. These grooves are located in close proximity to the fossa on the palmar surface of distal carpal I and may be functionally related. The ulnar one-third of the palmar surface is excavated to form a cup-like feature within which distal carpal 3 articulates.

The third distal carpal is the smallest. Its dorsal margin is eroded and it may have been larger in life. Its articular relationships are difficult to assess, but its distal surface makes a small contact with Mc III, and its radial surface fits within a shallow corresponding depression on the ulnar side of distal carpal II (Fig. 20). It is possible that the broken dorsal margin formed a small articular surface with the lateral-most side of the proximal surface of Mc II. The proximal surface of distal carpal III is sub-triangular in outline and shallowly concave. A low lip bounds the margin between its proximal and palmar surfaces. The palmar surface itself is rounded and strongly convex.

Metacarpus – Metacarpal (Mc) 1 is shorter than Mc II, but is transversely wide (with a maximum width to maximum length ratio of 0.87) giving it a squat appearance. The distal condyles are strongly asymmetrical, with the radial-side condyle placed considerably proximally relative to the ulnar-side condyle. Most of the following description is based on the left manus, supplemented with information from the right manus where appropriate (Fig. 20).

In proximal view, the articular surface has a radially tapering, sub-triangular outline. The dorsal margin is bounded by a low, proximally projecting, rounded lip of bone, which extends from the ulnar corner to a point approximately two-thirds of the transverse width. The palmar margin describes a low, dorsally concave arc. The radial margin is tapered and bluntly rounded, whereas the ulnar margin is much taller, and deeply concave. In palmar view, the radial portion of the proximal surface bears a small, sub-triangular fossa that is bounded dorsally and radially by the rounded lip of bone and grades into the ulnar portion of the surface. This fossa serves as the contact for the sub-triangular portion of the distal surface of distal carpal 1. In proximal view, the radial one-third of the proximal surface is flatter, with a sub-circular outline. This portion faces proximoradially and on the left hand this portion does not contact distal carpal 1. The plane of the proximal surface is oblique to the long axis of the bone, extending radiodistally so that the radial side of the metacarpal is proximodistally shorter than the ulnar side. The ulnar side of the proximal surface bears a robust, ulnarly projecting tab that forms a contact with the radial side of the proximal end of Mc II as well as the distal and radial surfaces of distal carpal 2. In dorsal view, this tab is abruptly everted from the shaft of the metacarpal, and the everted portion has a sub-rectangular outline. The ulnar surface of this tab is deeply concave, and in particular the dorsal margin forms a shelf of bone that strongly overhangs the radial side of the proximal end of Mc II dorsally.

The proximal end of the radial side of the shaft of Mc I bears a slightly rugose, convex eminence that is continuous with the proximal surface. The shaft of the bone is extremely short between this eminence and the distal condyle, but this short portion is radially convex. Distal to the deeply concave tab, the ulnar surface of the shaft is convex and considerably lower palmodorsally than the proximal end. The dorsal surface of the shaft is sub-trapezoidal in dorsal view, narrowing towards the distal end, and it is shallowly concave both transversely and proximodistally. The palmar surface is similarly sub-trapezoidal in palmar view, narrowing towards the distal end. Its surface is shallowly concave overall, but the boundaries between the palmar surface and the distal condyles are clearly marked by pronounced lips of bone. The radial distal condyle is greatly expanded dorsoventrally with respect to the shaft and is sub-semicircular in radial view. It bears a well-developed, deep collateral ligament fossa that is centrally located. The palmar side of the proximal end of the radial distal condyle is marked by a sharp lip of bone. The ulnar distal condyle is transversely wider, distally more extensive, and palmodorsally slightly taller than the medial condyle. Its ulnar surface bears a well-developed collateral ligament pit and its palmar margin bears a pronounced, ulnarly flaring tubercle. The area between the distal condyles on the dorsal surface is marked by a shallow, sub-circular extensor fossa.

Metacarpal II is the longest of the metacarpals and is much narrower than Mc I in dorsal view. The right element has been compressed slightly palmodorsally, giving each side a slightly different appearance. In palmar view, the shaft of the left metacarpal appears to bow radially, but this bowing is not apparent either in dorsal view or on the contralateral element, where the shaft appears straight. The proximal and distal ends are expanded radioulnarly relative to the shaft. The dorsal margin of the proximal surface is saddle-shaped, with a deep midline depression and dorsally expanded radial and ulnar sides that form rounded projections that extend on to the dorsal surface. The ulnar margin of the proximal surface is oriented strongly ulnodorsally, forming a broad sheet of bone that overhangs the radiodorsal surface of Mc III. The radial margin of the proximal end is radiopalmarly concave,

forming a broad sheet of bone that articulates with the ulnodorsal expansion of the proximal end of Mc I. The palmar margin of the proximal surface is shallowly concave palmarly. The proximal surface is strongly convex and rhomboidal in outline. Its dorsopalmar midline bears a low, transversely oriented, rounded ridge that extends across the entire surface, but is weakly developed in the radial portion.

The radial surface of the shaft distal to the proximal shelf is palmodorsally low and slightly convex. Immediately proximal to the distal condyle it bears a low rim of bone that surrounds a large, deep, centrally positioned collateral ligament fossa. The dorsal surface of the shaft is strongly concave proximally and is continuous with the saddle on the proximal margin. This concavity becomes progressively shallower towards the distal end. The radial projection of the proximal end of the dorsal surface grades into the dorsal surface of the shaft a short way from the proximal margin. Its terminus is marked by a low, rugose swelling. The ulnar projection gradually attenuates into the ulnar margin of the bone. The proximal end of the ulnar surface of the shaft is broad and flattened with a slightly rugose texture where it forms the articulation for Mc III, but distal to this it becomes palmodorsally low and slightly convex. More distally, the collateral ligament fossa on the ulnar surface lacks a distinct bounding lip, but the fossa is larger than that on the radial side. The most salient feature of the palmar surface is a rugose ridge of bone that extends distally along the centre of the shaft and terminates at a point approximately one-third of the length of bone. This ridge forms a buttress that articulates with the radial margin of the proximal end of Mc III. A shallow flexor fossa is present between the distal condyles. The distal condyles are best exposed in palmar view, where they are sub-symmetrical in outline and extend to the same level distally.

Metacarpal III is slightly shorter and much more slender than Mc II (Fig. 20). In dorsal view, both the proximal and the distal ends are transversely expanded relative to the shaft, but the expansion is less pronounced than in Mc II. The proximal surface is sub-triangular in outline, with a long, tapering ulnodorsally oriented apex. This structure supports a sheet-like projection that extends ulnarly from the ulnar surface, dorsally overlapping the proximal end of the radial side of Mc IV. The radiodorsal corner of the proximal surface in Mc III forms a right angle, while the radiopalmar corner is well rounded. Although the majority of the proximal surface is convex, a shallow groove extends palmodorsally along the midline and is more pronounced in its dorsal half. The proximal end of the radial surface is palmodorsally tall and shallowly concave. As it extends distally, this surface becomes palmodorsally lower and radially convex. A well-developed collateral ligament fossa is present, and the proximal margin of the fossa extends for a short distance as a shallow trough on to the distal end of the radial surface of the shaft. The ulnar surface of Mc III is obscured by matrix on both specimens. The margin between the proximal surface and the dorsal surface is formed by a low lip of bone. On the dorsal surface the transverse expansion of the proximal end abruptly narrows as it extends distally to join the shaft. The proximal end of the dorsal surface is concave, in contrast to the distal end, which is shallowly convex. The radial margin of the proximal end of the dorsal surface bears a small, dorsally projecting lip of bone that is closely appressed to Mc II. On its ventral surface, the proximal end of the ulnar margin has a rugose texture and bulges slightly towards Mc IV. The distal condyles are almost entirely obscured by matrix, but they are markedly expanded from the shaft. It is likely that the distal condyles were sub-symmetrical. The intercondylar groove appears to have been shallow. A faint lip marks the proximomedial margin of the radial condyle.

Metacarpal IV has been broken proximally on the left hand and is missing the entire proximal articular surface, as well as most of the lateral side of the shaft (Fig. 20). The right side is poorly preserved and badly encrusted, but some details can be assessed. It is a relatively slender bone, with a modestly expanded proximal end and a bulbous distal end. It is considerably shorter than Mc III. The proximal surface is triangular, with a dorsally directed apex. The radiodorsal surface underlies the overhanging shelf on Mc III. The palmar margin of the proximal surface is slightly convex. The proximal surface is convex over nearly its entire surface. The radial surface of both sides is obscured by matrix. The ulnar surface is proximally flattened and only slightly convex distally. The dorsal surface is generally convex but has been broken on both sides. A low, proximodistally-oriented ridge appears to have been present on the proximal end of this surface. The palmar surface is flattened, and on the right side it appears to overlie the dorsal surface of Mc V. The bulbous distal end has a hemispherical articular surface that lacks distinct condyles. The radial side of this articular surface bears a very faint collateral ligament fossa. The presence of this fossa is equivocal on the ulnar side. The articular surface continues proximally onto the shaft as a tapering triangular feature along the radial side of the palmar surface.

Metacarpal V is the shortest of the metacarpals. As preserved on the right hand, it lies palmar to the palmar surface of the proximal end of Mc IV. It is unclear if this represents its original life position, as the element has been completely prepared from the left hand and its original position was not noted (Fig. 20). Its proximal end is greatly expanded transversely and palmodorsally relative to both the shaft and the distal end in dorsal view. The distal end, as in Mc IV, is expanded from the shaft and globular. In the following description, directional terminology is used as if the metacarpal were held parallel to the rest of the hand.

The proximal surface is flat and sub-rectangular in proximal view. A pronounced lip of bone is present that extends along the radial, ulnar, and dorsal margins, strongly delineating the proximal end from the shaft. In proximal view, the dorsal margin is slightly convex whereas the radial, ulnar and palmar margins are flat. A transversely narrow, shallow, proximodistally-oriented groove excavates the radial side of the proximal palmar surface. The ulnar half of the proximal surface is shallowly

concave, and the radial half is weakly convex. The radial side of the proximal end is expanded into a tall, buttress like feature. This buttress is tall and rectangular in radial view, and its proximal and distal margins are marked by pronounced ridges of bone that extend palmodorsally from the palmar to the dorsal margins. Between these two ridges, the radial surface of the buttress is concave.

The radial, ulnar, dorsal and palmar surfaces of the shaft are convex and relatively featureless. The distal end is a sub-hemispherical, globular structure that lacks distinct condyles. A single collateral ligament fossa is present on its radial surface. The junction between the articular surface and the shaft is marked dorsally by a distinct lip of bone. The palmar portion of the articular surface extends a short way proximally onto the palmar surface of the shaft as a small, bulbous tubercle.

Digit I – Phalanx I-1 is the largest, most robust non-ungual phalanx of the hand. Its maximum radioulnar width, proximodistal length and palmodorsal height are subequal, giving it a blocky appearance. Its most salient feature is a strong ulnar twisting of the shaft relative to the proximal end, so that a line connecting the palmar margins of the proximal flexor processes and a similar line connecting the palmar margins of the distal condyles would cross at an angle of approximately 50°.

The proximal surfaces of each phalanx I-1 are concealed by matrix and the articulated first metacarpal, but radial and ulnar views indicate that it is deeply concave and likely subdivided asymmetrically into radial and ulnar cotyles by a vertical ridge of bone. The proximal end of the radial surface is greatly expanded palmodorsally. The proximodorsal corner of this surface bears a prominent, rounded tubercle that extends a short distance radially, to overhang the rest of the bone. Palmar to this tubercle, the mesial portion of the proximal end of the radial surface is deeply concave but expands radially into a rugose ridge along the radial surface of the flexor process. The more distal portion of the radial surface of the shaft tapers from the expanded proximal end, forming a sub-triangular, concave surface in radial view. The dorsal margin of this triangular concavity is formed by a low, rounded ridge that marks the radial border of the dorsal surface. This ridge deviates palmarly as it extends distally, traversing the distal end of the radial surface and connecting to the palmar margin of the radial distal condyle. The collateral ligament pit on the radial side is large, sub-circular, and positioned approximately at midheight on the distal end of the radial surface. Its dorsal margin is formed by a rugose ridge that bears strong transverse striations. The ulnar surface is considerably less expanded palmodorsally, and its proximal end is convex. The proximal margin is marked by faint horizontal striations. The ulnar surface of the shaft is proximodistally short. Its palmar half is convex, but the dorsal portion is shallowly concave. The proximodorsal and proximopalmar margins of the collateral ligament pit form a weak, semicircular ridge at the distal end of the shaft. The ulnar collateral ligament pit is slightly smaller than the radial one, and its dorsal margin is not marked by striations. The proximal end of the dorsal surface is developed as a low, transversely wide mound with a rugose texture. The dorsal surface of the shaft is relatively flat, but it becomes shallowly concave between the ridges formed by the distal condyles. The plane of the palmar surface is oblique to that of the dorsal surface due to the palmar expansion of the radial side. It is generally flat, although the proximal end of the ulnar margin bears a very low, rugose, triangular tubercle. In both hands, the distal condyles of phalanx I-1 are mostly covered by matrix or their articulated unguals, but they appear to be sub-symmetrical. They are palmodorsally taller than they are proximodistally long, and they expand both dorsally and palmarly from the shaft of the phalanx.

Phalanx I-2 (ungual) is the largest manual ungual in all dimensions (Fig. 20). It is strongly recurved, scribing nearly a quarter circle in the arc of its dorsal margin. The proximal surface is covered by matrix and obscured by the articulated phalanx I-1 in both hands, but it is clear from the radial and ulnar views that this surface was deeply concave. The proximal end of the radial surface is palmodorsally tall, and its proximal margin is marked by a rugose rim that is broken dorsally and palmarly by shallow concavities that are continuous with the groove for the claw sheath. The middle part of the proximal margin is marked by a low, mound-like tubercle that separates the proximal ends of the claw sheath grooves. The radial claw sheath groove is prominent and forms a narrow channel that begins proximally immediately dorsal to the radial side of the flexor tubercle. A short distance from the flexor tubercle, it bends sharply dorsally, then continues distally along the midline of the radial surface, extending all the way to the distal tip of the ungual. Dorsal to the groove, a shallow, subtriangular fossa follows its arc, expanding proximally. The morphology of the ulnar surface is generally similar, but the proximal margin is marked by more prominent striations, and the claw sheath groove appears to be deeper, particularly proximally (although this may due to preservation). The proximal end of the palmar surface bears a hypertrophied, rugose flexor tubercle. The palmar surface of this tubercle is flattened and transversely broad. A shallow fossa is present on the distal end of the mesial portion in the left hand, but preservation of the right ungual I-2 is too poor to confirm this. The palmar surface of the tubercle is also slightly asymmetrical – the radial side extends slightly further palmarly than the ulnar side. Distal to the flexor tubercle, the palmar surface narrows transversely and is uniformly convex. The dorsal surface is convex and relatively featureless. The proximal margin extends proximally over the articular surface as a triangular extensor process.

Digit II – The phalanges of the digits II–V are considerably smaller and less robust than those of digit I (Fig. 20).

Phalanx II-1 is a robust element, with expanded proximal and distal ends. The proximal surface is obscured by matrix and the articulated distal end of Mc II, but it appears to be deeply concave. A low rim defines the radial, dorsal, and ulnar margins of the proximal surface. The proximal end of the palmar surface bears a well-developed flexor region that forms a rugose, semicircular platform. This platform is slightly asymmetrically devel-

oped, with a more palmarly extensive radial margin that forms a low hemispherical tubercle. The shaft is proximodistally short, and its radial and ulnar surfaces are convex. The distal end of the dorsal surfaces bears a prominent sub-circular extensor ligament pit. The palmar surface is flattened and transversely broader than the dorsal surface. A faint flexor pit is present along the midline, immediately proximal to the distal condyles. The distal condyles are well-developed and sub-symmetrical. The bear a pronounced ginglymus, and their radial and ulnar surfaces bear well developed, sub-circular, centrally positioned collateral ligament pits.

Phalanx II-2 is proximodistally shorter and transversely narrower than II-1. The right element has been more thoroughly prepared, exposing the proximal surface. This surface is tall and deeply concave, with a sub-trapezoidal outline in proximal view. It bears two prominent cotylae, which are divided by a sharp, proximally projecting ridge. The ulnar cotyle is transversely broader. The dorsal margin of the proximal end forms a well-developed, rounded extensor process, which projects far dorsally and a short distance proximally above the ginglymus on the distal end of II-1. As in II-1, the radial, ulnar and dorsal surfaces of the shaft are slightly convex, and the palmar surface is flattened. The proximal end of the palmar surface also bears a striated rim, which is similar to II-1 in being more palmarly extensive on the radial side. The remaining portion of the palmar surface is flat. The distal condyles are strongly expanded from the shaft, and bear prominent, circular collateral ligament pits. There is no extensor pit on the dorsal surface at the proximal end of the condyles.

Phalanx II-3 (ungual) is considerably shorter proximodistally, narrower transversely, lower palmodorsally, and less recurved than phalanx I-2. Its dorsal margin scribes approximately one-eighth of a circle in radial view. The proximal surface is mostly obscured by matrix and the articulated distal end of phalanx II-2, but radial and ulnar views suggest that it is deeply concave. The claw sheath grooves on the radial and ulnar sides lack the associated triangular fossae present in phalanx I-2, but they are similarly developed as well-defined, narrow channels. On both the radial and the ulnar surface, they diverge proximally to form a 'Y' shape and continue proximally to wrap around the dorsal margins of the flexor tubercle, ultimately terminating at palmar end of the proximal surface. As the claw sheath grooves extend distally, they become more dorsally positioned. The flexor tubercle is large and its outline is sub-circular in palmar view. The palmar surface of the tubercle is rugose and its midline features a shallow, proximodistally oriented groove.

Digit III – Phalanx III-1 is relatively short and squat, and its proximal and distal ends are expanded with respect to the shaft (Fig. 20). The proximal surface cannot be seen, but the palmar margin is transversely much broader than the dorsal margin, giving it a low, rounded triangular outline in proximal view. The radial and ulnar surfaces are slightly convex, and due to the triangular cross-section of the bone they face radiodorsally and ulnodorsally, respectively. The dorsal surface is more convex than the radial and ulnar surfaces, and its proximal end is dorsally expanded to form a prominent extensor region. Its distal end bears a sub-circular, shallow extensor ligament pit. The proximal end of the palmar surface is convex, and as with the other proximal phalanges it bears a rugose margin that is asymmetrically developed so that the radial side extends farther palmarly than the ulnar side. Distal to this rugose region, the palmar surface of the shaft flattens. The distal condyles are sub-symmetrical and ginglymoid. The collateral ligament pits are well developed, and they bear an accessory groove that extends proximally, interrupting the ridge that marks their proximal boundary.

Phalanges III-2 and III-3 are similar in shape to phalanx III-1, but decrease in proximodistal length, transverse breadth and palmodorsal height. Unlike phalanx III-1, in palmar view the proximal margin of the palmar surface forms a proximally projecting point, and the mesial portion of the palmar surface is concave rather than flat. The collateral ligament pit on III-3 is particularly well developed, forming a deep, sub-circular feature with a raised rim.

Phalanx III-4 (ungual) is only 72% the length of phalanx II-3 and is considerably lower and narrower. Its claw sheath grooves are still prominent, however, and as in II-3 they diverge proximally to form a 'Y' shape and move dorsally as they extend distally. The extensor process is weakly developed and proximally rounded, and the flexor tubercle is a moderately developed structure with fewer striations than the other manual unguals. It grades into the palmar surface of the ungual a short distance from the proximal articular surface.

Digit IV – Neither digit IV nor digit V bear ungual phalanges (Fig. 20). Phalanx IV-1 is proximodistally short and transversely broad. The proximal end is expanded palmodorsally and transversely from the shaft, but the distal end is only slightly expanded in these dimensions. The proximal surface is partially obscured, but it is sub-circular in outline and appears to only bear a single, shallowly concave cotyle for articulation with the metacarpal. The dorsal surface of the proximal end lacks the prominent dorsal expansion of the extensor process seen in other phalanges. The radial and ulnar surfaces are flat. The palmar surface is slightly convex, and the proximal margin bears a weakly developed rugose area that is more symmetrically developed than in other proximal phalanges. The distal condyles are sub-ginglymoid, with only a faint suggestion of a midline groove separating the radial and ulnar sides. Only a faint suggestion of a collateral ligament pit is visible on the ulnar side of the distal end.

Phalanx IV-2 is markedly smaller than IV-1 but agrees closely in its morphology. In palmar view, the proximal margin forms a sub-angular proximal projection and the palmar surface distal to this projection is faintly rugose. The distal end is sub-ginglymoid, and lacks collateral ligament pits, although a faint tubercle along the palmar end of the ulnar surface likely marks the margin of the ligamentous insertion.

Only the proximal portion of phalanx IV-3 is preserved, and little of its morphology can be ascertained. It is much narrower and lower than the preceding phalanx, and the

preserved portion suggests is was reduced to a small, nubbin-like element.

Digit V – Phalanx V-1 is a short bone that is only moderately expanded proximally and distally relative to other phalanges (Fig. 20). Its proximal surface is shallowly concave, with a sub-circular outline in proximal view. A low lip that lacks prominent striations delineates the radial, ulnar and dorsal margins. The radial, ulnar and dorsal surfaces of the shaft are shallowly concave, giving the phalanx a spool-like morphology in dorsal view, but the palmar surface is convex and marked by a few faint longitudinal striations. The distal articular surface is poorly preserved on both sides. It is clear that the distal end is delineated by a relatively sharp rim that extends along the distal end of the radial, ulnar and dorsal surfaces. Faint suggestions of collateral ligament pits are present immediately proximal to this ridge on the radial and ulnar surfaces. The distalmost surface appears on both sides to be shallowly concave.

Phalanx V-2 is little more than a wedge-like nubbin of bone. Its palmar surface is flattened, and the radial and ulnar surfaces slope dorsally, giving it a sub-triangular cross-section. The distal tapers to a blunt point, which appears incapable of supporting an additional phalanx.

Pelvic girdle

Ilium

The left ilium is visible in lateral view only and is broken posteriorly; the right ilium is exposed both laterally and medially (Figs 21–23; Supplementary Model 4). In lateral view, the anterior iliac process is sub-triangular in outline and its blunt, rounded apex extends anteriorly. This process is relatively deep, with subequal maximum length (measured from the apex to a point level with the anterior margin dorsal to the origin of the pubic peduncle) and height (as measured where the process merges with the main body of the ilium). This is similar to the condition in *Ignavusaurus* (Knoll 2010), *Lufengosaurus* (Young 1941) and *Sarahsaurus* (Rowe *et al*. 2011), but contrasts with the slender process present in *Adeopapposaurus*, which has a maximum length/height ratio of ~0.50 (Martínez 2009) (see Table 8 for other measurements). In lateral view, the anterior iliac process of *M. carinatus* does not extend as far anteriorly as the anterior margin of the distal end of the pubic peduncle, and a line drawn ventrally from the apex of the process intersects the pubic peduncle at a point approximately halfway along its length (Fig. 23A), as also occurs in *Ignavusaurus* (Knoll 2010), *Lufengosaurus* (Young 1941) and *Sarahsaurus* (Rowe *et al*. 2011), whereas in *Adeopapposaurus* such a line would intersect with the distal end of the pubic peduncle (Martínez 2009). In *M. carinatus*, the ventral margin of the anterior iliac process of the process forms an angle of approximately 80° with the anterior margin of the pubic peduncle. The lateral surface of the anterior process is dorsoventrally convex and bears a low swelling at its centre that was presumably a muscle attachment site. Its dorsal margin is gently convex but slopes upward slightly as it merges into the main iliac body posteriorly. The remainder of the iliac dorsal margin is smoothly and shallowly convex across its entire length, with the exception of this small, but distinct, inflexion, at the junction between the anterior process and the main iliac body (Fig. 23A). This inflexion is absent in *Lufengosaurus* (Young 1941).

Table 8. Measurements of pelvic girdle elements in BP/1/4934. All measurements are in mm. Those marked with an asterisk are minima due to breakage. Some measurements were not possible due to either extensive breakage or the presence of matrix/overlapping elements. Measurements from the left ilium are in lateral view; those from the right ilium (except pubic peduncle length) are in medial view.

Element	Measurement	Value (mm)
l ilium	Total length	248*
	Main body height dorsal to supraacetabular flange	97
	Anterior process length	50
	Pubic peduncle length	135
	Pubic peduncle distal end, anteroposterior length	47
	Ischiac peduncle length	61
	Maximum acetabulum length (between peduncles)	142
r ilium	Total length	309
	Main body height dorsal to acetabulum	120
	Pubic peduncle length	135
	Ischiac peduncle length	50
	Pubic peduncle distal end, anteroposterior length	60
l pubis	Total length (iliac articulation to distal end)	365
	Proximal end, maximum width	165
	Obturator foramen, maximum diameter (anteroposterior)	49
	Obturator foramen, minimum diameter (mediolateral)	15
	Shaft, minimum width	70
	Shaft, distal width	96
	Shaft, anteroposterior length distal end	28
r pubis	Total length (iliac articulation to distal end)	367
	Shaft, minimum width	69
	Shaft, distal width	84

In lateral view, the main iliac body reaches its greatest height at a point level with the ischiac peduncle (Fig. 23A). The dorsal half of the main body is anteroposteriorly and dorsoventrally concave, forming an extensive depression. The dorsal margin of this depression bears numerous dorsoventrally extending striations, indicating areas of muscle attachment. A distinct change in slope separates this depression from the ventral part of the main body, producing a dorsoventrally convex swelling that lies dorsal to the acetabular margin. The acetabular margin is mainly smooth-edged but bears a short anteroposteriorly-extending ridge that lies close to its junction with the pubic peduncle, which probably represents a reduced supraacetabular flange. Posterior to this ridge the ventrolateral surface of the iliac body flattens as it merges into the ischiadic peduncle. The posterior iliac process is triangular in outline. It is considerably larger than the anterior process and its posterodorsal corner projects beyond the posterior margin of the ischiadic peduncle. Its lateral surface is dorsoventrally convex and it bears a heavily striated swelling at its junction with the main iliac body.

In medial view, the dorsal part of the iliac blade is gently convex anteroposteriorly, slightly convex dorsoventrally and heavily striated for muscle attachment (Fig. 23B). This region is divided from the sacral rib scars by a sinusoidal

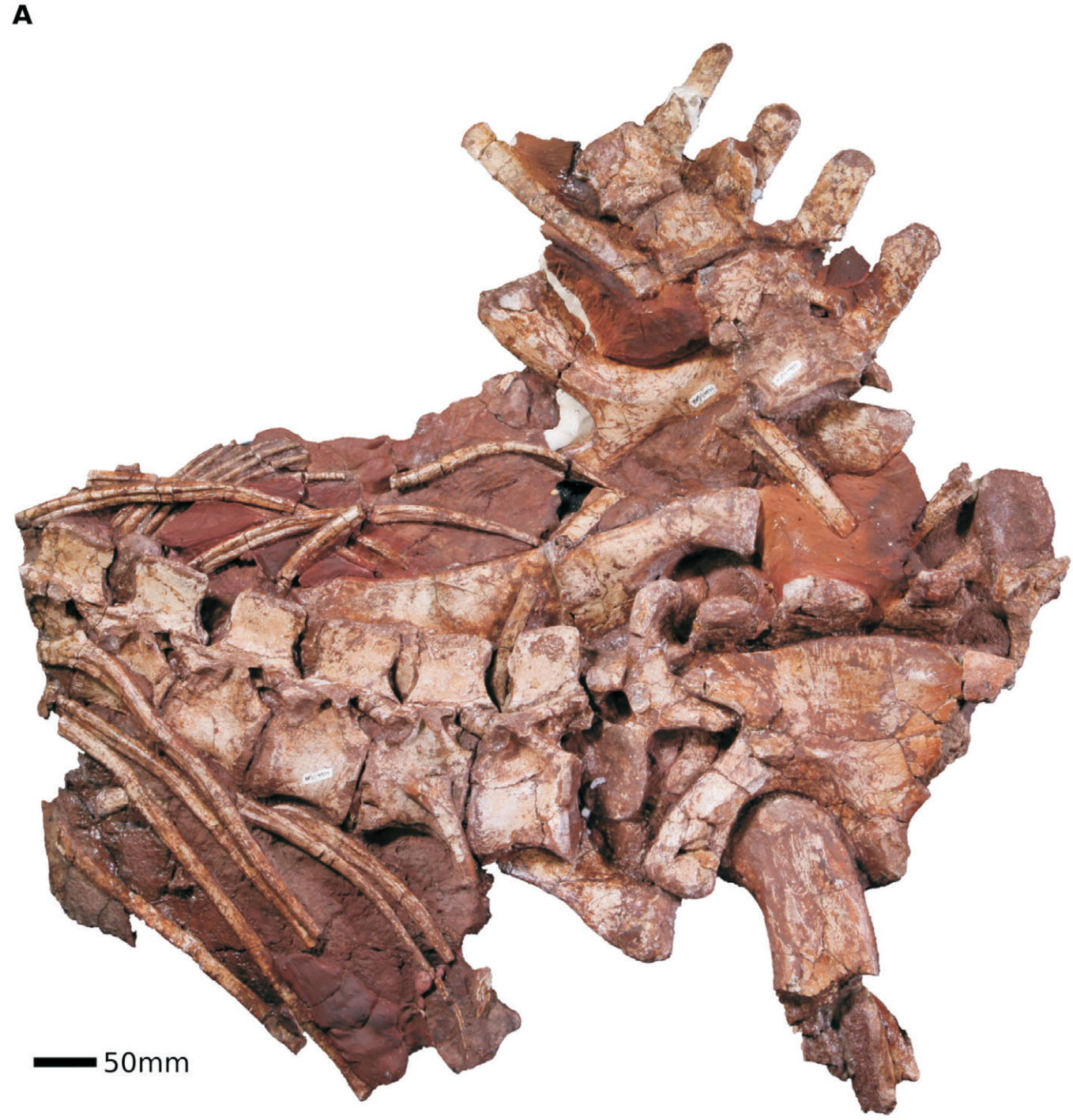


Figure 21. Posterior thoracic and pelvic region of *Massospondylus carinatus* (BP/1/4934) in left lateral view, including the posterior dorsal vertebral column (D8, in part, to D14), dorsal ribs, sacrum, anterior caudal vertebrae, gastralia, pelvic girdles and left femur. **A**, photograph; **B**, interpretative line drawing. Scale bar = 50 mm. (Continued on p. 161.)

sacricostal ridge that extends posteriorly from the base of the anterior process. The sacricostal ridge is most prominent anteriorly but becomes lower in the central part of the ilium and fades into the medial surface: it does not reach the posterior margin of the iliac blade. A trough-like depression lies below the sacricostal ridge, whose undulating morphology corresponds with that of the three sacral ribs (Fig. 23B). Sacral rib 1 would have articulated with a small sulcus that lies partially on the anterior process and partially on the iliac blade, which is defined by the strongly dorsally convex anterior part of the sacricostal ridge. A shallow facet for sacral rib 2 is defined by the adjacent ventrally convex portion of the sacricostal ridge in the anterior-to-central part of the iliac blade. Finally, a broad, shallow scar defined dorsally by the lowest portion of the sacricostal ridge would have received sacral rib 3. Ventral to the sacral rib scars the area immediately dorsal to the acetabulum is dorsoventrally convex. In medial and posterior views, the posterior process is excavated ventrally to form a low, ridge-like brevis shelf and shallow brevis fossa (Fig. 23B). Neither of these structures is visible laterally, as in *Lufengosaurus* (Young 1941), but in contrast to *Adeopapposaurus* where the brevis fossa is visible (Martínez 2009). Ventral to the brevis fossa, the posterior margin of

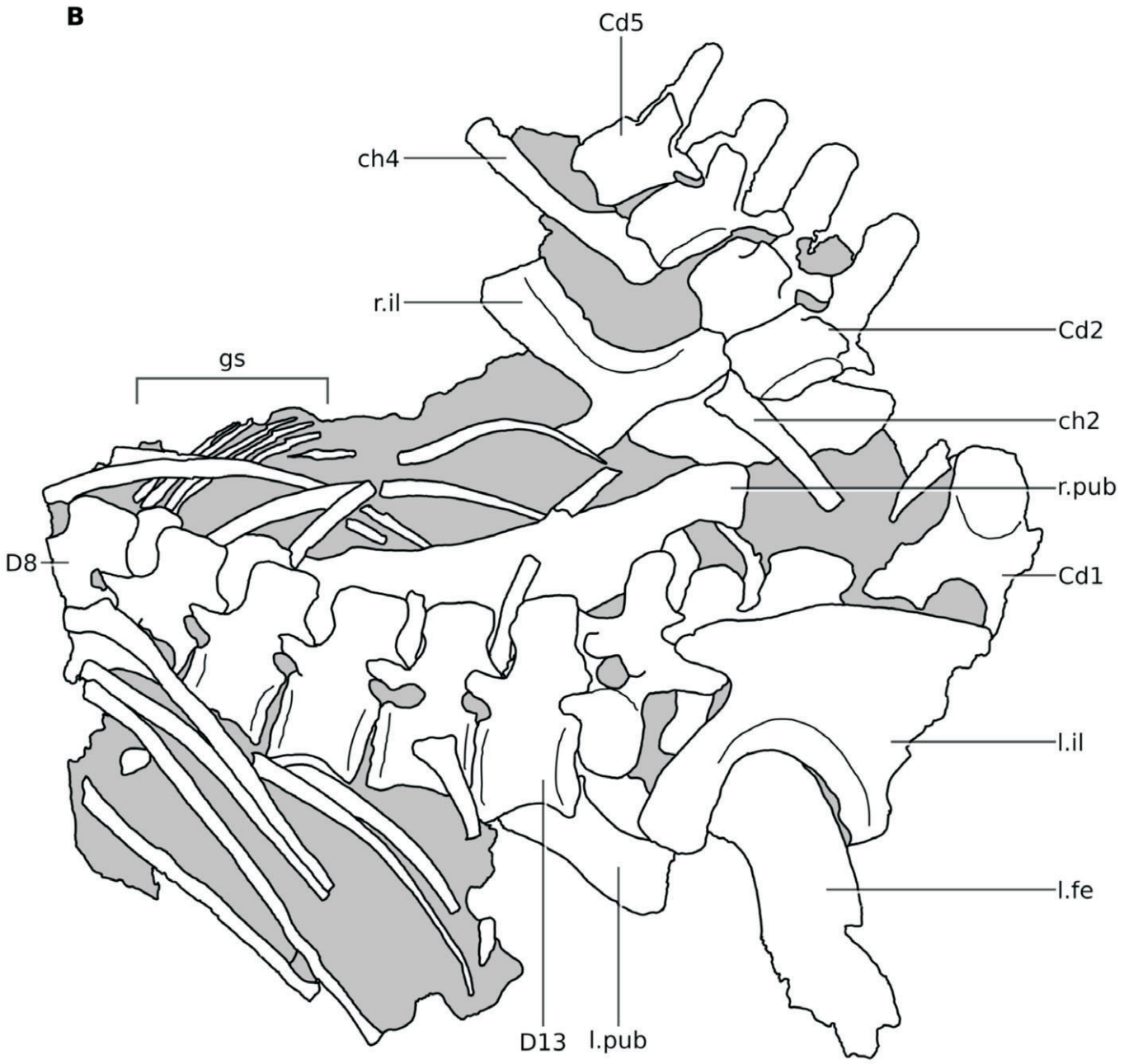


Figure 21 (continued).

the iliac body forms a mediolaterally compressed sheet that merges with the ischiac peduncle ventrally.

The pubic peduncle projects anteroventrally and has a gently sinuous and convex anterior margin and a correspondingly concave posteriorly margin, with the latter forming the anterior border of the acetabulum (Fig. 23A). Its dorsal part is anteroposteriorly narrow, but it increases in width distally, so that it has a sub-rectangular outline in lateral view. The lateral surface of the peduncle is slightly concave dorsally but flattens ventrally; its posterior surface is mediolaterally concave; and its medial surface is shallowly concave. The lateral margin of the pubic peduncle is broken in both ilia, but it clearly formed an extensive, laterally and posteriorly projecting flange of bone that enclosed the anterior margin of the acetabulum, hiding it from lateral view. This lateral flange is continuous with the supraacetabular flange, dorsally. The peduncle has a sub-triangular cross-section, with the apex of this triangle pointing anteriorly. It is approximately twice the length of the ischiadic peduncle.

The acetabulum is open, but its dorsal part is partially enclosed medially by a mediolaterally broad and ventrolaterally inclined sheet of bone that is deepest medially and that shallows laterally (Fig. 23). The anterior acetabular margin is mediolaterally and dorsoventrally concave, the dorsal margin is dorsoventrally convex and anteroposteriorly concave and its posterior margin (anterior margin of the ischiadic peduncle) is antero-



Figure 22. Posterior thoracic and pelvic region of *Massospondylus carinatus* (BP/1/4934) in ventral view, including the posterior dorsal vertebral column (D8, in part, to D14), dorsal ribs, sacrum, anterior caudal vertebrae, gastralia, pelvic girdles and left femur. **A**, photograph; **B**, interpretative line drawing. Scale bar = 50 mm. (Continued on p. 163.)

laterally inclined. As a result, the dorsal and posterior acetabular surfaces are partially visible in lateral view, whereas the anterior surface is obscured (see above).

In lateral view, the ischiadic peduncle has a sub-triangular outline and projects ventrally and slightly posteriorly from the main body of the ilium (Fig. 23A). It tapers ventrally and has an almost symmetrical outline, with gently convex anterior and posterior margins, and terminates in a blunt, rounded apex. Its lateral surface is flat dorsally, but becomes a broad, low rounded ridge ventrally, which extends to the apex of the peduncle. It has a sub-triangular to sub-elliptical transverse cross-section, with a shallowly convex medial surface.

Pubis

The pubes appear to be largely complete, although small sections of both are concealed by matrix and the right pubis has a broken dorsal margin. In anterior view, the left pubis is hidden by the posterior dorsals, but the right pubis is almost completely exposed. By contrast, the left pubis is almost fully exposed in posterior view, whereas the proximal end of the right pubis is obscured. The pubes lie in their approximate life positions but are disarticulated and are not in contact with each other (Figs 21, 22, 24; Supplementary Model 4). Measurements are provided in Table 8.

In anterior view, the pubis is an elongate strap-like

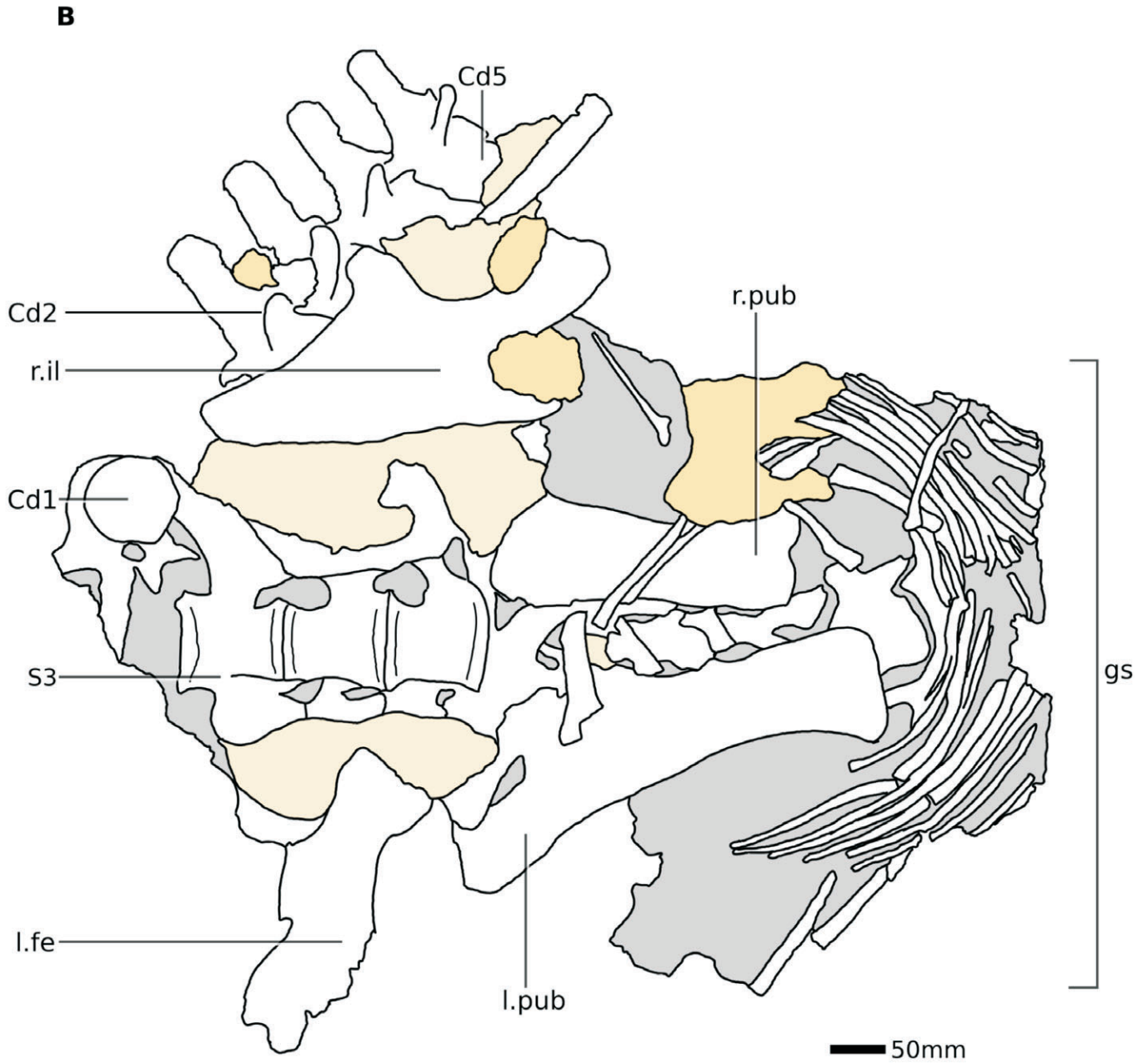


Figure 22 (continued).

element that is divided into a mediolaterally expanded, fan-like proximal plate that narrows ventrally, and whose medial side is extended ventrally to form the pubic apron (Fig. 21). The proximal plate and pubic apron are twisted with respect to each other, with the long axis of the proximal end extending anterolaterally/posteromedially and that of pubic apron anteroventrally.

In proximal view, the iliac articulation has a narrow, elliptical outline, with its long axis oriented anterolaterally, and the surface is shallowly concave and rugose. In anterior or posterior view, the articular surface slopes slightly medially. Posterior to the iliac articulation, the pubis provides a short contribution to the acetabular margin. This region is flat adjacent to the iliac articulation but becomes strongly convex more posteriorly. The ischial articular surface has an elongate triangular outline that is broadest proximally and tapers ventrally to form a thin point. Dorsally, the ischial articular surface is almost flat but it becomes concave ventrally. In anterior or posterior view, the iliac articular and acetabular margins lie in approximately the same plane, but the proximal margin of the ischiac articular surface extends medioventrally from its junction with the acetabular margin, forming an angle of approximately 120° with respect to the rest of the proximal margin. A large, elliptical obturator foramen is present, piercing the proximal plate just ventral to the acetabular margin (Figs 21, 22, 24). It is approximately three times as long dorsoventrally as it is wide mediolaterally, and its long axis is oriented anteromedially/laterodorsally. The foramen is completely enclosed by

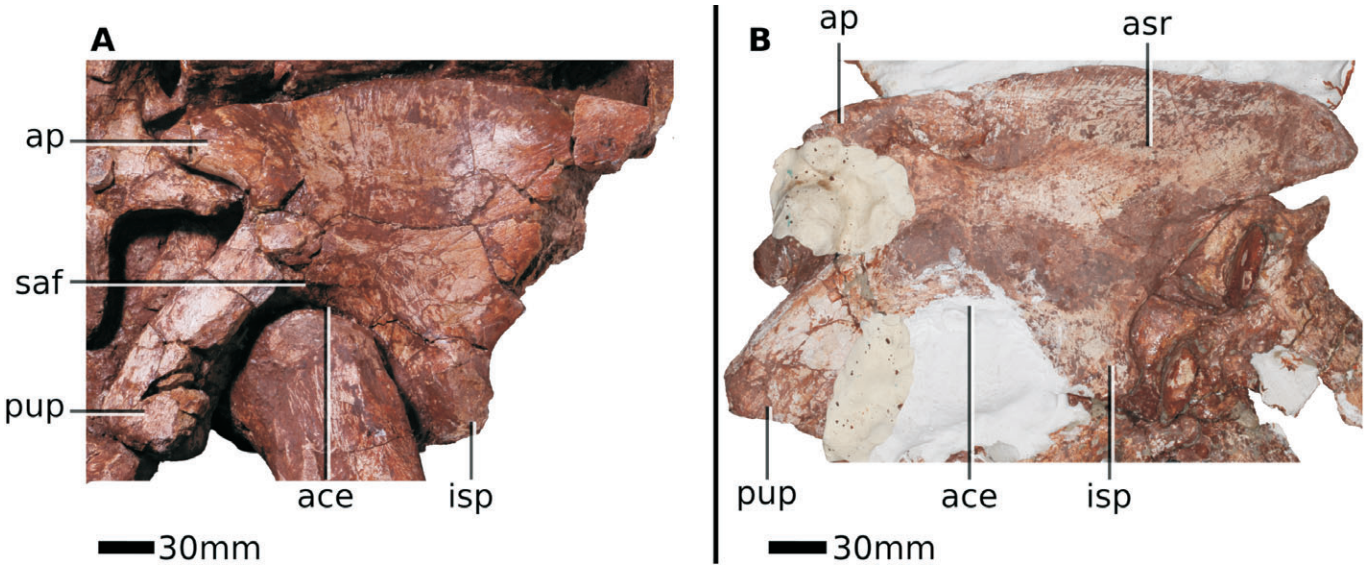


Figure 23. Left and right ilia of *Massospondylus carinatus* (BP/1/4934). **A**, left ilium in lateral view; **B**, right ilium in medial view. Scale bars = 30 mm.

bone in the left pubis, although there is some damage to the proximal plate in this region. The foramen subdivides the proximal plate into a broad triangular region ventral to the iliac articulation, which is mediolaterally concave posteriorly, and a narrower, hook-like region ventral to the ischiac articulation. The posterolateral margin of the proximal plate bears an elongate, low protuberance, which probably represents a muscle scar, immediately below the iliac articulation, lying at a point level with the obturator foramen.

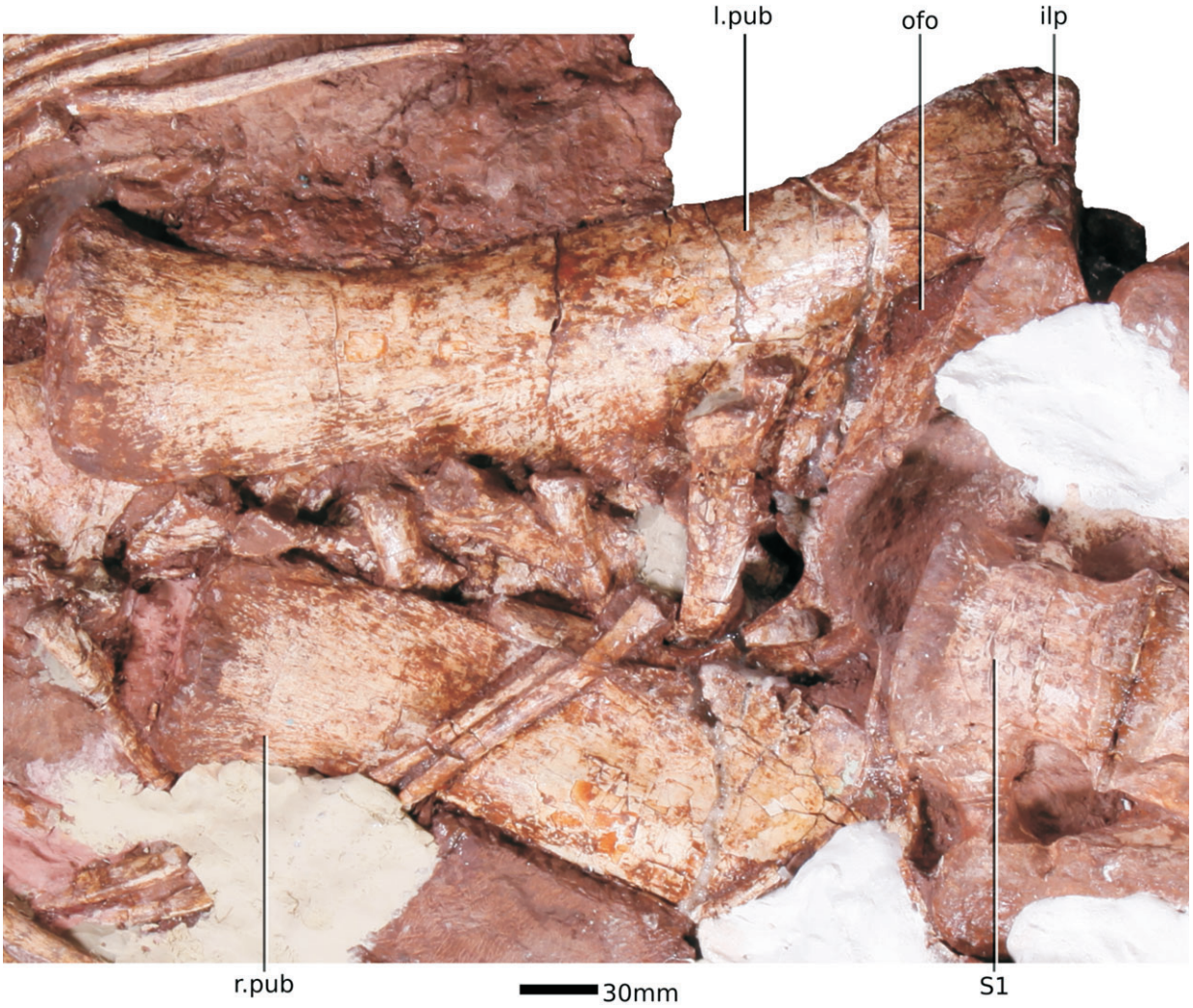


Figure 24. Left and right pubes of *Massospondylus carinatus* (BP/1/4934) in posteroventral view. Scale bar = 30 mm.

In anterior or posterior view, the pubic apron tapers slightly in width ventrally due to the curvature of its lateral margin, which is very gently concave (Figs 21, 24). This is similar to the condition in *Coloradisaurus* (Apaldetti *et al*. 2013) and *Seitaad* (Sertich & Loewen 2010) but differs from the condition in *Adeopapposaurus* (Martínez 2009) and *Lufengosaurus* (Young 1941), where this junction is much more strongly concave. In *M. carinatus* the medial margin of the pubic apron is straight. In posterior view, the proximal part of the pubic apron is thickened along its lateral margin, forming a stout ridge that extends ventrally for approximately two-thirds of the length of the element. By contrast, the apron thins medially, so that its proximal and middle parts have an elongated comma-shaped transverse cross-section. Ventrally, the lateral swelling reduces in prominence and the ventral part of the posterior surface is mediolaterally convex, whereas the corresponding part of the anterior surface is flat. The ventral-most part of the pubis expands slightly laterally, to form a small, hook-like process (Fig. 24). In distal view, the pubis is only slightly expanded anteroposteriorly with respect to the rest of the pubic apron and has a strongly rugose distal end. The anterior margin of the distal end is almost straight, whereas its posterior margin is shallowly convex to produce a flattened hemispherical outline. The anteriorly flat distal pubes contrast with those in *Adeopapposaurus* (Martínez 2009), *Coloradisaurus* (Apaldetti *et al*. 2013), *Lufengosaurus* (Young 1941) and *Seitaad* (Sertich & Loewen 2010), whose anterior surfaces are convex, thereby contributing to their greater anteroposterior expansions, and the condition present in *M. carinatus* is considered a potential autapomorphy. It seems likely that the pubes of *M. carinatus* articulated along for midline for most of their length and that their proximal ends would have enclosed a broad, 'U'-shaped pubic fenestra. The surfaces of the pubes are heavily striated, reflecting the origin and insertions of the pelvic musculature.

Hind limb

Femur

The poorly preserved proximal end of the left femur is preserved in articulation with the acetabulum and is broken just below the level of the fourth trochanter (Fig. 25; Supplementary Model 4). The femoral head is in-turned to extend dorsomedially and its articular surface is mediolaterally and dorsoventrally convex but is partially obscured by plaster. The ventral margin of the femoral head is smoothly concave in anterior view, lacks a ventral projection, and merges with the medial surface of the proximal shaft (Fig. 25A). It is not set on a distinct, constricted neck and its dorsal part merges laterally with the greater trochanter. The greater trochanter has a convex dorsal margin and its medial part is anteroposteriorly expanded relative to its lateral corner. The lateral part of the proximal end is damaged, but there is no evidence for the presence of a dorsolateral trochanter. A damaged, low ridge on the centre of the proximal anterior surface, which terminates below the dorsal margin of the greater trochanter, probably represents the anterior trochanter (Fig. 25A), which is more laterally situated in *Adeopapposaurus* (Martínez 2009). The shaft medial to this ridge is convex, whereas medially it is concave, though this has been accentuated by deformation and breakage. In posterior view, a shallow concavity extends across the posterior surface of the proximal femur, which is defined medially by a sharp, raised rim of bone that forms the posterolateral margin of the femoral head. The lateral border of this concavity is a low, dorsoventrally extending ridge that originates from the greater trochanter dorsally that merges with the shaft at a point level with the ventral margin of the femoral head.

The femoral shaft has an elliptical cross-section immediately ventral to the anterior trochanter, with its long axis extending mediolaterally. The preserved portion of the femur suggests that it would have been at least slightly sigmoidal in anterior view and the proximal part of the lateral surface is convex, while its ventral part, in the region of the fourth trochanter, is concave. The fourth trochanter is situated on the posterior surface of the shaft (Fig. 25B,C). It is elongate dorsoventrally and its base is a mediolaterally-thickened flange that tapers laterally to a thin margin. The ventrolateral corner of the fourth trochanter is slightly hooked, but it is not pendant. In lateral view, the fourth trochanter has a sub-crescentic lateral outline and its margins are heavily striated.

Pes

The only part of the hind limb remaining in articulation with the specimen is the left femur. However, partial metatarsals and pedal phalanges (including unguals) are associated with the specimen, although they are stored separately. Measurements where possible are listed in Table 9.

Metatarsus–Left metatarsals (Mt) I and II are represented by their proximal and distal ends only (the shaft is missing in both cases). Several other fragments of metatarsals are also present but cannot be identified with confidence. The proximal end of Mt I has been cracked but has a sub-triangular outline with its longest margin facing medially with the apex of the triangle pointing laterally. This lateral process articulates with a sulcus on the medial surface of Mt II. The proximal articular surface is slightly convex anteroposteriorly and more strongly convex mediolaterally. In anterior view, Mt I tapers slightly from the proximal end as it extends ventrally. The medial surface of the proximal end is flat to slightly convex, whereas

Table 9. Measurements of pedal elements in BP/1/4934. All measurements are in mm. Those marked with an asterisk are minima due to breakage.

Element	Measurement	Value (mm)
Mt I	Maximum anteroposterior length (proximal)	53
	Maximum mediolateral width (proximal)	34
	Maximum anteroposterior length (distal)	31
Mt II	Maximum anteroposterior length (proximal)	48
	Maximum mediolateral width (proximal)	49
	Maximum mediolateral length (distal)	45*

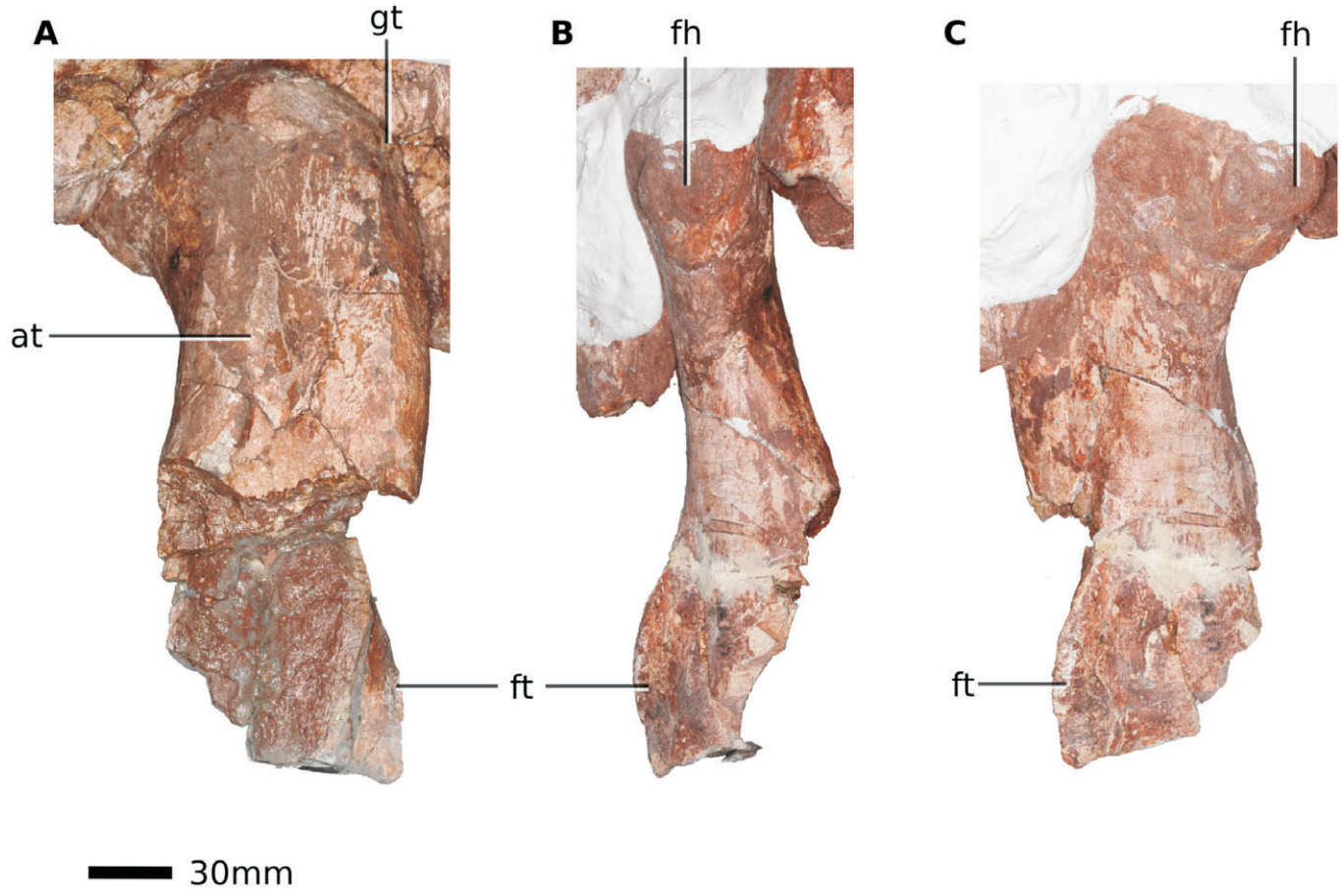


Figure 25. Left femur of *Massospondylus carinatus* (BP/1/4934) in anterolateral (**A**), medial (**B**) and posteromedial (**C**) views. Scale bar = 30 mm.

its anterolateral and posterolateral surfaces are shallowly concave and separated by a ridge that extends ventrally from the laterally projecting triangular process of the proximal surface. The broken ventral surface of the proximal part has a triangular cross-section. In anterior view, the distal part of Mt I is parallel-sided in its proximal part, but distally it expands to form the articular condyles for phalanx I-1. In lateral view, the articular surface expands anteroposteriorly with respect to the base of the shaft. Proximally, the broken shaft has a figure-of-eight-shaped cross-section due to the presence of shallow excavations on the anterior and posterior surfaces of the shaft. The lateroventral surface bears a shallow excavation surrounded by a raised rim of bone, but it does not form a well-defined collateral ligament pit. The medial part of the articular surface is damaged, but it is clear that it was asymmetrical and more strongly expanded anteroposteriorly along its lateral margin. In distal end view, the articular surface is rugose and has a sub-triangular margin with a flat medial surface and very weakly convex anteromedial and anterolateral surfaces that meet at a blunt apex. The articular surface is strongly convex both anteroposteriorly and mediolaterally.

The proximal surface of Mt II has an hourglass-shaped outline, as is common among sauropodomorphs, with strongly concave medial and lateral margins (which have been accentuated by crushing) a weakly concave anterior margin and a weakly convex posterior margin. The anterior margin appears to be longer than the posterior margin, but this is due to the abrasion and breakage of the latter. The articular surface is slightly rugose and weakly convex anteroposteriorly and more strongly convex mediolaterally. The anterior, medial, lateral and posterior surfaces of the proximal end all bear ventrally extending shallow sulci, with those on the medial and lateral surfaces for the reception of Mt I and III, respectively. The broken base of this section has an elliptical cross-section, with its long axis trending mediolaterally. The distal part of Mt II is poorly preserved but exhibits development of a shallow pit on its lateroventral corner and a shallow sulcus is present on its posteroventral surface. The articular surface has a sub-rectangular outline in distal view, with its long axis trending horizontally, and is strongly convex anteroposteriorly and straight mediolaterally to produce a strongly curved roller surface.

Phalanges – Six partial pedal phalanges are preserved, including two unguals. The proximal articular surfaces of the non-ungual phalanges are strongly concave dorsoventrally and mediolaterally and lack a dorsal lappet. They have an asymmetrical, 'D'-shaped outline in posterior view. The medial, lateral and dorsal surfaces of the proximal part grade into each other along a smooth convex curve, but the shallowly concave ventral surface is offset from the others by distinct breaks in slope medially and laterally. The non-ungual phalanges taper in mediolateral width anteriorly prior to expanding again at their distal ends to produce the articular surface. In all of the preserved phalanges the distal ends are divided into distinct medial and lateral ginglymi, which are separated by a shallow sulcus that wraps around the midline from

the dorsal to the ventral surface of the phalanx. Deep collateral ligament pits are present medially and laterally and in distal end view the articular surface has a sub-trapezoidal outline as the ventral margin of the articular region is wider than its dorsal margin. The medial and lateral ginglymi are subequal in size in all preserved non-ungual phalanges, but the lateral ginglymus is very slightly smaller as it is not expanded dorsoventrally to the same degree as the medial ginglymus.

Both ungual phalanges are missing their distal tips. In proximal view, they have a sub-ovate outline that is widest approximately one-third of the distance from the ventral margin and that tapers dorsally to a blunt apex. The articular surface is divided into two parallel, dorso-ventrally concave sulci by a low midline ridge. In lateral view, the proximal margin of the ungual is strongly concave, the dorsal margin is convex and the ventral margin is more strongly concave. The dorsal and ventral margins converge anteriorly. The junctions between the proximal and lateral surfaces are ornamented with a series of fine ridges. Prominent sheath attachment grooves are present on the medial and lateral surfaces, positioned at approximately one-third of the distance from the dorsal margin of the ungual. In dorsal view, the unguals are broadest proximally and taper anteriorly.

OSTEOHISTOLOGY

The right humeral sample was taken just below the deltopectoral crest and, due to the incomplete nature of this region, the sections comprise only a small portion of the medullary cavity and the anteromedial side of the compact cortex (Fig. 26). The centre of the medullary cavity is not preserved, but the outer portion is relatively clear. The perimedullary region, however, contains numerous broken bony trabeculae and resorption cavities (Resorption Front: see Fig. 26A). The compact cortex is thinner than that of the femur. The primary bone tissue of the inner cortex has been almost completely destroyed by secondary reconstruction. Dense Haversian bone, with up to two generations of secondary osteons (Fig. 26B), extends into the innermost part of the cortex, but isolated scattered secondary osteons are present in the middle and outer cortex as well. We place the Haversian Front (Klein & Sander 2008) in the outer cortex in a region of closely distributed secondary osteons, based on Klein & Sander's (2008) definition, although there are numerous areas of primary bone inside this Haversian Front (Fig. 26A). The primary bone tissue primarily consists of well-vascularized fibrolamellar bone. The patches of preserved primary interstitial matrix in the inner cortex contain both a woven-fibred matrix with round, haphazardly arranged osteocyte lacunae as well as areas of flattened osteocyte lacunae arranged parallel to one another indicating a lamellar bone matrix (Fig. 26C). The primary bone of the mid-cortex contains numerous longitudinally-oriented primary osteons arranged either haphazardly or in circumferential rows in a woven-fibred bone matrix (Fig. 26D). The vascular canals in some regions also form a laminar network. The tissue gradually transitions into predominantly parallel-fibred bone towards the sub-periosteal surface. Irregularly spaced growth marks are present throughout the cortex. Most comprise lines of arrested growth (LAGs), which indicate a temporary cessation in growth, however, annuli (indicating a temporary decrease in growth) of lamellar bone associated with some LAGs were also observed (Fig. 26A). Spacing between LAGs becomes smaller and double LAGs become increasingly prevalent in the outer cortex, with a triple LAG being observed at the sub-periosteal surface (Fig. 26E). Double and triple LAGs were counted as single LAGs as they are likely deposited within one year (Castanet 1994). Using this method we counted 10 LAGs in the cortex. However, we note here that three LAGs in the outer cortex are relatively closely spaced and two of them merge on the anterior side of the bone, suggesting that at least two if not all three represent one season. Although there are fewer vascular canals at the bone periphery, they still occur after the triple LAG. An external fundamental system (EFS), which typically consists of avascular lamellar bone with multiple, closely-spaced LAGs, was not observed. An EFS indicates that the animal has reached maximum size (Cormack 1987).

The left femoral sample was taken just below the fourth trochanter. Due to the incomplete nature of this region, the sections comprise a small portion of the medullary cavity and the posterolateral corner of the compact cortex (Figs 27, 28A). The medullary cavity is likely open (based on previous work on the femur of *Massopondylus carinatus*: see Chinsamy 1993), although only the outer portion is clearly preserved. Similar to the humerus, the peri-medullary region contains several large bony trabeculae, some of which are broken. Resorption cavities extend into the innermost portion of the compact cortex (Resorption Front: see Fig. 27). Secondary remodelling has almost completely destroyed the primary bone tissue in the inner third of the cortex with, frequently two and occasionally three, generations of secondary osteons being found (Fig. 28B). Abundant secondary osteons extend to the outer part of the mid-cortex (Haversian Front: see Fig. 27), but decrease in size and become increasingly isolated towards the sub-periosteal surface. Similar to the humerus, the primary bone tissue transitions from fibrolamellar bone to parallel-fibred bone tissue (Fig. 28C–E). The vascular canals are predominantly arranged as longitudinally-oriented primary osteons in circumferential rows, with some areas being more haphazard in the inner and mid-cortex. The number of circumferential vascular canals increases towards the sub-periosteal surface, but not to the degree of forming a laminar network. Seven LAGs were counted in the middle and outer cortex, including several double LAGs (Fig. 28A,E). A definitive count is hindered by the presence of secondary remodelling. A few vascular canals are still present after the last clear LAG, indicating that the animal was still growing. However, the small distance separating LAGs as well as the amount of secondary remodelling in the middle and inner cortex indicate that this animal was an adult at the time of death.

Extensive Sharpey's fibres were observed extending from the periphery of the cortex to the medullary cavity along the lateral and posterior sides, forming a 70° angle

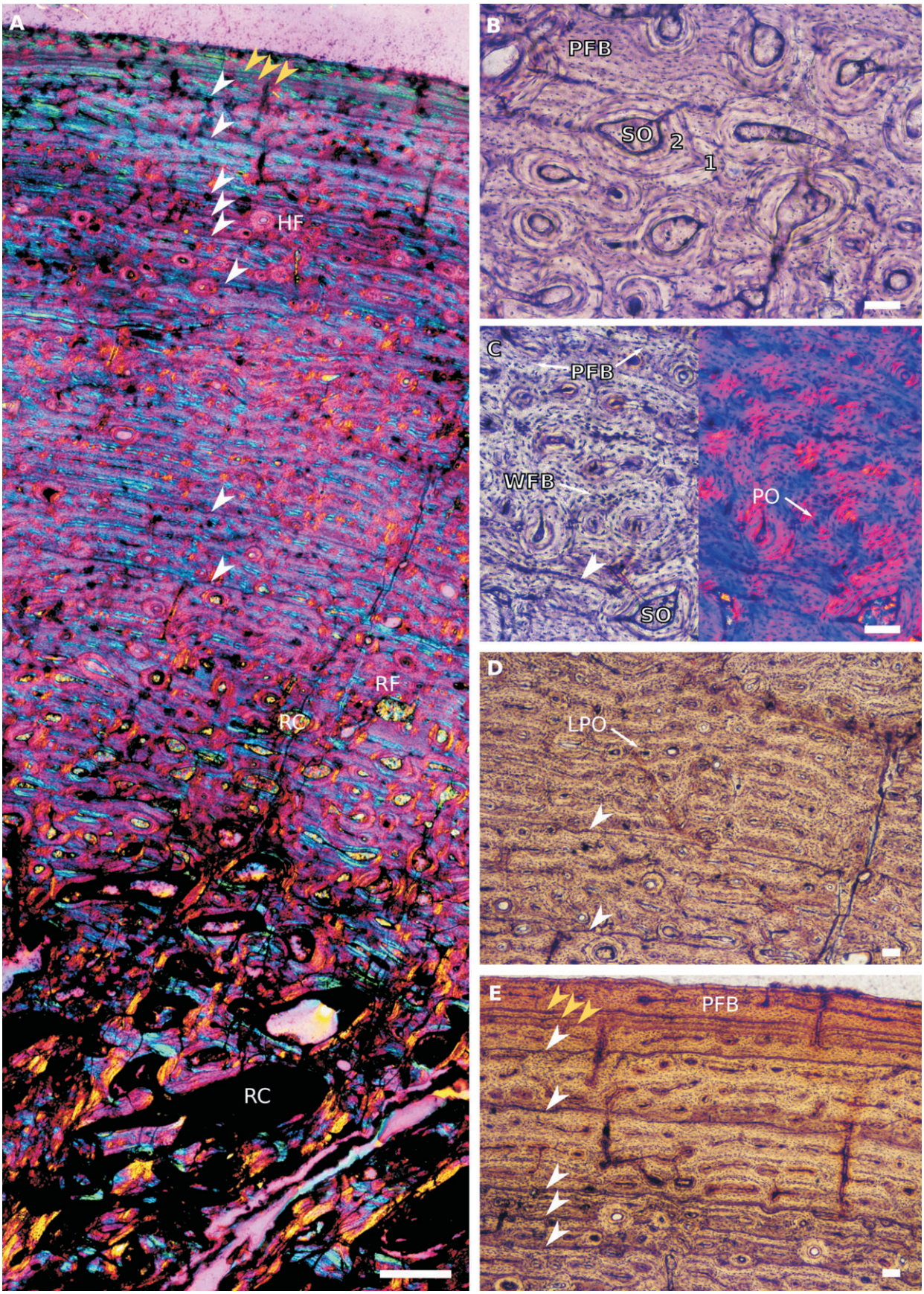


Figure 26. Humeral osteohistology of *Massospondylus carinatus* (BP/1/4934). **A**, overall view in cross-polarized light showing resorption cavities demarcating the Resorption Front in the perimedullary region. Note the Haversian Front decreased spacing between LAGs in the outer cortex. **B**, high magnification of the inner cortex in normal light showing multiple (1 and 2) generations of secondary osteons. **C**, high magnification of the mid-cortex in normal and cross-polarized light showing a mixture of parallel-fibred and woven-fibred bone as well as primary and secondary osteons. **D**, mid-cortex in normal light showing fibrolamellar bone tissue with longitudinally-oriented primary osteons in circumferential rows. **E**, outer cortex in normal light showing a triple lag and parallel fibred bone at the sub-periosteal surface. White arrowheads indicate LAGs and yellow arrowheads indicate a triple LAG. Scale bars = 500 μm (**A**) and 100 μm (**B**–**E**).

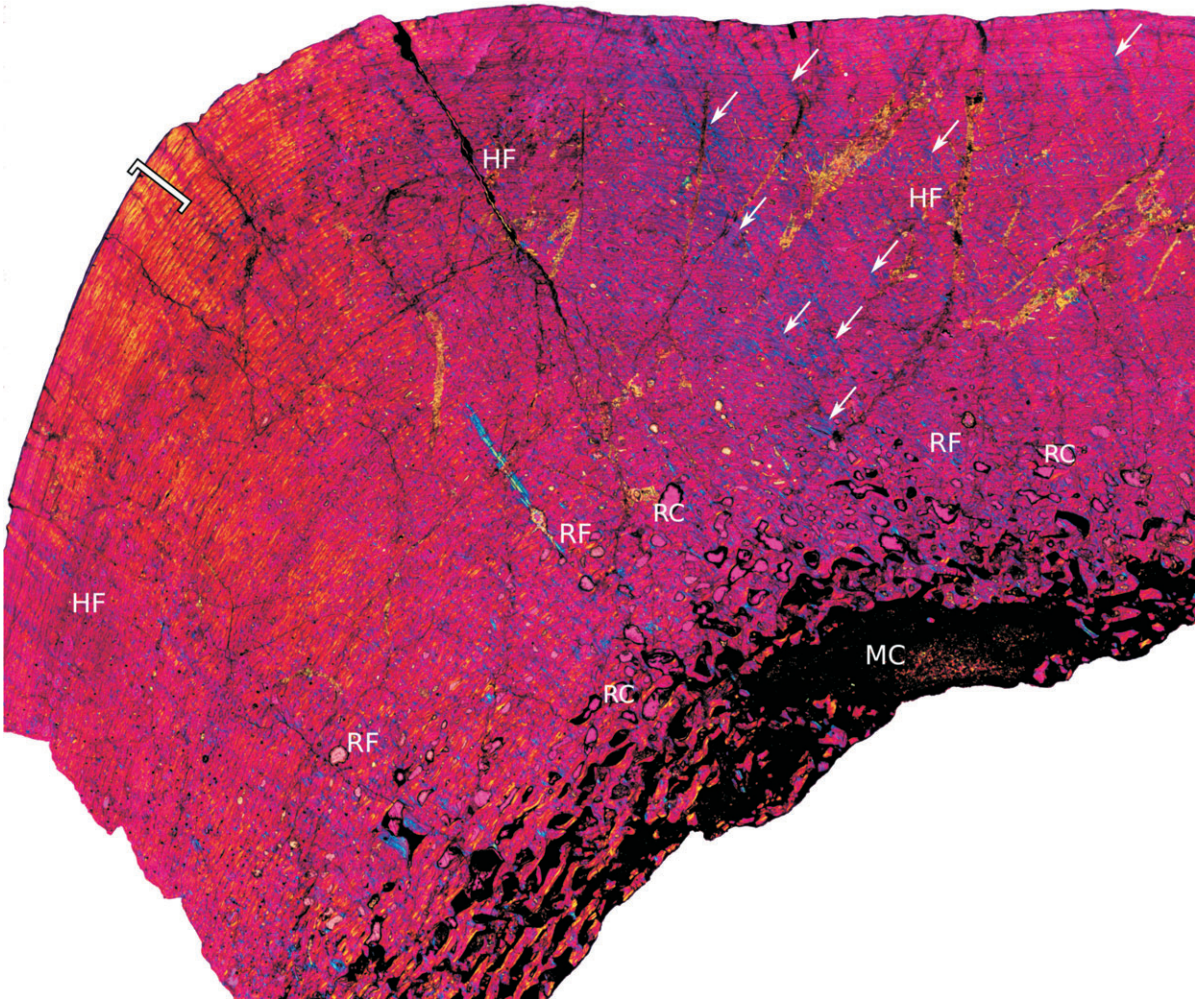


Figure 27. Femoral osteohistology of *Massospondylus carinatus* (BP/1/4934) in cross-polarized light. Resorption cavities demarcate the Resorption Front. The Haversian Front is located in the outer part of the middle cortex. Bracket indicates parallel-fibred bone in the outer cortex. Arrows indicate extensive Sharpey's fibres. Scale bar = 500 μm.

with the margin of the bone (Fig. 27). These are best seen in polarized and cross-polarized light and probably correspond to the attachment points of the m. femorotibialis lateralis.

DISCUSSION

Diagnosis of *M. carinatus*

Various authors have proposed diagnostic characters for *Massospondylus*, primarily on the basis of referred crania, including that of BP/1/4934 (e.g. Galton 1990; Hinic 2002, cited in Galton & Upchurch 2004; Sues *et al*. 2004; Chapelle & Choiniere 2018). Many of these were proposed as parts of a unique character combination for the taxon, rather than as distinct autapomorphies (Sues *et al*. 2004; Chapelle & Choiniere 2018). Unfortunately, however, in the light of more recent work on sauropodomorph anatomy and taxonomy, the majority of these do not stand up to detailed scrutiny and can no longer be considered useful diagnostic features. Here, we deal with each of these proposed characters in turn:

1) 'Greatest transverse width of skull exceeding height of skull by at least 10%' (Sues *et al*. 2004: 242). This feature was proposed by Sues *et al*. (2004), who attributed this character to Sereno (1999). However, Sereno (1999) did not discuss the taxonomy of *Massospondylus* (*contra* Sues *et al*. 2004) and it is more likely that this feature should be attributed to Hinic (2002), as noted by Galton & Upchurch (2004). Although this feature does characterize one of the specimens referred to *M. carinatus* by Gow *et al*. (1990) and Sues *et al*. (2004) – BP/1/4779, which has an exceptionally broad, low skull – it does not describe the condition in either the neotype or BP/1/5241, in which the maximum skull width (measured between the postorbital/frontal junctions), is equal to maximum skull height (measured from the ventral margin of the jugal to the dorsal margin of the frontal above the orbit). As a result, this character is rejected as a diagnostic feature of the taxon.
2) 'Orbit proportionally large and snout proportionally short even in presumably adult specimens' (Sues *et al*. 2004: 242). Precise definitions of how these ratios were obtained were not provided in Sues *et al*. (2004), but in lateral view, the long axis of the orbit in BP/1/4934 accounts for ~30% of total skull length (as measured from the tip of the premaxilla to the posteroventral corner of the quadratojugal) and the snout extends for ~55% of the same distance (with the snout defined as the preorbital region of the skull, as measured from a straight line meeting the anterior margin of the orbit

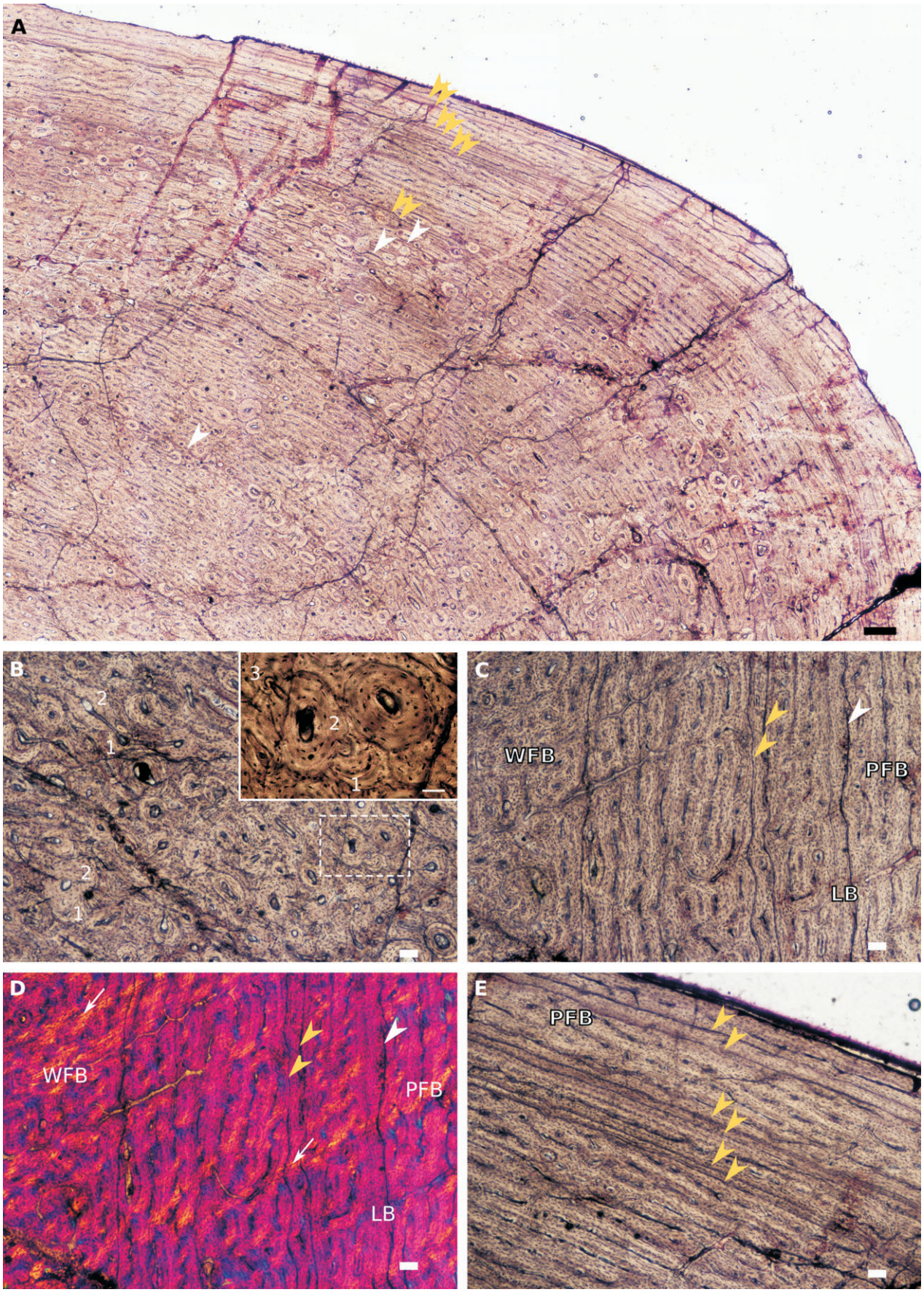


Figure 28. Femoral osteohistology of *Massospondylus carinatus* (BP/1/4934). **A**, middle to outer cortex in normal light showing multiple double LAGs. **B**, inner cortex in normal light showing multiple (1, 2 and 3) generations of secondary osteons. Inset corresponds to high magnification of dashed box showing three generations of secondary osteons. **C**, middle cortex in normal light showing a mixture of woven-fibred and parallel-fibred bone, as well as multiple LAGs. Note the annulus of lamellar bone associated with a LAG. **D**, same view as in C, but in cross-polarized light. Arrows indicate Sharpey's fibres. **E**, outer cortex in normal light showing several double LAGs and parallel-fibred bone. White arrowheads indicate LAGs and yellow arrowheads indicate double LAGs. Scale bars = 500 μm (**A**), 100 μm (**B**–**E**) and 50 μm (**B**, inset).

and extending perpendicular to the skull long axis. Similar orbit ratios are present in BP/1/5241 (~31%) and BP/1/4779 (33%), but these specimens differ in having snout ratios of ~56% and ~42%, respectively. This contrasts to some extent with the condition in *Plateosaurus* (e.g. Galton 1985b), whose adults have relatively smaller orbits (orbit ratio = ~22%), but where the snout ratio is the same as that in *M. carinatus*. Reconstructions of *Adeopapposaurus* and *Lufengosaurus* (which have almost complete skulls) have orbital length/skull length ratios of around ~33% and ~29%, respectively, and similar snout proportions to those of *M. carinatus* and *Plateosaurus* (Martínez 2009; Barrett *et al*. 2005). As these proportions are consistent among other massospondylids and are also present in some other non-massospondylid sauropodomorphs, these features are rejected as diagnostic characters of *M. carinatus*. Moreover, relative orbit size and snout length are both known to vary considerably during dinosaur ontogeny (e.g. Varricchio 1997), so should be avoided as taxonomic characters.

3) 'Dorsal process of maxilla tall and nearly vertical' (Galton 1990: 339; Sues *et al*. 2004: 242). The height and orientation of the maxillary ascending process is very similar in a broad range of sauropodomorphs and that of *M. carinatus* is very similar to those of *Coloradisaurus* (Apaldetti *et al*. 2014), *Lufengosaurus* (Young 1941; Barrett *et al*. 2005), *Mussaurus* (Pol & Powell 2007) and some individuals of *Plateosaurus* (Galton 1985b), among others, so this feature is rejected as a diagnostic character of *M. carinatus*.
4) 'Medial sheet of maxilla narrow anteroposteriorly' (Sues *et al*. 2004: 242). A similarly narrow medial lamina is present on the maxillary ascending process of a wide range of sauropodomorph taxa, including *Adeopapposaurus* (Martínez 2009), *Coloradisaurus* (Apaldetti *et al*. 2014), *Lufengosaurus* (Young 1941; Barrett *et al*. 2005) and *Sarahsaurus* (Attridge *et al*. 1985), so it cannot be regarded as an autapomorphy of *M. carinatus*.
5) 'Prefrontal with long posterior process along dorsal margin of the orbit, but frontal still contributing significantly to formation of orbital margin' (Sues *et al*. 2004: 242). Similarly, proportionally lengthy prefrontals are found in combination with a substantial frontal contribution to the orbit in other putative massospondylids, including *Adeopapposaurus* (Martínez 2009), *Coloradisaurus* (Apaldetti *et al*. 2014), *Leyesaurus* (Apaldetti *et al*. 2011), *Lufengosaurus* (Young 1941; Barrett *et al*. 2005) and *Sarahsaurus* (Attridge *et al*. 1985), so this feature is not distinctive for *M. carinatus*.
6) 'Lacrimal with lateral sheet overhanging the posterodorsal corner of antorbital fenestra' (Sues *et al*. 2004: 242). This feature also occurs in a number of other sauropodomorphs, including *Leyesaurus* (Apaldetti *et al*. 2011), *Lufengosaurus* (Barrett *et al*. 2005) and some individuals of *Plateosaurus* (Galton 1985b), so it cannot be regarded as useful for diagnosing *M. carinatus*.
7) 'Distinct ridge on dorsolateral aspect of lacrimal, continuous with lateral knob on the prefrontal' (Sues *et al*. 2004: 242). Similar features are also present in *Lufengosaurus* (Barrett *et al*. 2005), *Melanorosaurus* (Yates 2007a) and *Mussaurus* (Pol & Powell 2007), so they cannot be considered as distinctive for *M. carinatus*.
8) 'Width of the base of the cultriform process at least 20% of its length' (Hinic 2002, cited in Galton & Upchurch 2004: 252). Similar proportions of the cultriform process are also seen in *Pantydraco* (Yates 2003) and *Plateosaurus* (Prieto-Márquez & Norell 2011), so this is not considered to be a reliable diagnostic character.
9) 'Prominent muscle scar on lateral surface of fibula at midlength' (Hinic 2002, cited in Galton & Upchurch 2004: 252). The fibulae are not preserved in the *M. carinatus* neotype, so the status of this character cannot be confirmed. In addition, a similar muscle scar has been reported in *Mussaurus* (Otero & Pol 2013), so its utility as a diagnostic feature is doubtful.
10) 'Basipterygoid processes that are separated by an angle smaller than 60°' (Chapelle & Choiniere 2018: 6). This feature is present in both the neotype of *M. carinatus* and BP/1/5241 and differs from the conditions present in other sauropodomorphs, including *Plateosaurus* and *Efraasia* (interbasipterygoid process angles of ~70°: Chapelle & Choiniere 2018) and *Adeopapposaurus*, *Coloradisaurus* (*contra* Chapelle & Choiniere 2018) and *Pantydraco* (interbasipterygoid process angles of ~90°: Kermack 1984; Martínez 2009; Apaldetti *et al*. 2014). This character is accepted as a potential autapomorphy of *M. carinatus* herein.
11) 'Jugal process of the ectopterygoid is strongly curved' (Chapelle & Choiniere 2018: 7). As noted by Chapelle & Choiniere (2018) this feature is present in BP/1/5241, but cannot be evaluated in the neotype. However, as these authors argue, there are strong grounds for accepting the referral of BP/1/5241 to *M. carinatus* (see below). The strong recurvature of the ectopterygoid in BP/1/5241 is distinct from that seen in other putative massospondylids, such as *Lufengosaurus* and *Sarahsaurus*, though it is similar to that of *Leyesaurus* (Chapelle & Choiniere 2018). Although this feature cannot be considered an autapomorphy it can be regarded as part of a unique character combination that distinguishes *M. carinatus* from other massospondylids.

As a result of the foregoing discussion, we restrict the diagnosis of *M. carinatus* to include one cranial and six postcranial autapomorphies (see Diagnosis and Description, above), providing a range of features that can be used characterize the taxon from other massospondylids and other non-sauropod sauropodomorphs. Additional character combinations may also prove useful in further distinguishing *M. carinatus* from other basal sauropodomorphs.

Status of BP/1/5241

Chapelle & Choiniere (2018) referred a complete skull and partial postcranial skeleton (BP/1/5241) to *M. carinatus*, following Gow *et al*. (1990) and Sues *et al*. (2004). Their referral was based on the shared presence of a single feature, which they considered to be autapomorphic for the taxon, namely the possession of a strongly, curved

hook-like ectopterygoid in BP/1/5241 and BP/1/4934 (Chapelle & Choiniere 2018), in addition to many general similarities between the crania (see also Gow *et al*. 1990; Sues *et al*. 2004). Here, we confirm the presence of four postcranial autapomophies of *M. carinatus* in BP/1/5241, supporting its referral to this taxon. These are: 1) the presence of very elongate anterior cervical centra (centrum length/anterior centrum height ratio of ~7.2 in Cv5); 2) the presence of a hook-like process on the anterior margin of the anterior cervical neural spines (present in Cv5, but damaged in the other cervicals); 3) a scapula whose distal blade is expanded dorsally and ventrally with respect to the long axis of the blade; and 4) the presence of an elongate deltopectoral crest (~57% of humeral length in BP/1/5241, which although not as extensive as that in BP/1/4934 is still more elongate than in any other massospondylid, see above). BP/1/5241 lacks an ulna and the distal pubes are missing, so the other proposed autapomorphies cannot be confirmed in this specimen. Nevertheless, the presence of shared cranial and postcranial features strongly supports the referral of BP/1/5241 to *M. carinatus* and until further taxonomic revisions are conducted, the hypodigm should be limited to these two specimens.

Implications for the referral of additional material

Since Owen's (1854) description of *M. carinatus*, many additional sauropodomorph taxa have been proposed on the basis of specimens recovered from the upper Elliot and Clarens formations. Although some of these are based on recent work and are regarded as valid (e.g. *Aardonyx*, *Antetonitrus*, *Arcusaurus*, *Ignavusaurus*, *Pulanesaura*: Yates & Kitching 2003; Knoll 2010; Yates *et al*. 2010, 2011; McPhee *et al*. 2015) the majority of historically proposed taxa have been relegated to the status of *nomina dubia* or regarded as junior synonyms of *M. carinatus* (e.g. Seeley 1895a; Galton & Cluver 1976; Cooper 1981; Galton 1990; Galton & Upchurch 2004). However, in many cases, these taxonomic decisions were made on the basis of the provenance of material, and the assumption that there was only a single valid upper Stormberg Group sauropodomorph taxon, rather than on detailed consideration of anatomy. Perhaps significantly, almost all of the taxa synonymized with *M. carinatus* have been erected on material consisting solely of postcranial elements (see Table 10 for a list of these taxa and the composition of their type specimens), but as the postcranial skeleton of *M. carinatus* has not been fully characterized until now comparisons between these specimens have had a weak basis. Description of the neotype specimen (BP/1/4934) provides a benchmark for re-assessing these taxonomic decisions and for determining whether the referral of historically collected and new material to this iconic taxon can be justified on the basis of shared anatomical features.

A thorough revision of the hundreds of specimens referred to *M. carinatus* that are housed in museum collections around the world lies beyond the scope of this contribution, but it is important to note that it is essential to refer to the neotype in all future discussions of sauropodomorph taxonomy and systematics, as it should be regarded as the primary reference specimen for this taxon. Until recently, the detailed monograph published by Cooper (1981) was used extensively as the primary source of information on the postcranial skeleton of *Massospondylus* or as a supplement to personal observations on the neotype (e.g. Benton *et al*. 2000; Galton & Upchurch 2004; Upchurch *et al*. 2007; Martínez 2009; Knoll 2010; Apaldetti *et al*. 2011, 2013), but as mentioned above there has been no critical assessment of whether this Zimbabwean material is conspecific, or even congeneric, with that from the main Karoo Basin. To illustrate this problem, it is noteworthy that although some of the specimens illustrated by Cooper (1981) do appear very similar or identical to those in BP/1/4934, such as the ilium (Cooper 1981: fig. 51), others are clearly distinct. For example, the deltopectoral crests of the humeri illustrated by Cooper (1981: figs. 26 and 27) are proportionally shorter than those in *M. carinatus* (Fig. 18A), with the crest extending for only 50% or less of humeral length in the former, but up to 60% in the latter, (see above). Also, some of the posterior dorsal vertebrae reported from Zimbabwe (Cooper 1981: fig. 10) have centra that are much more elongate than those in BP/1/4934, with centrum length/anterior height ratios of 1.6 *vs* 1.1 in BP/1/4934 (see Table 2). A thorough revision of the material described by Cooper (1981) is now warranted to establish its taxonomic affinities and the latter work should no longer be used uncritically as a source of information on *M. carinatus*, as to do so might misrepresent the anatomy and affinities of the taxon.

In addition, as the taxonomic affinities of many specimens referred to *M. carinatus* require reappraisal, further consideration needs to be given to the roles that ontogenetic and individual variation might play in the definition of potential autapomorphies. Hopefully, this description of the adult neotype individual will now form a firmer baseline against which such comparisons can be made.

Ontogenetic status of BP/1/4934

Previous work has attempted to determine growth rates and patterns in *Massospondylus carinatus* (Chinsamy 1991, 1993; Cerda *et al*. 2017), but the taxonomic status of many of the specimens used in these studies requires reassessment as it can no longer be assumed that all sauropodomorphs from the upper Elliot Formation are referable to this taxon (see above). Nevertheless, in agreement with these earlier studies the primary bone tissue of BP/1/4934 is predominantly characterized by rapidly forming well-vascularized fibrolamellar bone, with a transition to slower forming parallel-fibred bone towards the sub-periosteal surface. The presence of fibrolamellar bone indicates rapid growth rates similar to other massospondylids such as *Adeopapposaurus* and *Leyesaurus* (Cerda *et al*. 2017). The decrease in overall growth rate and increased abundance and decreased spacing between LAGs indicates a late ontogenetic stage for this individual. Although an EFS was not observed, the extensive secondary remodelling, increased incidence of double and triple LAGs, and the predominance of parallel-fibred bone towards the

Table 10. Taxa referred to *Massospondylus*, with comments on the material and its provenance (following Seeley, 1895a; Galton & Cluver 1976; Cooper 1981; Galton 1990; Galton & Upchurch 2004).

Taxon	Type material	Locality and Horizon	Notes and current status
Massospondylus carinatus Owen, 1854	Almost complete skeleton with skull (neotype: BP/1/4934)	Bormansdrift Farm, Clocholan District, Free State Province, South Africa; upper Elliot Formation (Kitching & Raath 1984)	Valid species. Neotype replaces the original syntype series (formerly in the Hunterian Museum of the Royal College of Surgeons, London), which was destroyed during WW2, although casts of these remains are available (NHMUK PV R1312 and R3027–3028/SAM-PKC-958-962), as well as casts of other specimens referred to *Massospondylus* by Owen (1854) (NHMUK PV R3030–3034)
Leptospondylus capensis Owen, 1854	Two caudal vertebrae	Farm Beauchef Abbey 215, Harrismith, Free State Province, South Africa; unknown but probably upper Elliot Formation (Kitching & Raath 1984)	Original specimens destroyed during WW2 (see above), but cast available of one syntype (NHMUK PV R3025) and one specimen referred to *Leptospondylus* by Owen (1854) (NHMUK PV R3026); junior subjective synonym of *M. carinatus* (Seeley 1895a) or *nomen dubium*, Sauropodomorpha indet. (Galton 1990; Galton & Upchurch 2004)
Pachyspondylus orpenii Owen, 1854	Nine sacral and caudal vertebrae	Farm Beauchef Abbey 215, Harrismith, Free State Province, South Africa; unknown but probably upper Elliot Formation (Kitching & Raath 1984)	Original specimens destroyed during WW2 (see above), but casts available of some syntypes (NHMUK PV R3035 *partim*), as well as casts of other specimens referred to *Pachyspondylus* by Owen (1854) (NHMUK PV R1312a, NHMUK PV R3035 *partim* and R3036–3037); junior subjective synonym of *M. carinatus* (Seeley 1895a) or *nomen dubium*, Sauropodomorpha indet. (Galton 1990; Galton & Upchurch 2004)
Massospondylus hislopi Lydekker, 1890a	Isolated partial vertebra (IM G.281/1-u)	Maleri, Andhra Pradesh, India; Lower Maleri Formation (Lydekker 1885)	*Nomen dubium*, Sauropodomorpha indet. (Huene 1906; Cooper 1981; Galton 1990; Galton & Upchurch 2004)
Massospondylus rawesi Lydekker, 1890a	Isolated tooth (NHMUK PV R4190)	Takli, Maharashtra, India; Lameta Beds (Lydekker 1890a)	*Nomen dubium*, Theropoda indet. (Cooper 1981; Carrano et al. 2010)
Hortalotarsus skirtopodus Seeley, 1894	Partial hind limb (AM 455)	Exact locality unknown, but near Barkley East, Eastern Cape Province, South Africa; Clarens Formation (Kitching & Raath 1984)	The hind limb is the only surviving part of a partial skeleton that was largely destroyed during an attempt to extract it; junior subjective synonym of *M. carinatus* (Cooper 1981) or *nomen dubium*, Sauropodomorpha indet. (Galton 1990; Galton & Upchurch 2004)
Massospondylus browni Seeley, 1895b	Vertebrae, femora, partial foot (NHMUK PV R3302)	Exact locality unknown, but Telle River, Eastern Cape Province, South Africa; upper Elliot Formation (Kitching & Raath 1984)	Junior subjective synonym of *M. carinatus* (Cooper 1981; Galton 1990) or *nomen dubium*, Sauropodomorpha indet. (Galton & Upchurch 2004)
Aetonyx palustris Broom, 1911	Partial postcranial skeleton (SAM-PK-2768-2770)	Foutanie Farm, near Fouriesburg, Free State Province, South Africa; upper Elliot Formation (Kitching & Raath 1984)	Junior subjective synonym of *M. carinatus* (Cooper 1981; Galton 1990) or *nomen dubium*, Sauropodomorpha indet. (Galton & Upchurch 2004)
Gryponyx africanus Broom, 1911	Partial postcranial skeleton (SAM-PK-3357-3359)	Foutanie Farm, near Fouriesburg, Free State Province, South Africa; upper Elliot Formation (Kitching & Raath 1984)	Junior subjective synonym of *M. carinatus* (Cooper 1981; Galton 1990) or *nomen dubium*, Sauropodomorpha indet. (Galton & Upchurch 2004)
Gyposaurus capensis Broom, 1911	Partial skeleton lacking skull, preserved partly as natural moulds (SAM-PK-K990)	Exact locality unknown, but near Ladybrand, Free State Province, South Africa; Clarens Formation (Kitching & Raath 1984)	Junior subjective synonym of *M. carinatus* (Cooper 1981; Galton 1990) or *nomen dubium*, Sauropodomorpha indet. (Galton & Upchurch 2004)

Continued on p. 174

Table 10 (continued)

Taxon	Type material	Locality and Horizon	Notes and current status
Massospondylus harriesi Broom, 1911	Incomplete forelimb and hindlimb (SAM-PK-3394)	Foutanie Farm, near Fouriesburg, Free State Province, South Africa; upper Elliot Formation (Kitching & Raath 1984)	Junior subjective synonym of *M. carinatus* (Cooper 1981; Galton 1990) or *nomen dubium*, Sauropodomorpha indet. (Galton & Upchurch 2004)
Gryponyx transvaalensis Broom, 1912	Ungual and metatarsal (TM 120)	Farm Wiepe 1258, Limpopo Province; Bushveld Sandstone Formation (Broom 1912)	Junior subjective synonym of *M. carinatus* (Cooper 1981) or *nomen dubium*, Sauropodomorpha indet. (Galton 1990; Galton & Upchurch 2004)
Thecodontosaurus minor Haughton, 1918	Cervical, tibia and ilium (SAM-PK-3451)	Pitsing, near Maclear, Eastern Cape Province, South Africa; Elliot Formation (not known if lower or upper Elliot) (Kitching & Raath 1984)	Junior subjective synonym of *M. carinatus* (Cooper 1981) or *nomen dubium*, Sauropodomorpha indet. (Galton 1990; Galton & Upchurch 2004)
Aristosaurus erectus Van Hoepen, 1920a	Partial skeleton (TM 130)	Exact locality unknown, Ficksburg, Free State Province, South Africa; Clarens Formation (Kitching & Raath 1984)	Junior subjective synonym of *M. carinatus* (Cooper 1981) or *nomen dubium*, Sauropodomorpha indet. (Galton 1990; Galton & Upchurch 2004)
Dromicosaurus gracilis Van Hoepen, 1920b	Partial skeleton (TM 123)	Noupoortsnek, Bethlehem, Free State Province, South Africa; Elliot Formation (not known if lower or upper Elliot) (Kitching & Raath 1984)	Junior subjective synonym of *M. carinatus* (Cooper 1981) or *nomen* dubium, Sauropodomorpha indet. (Galton 1990; Galton & Upchurch 2004)
*Gryponyx taylor*i Haughton, 1924	Partial pelvis (SAM-PK-3453)	Fouriesburg, Free State Province, South Africa; upper Elliot Formation (Kitching & Raath 1984)	Junior subjective synonym of *M. carinatus* (Cooper 1981; Galton 1990) or *nomen dubium*, Sauropodomorpha indet. (Galton & Upchurch 2004)
Massospondylus schwarzi Haughton, 1924	Partial tibia and pes (SAM-PK-5134)	Makomoreng, Eastern Cape Province, South Africa; Elliot Formation (not known if lower or upper Elliot) (Kitching & Raath 1984)	Junior subjective synonym of *M. carinatus* (Cooper 1981; Galton 1990) or *nomen dubium*, Sauropodomorpha indet. (Galton & Upchurch 2004)
Massospondylus kaalae Barrett, 2009	Partial skull (SAM-PK-K1325)	Voyizane, Eastern Cape Province, South Africa; upper Elliot Formation (Barrett 2009)	Provisionally valid species

periphery in both elements suggests that BP/1/4934 was an adult at the time of death. The lack of an EFS, however, indicates that it had not reached maximum size. The features noted above, including the position of the Resorption Front and the Haversian Front suggest that the bone tissue is equivalent to the Type F bone tissue or an early Histologic Ontogenetic Stage 12, as described by Klein & Sander (2008).

CONCLUSIONS

This description of the neotype postcranial skeleton of *Massospondylus carinatus* (BP/1/4934), the first ever attempted, can act as a basis for more rigorously evaluating the taxonomic status of the copious material referred to this species that resides in museum collections, as well as that being recovered by new fieldwork initiatives. *M. carinatus* can be diagnosed on the basis of one cranial and six postcranial autapomorphies, all of which are present in the neotype, and that relate to the basicranium, cervical vertebrae, scapula, humerus, ulna and pubis. This information can be used to assess the taxonomy of other sauropodomorph dinosaurs from the main Karoo Basin and elsewhere in southern Africa, which will lead to an improved understanding of species diversity, palaeoecology and faunal succession in these critical early dinosaur faunas.

SUPPLEMENTARY MATERIAL

Supplementary information is provided in five online supplements.

ABBREVIATIONS

Institutional

AM	Albany Museum, Rhodes University, Grahamstown, South Africa
BP	Evolutionary Studies Institute (ESI: formerly Bernard Price Institute), University of the Witwatersrand, Johannesburg, South Africa
IM	Indian Museum, Kolkata, India
IVPP	Institute of Vertebrate Paleontology and Paleoanthropology, Academia Sinica, Beijing, People's Republic of China
NHMUK	Natural History Museum, London, UK
SAM	Iziko South African Museum, Cape Town, South Africa
TM	Ditsong National Museum of Natural History, Pretoria, South Africa

Anatomical

ace	acetabulum
acr	acromion process
ap	anterior process
ant	anterior
asr	attachment sites for sacral ribs
at	anterior trochanter
Ax	axis
c	carpal
Cd	caudal vertebra(e)
CDF	centrodiapophyseal fossa
ce	centrum
ch	chevron
cl	clavicle
cot	coracoid tubercle
cr	cervical rib
Cv	cervical vertebra(e)
D	dorsal vertebra(e)
dep	slit-like depression at neurocentral boundary
dia	diapophysis
dpc	deltopectoral crest
entc	entepicondyle
ep	epipophysis
EPRL	epipophyseal-prezygapophyseal lamina
fe	femur
fh	femoral head
ft	fourth trochanter
gl	glenoid
gs	gastralia
gt	greater trochanter
hh	humeral head
hp	hook-like process on neural spine
hu	humerus
il	ilium
ilp	iliac process
IPRL	interprezygapophyseal lamina
isp	ishiac peduncle
it	internal tuberosity
k	keel
l	left
LB	lamellar bone
LPO	longitudinally-oriented primary osteons
man	manus
Mc	metacarpal
MC	medullary cavity
Mt	metatarsal
ncs	neurocentral suture
ns	neural spine
of	olecranon fossa
ofo	obturator foramen
olp	olecranon process
PCDL	posterior centrodiapophyseal lamina
PFB	parallel-fibred bone
Ph	phalanx
PO	primary osteons
poz	postzygapophysis
POCDF	postzygapophyseal centrodiapophyseal fossa
PPDL	paradiapophyseal lamina
PRDL	prezygodiapophyseal lamina
PRPADF	prezygopophyseal paradiapophyseal fossa
PRPL	prezygoparapophyseal lamina
prz	prezygapophysis
PSF	prespinal fossa
pub	pubis
pup	pubic peduncle
r	right
ra	radius
rc	radial condyle
RC	resorption cavities
RF	resorption front
S	sacral vertebra(e)
saf	supra-acetabular flange
sb	scapular blade
sco	scapulocoracoid
SO	secondary osteons
SPOL	spinopostzygapophyseal lamina
SPRL	spinoprezygapophyseal lamina
st	sternum
stp	sternal process
tp	transverse process
uc	ulnar condyle
ul	ulna
Un	ungual
WFB	woven-fibred bone

Measurements

ACH	anterior centrum height
ACW	anterior centrum width
CL	centrum length
LPL	lateral process of sacral rib length (anteroposterior)
MPL	medial process of sacral rib length (anteroposterior)
NAL	neural arch length
NSH	neural spine height
NSL	neural spine length
PCH	posterior centrum height
PCW	posterior centrum width
SRL	sacral rib length (mediolateral)
VH	total height of vertebra

P.M.B. would like to offer his sincere thanks to his coauthors and all of the other staff and students of the ESI for their assistance and hospitality during the course of this work. We especially thank Sifelani Jirah for facilitating collections access, Bernhardt Zipfel for allowing further preparation and osteohistological sampling, Charlton

Dube for conservation and preparation, and Bruce Rubidge for his long-term support of the project. Mark Graham (NHMUK) provided further advice on conserving the specimen. Pia Viglietti (ESI) offered useful discussion on the type locality, while Heinrich Mallison (Museum für Naturkunde, Berlin) gave advice on photogrammetry. Zaituna Skosan (SAM) and Heidi Fourie (TM) afforded catalogue information on specimens in their care. Cecilia Apaldetti and Ricardo Martínez (both of the Universidad Nacional de San Juan) are thanked for providing unpublished comparative information on *Leyesaurus* and *Adeopapposaurus*, respectively. K.E.J.C. would like to express her thanks to Valerie and Charles Rose-Innes for their hospitality in Bloemfontein during data collection. All of the authors thank the referees, Cecilia Apaldetti and Peter Galton (University of Bridgeport), for their comments, as well as the handling editor, Roger Benson (University of Oxford). Funding for this work was provided by: a Royal Society International Exchange Grant (jointly to P.M.B. and J.N.C.), the Earth Sciences Departmental Investment Fund of the Natural History Museum, London (to P.M.B.), the National Research Foundation (UID 104688, 98819: to J.B.), The Palaeontological Scientific Trust (PAST: to K.E.J.C. and J.B.), and the DST-NRF Centre of Excellence in Palaeosciences (CoE-Pal: to K.E.J.C., J.B. and J.N.C.). PAST also awarded generous funds for conservation of the specimen (to J.N.C.).

§ORCID iDs

P.M. Barrett: orcid.org/0000-0003-0412-3000
K.E.J. Chapelle: orcid.org/0000-0002-9991-0439
J. Botha: orcid.org/0000-0001-8824-9334
J.N. Choiniere: orcid.org/0000-0002-1008-0687

REFERENCES

ANONYMOUS. 1969. Lesotho. **In**: Anonymous (ed.), *Report on the British Museum (Natural History), 1966–1968*, 31–35. London, Trustees of the British Museum (Natural History).

APALDETTI, C., POL, D. & YATES, A.M. 2013. The postcranial anatomy of *Coloradisaurus brevis* (Dinosauria: Sauropodomorpha) from the Late Triassic of Argentina and its phylogenetic implications. *Palaeontology* **56**(2), 277–301. DOI:10.1111/j.1475-4983.2012.01198.x

APALDETTI, C., MARTINEZ, R.N., ALCOBER, O.A. & POL, D. 2011. A new basal sauropodomorph (Dinosauria: Saurischia) from Quebrada del Barro Formation (Marayes-El Carrizal Basin), northwestern Argentina. *PLOS ONE* **6**(11), e26964. DOI:10.1371/journal.pone.0026964

APALDETTI, C., MARTINEZ, R.N., POL, D. & SOUTER, T. 2014. Redescription of the skull of *Coloradisaurus brevis* (Dinosauria, Sauropodomorpha) from the Late Triassic Los Colorados Formation of the Ischigualasto-Villa Union Basin, northwestern Argentina. *Journal of Vertebrate Paleontology* **34**(5), 1113–1132. DOI:10.1080/02724634.2014.859147

ATTRIDGE, J. 1963. The Upper Triassic Karroo deposits and fauna of southern Rhodesia. *South African Journal of Science* **59**(5), 242–247.

ATTRIDGE, J. & CHARIG, A.J. 1967. Crisis in evolution: the Stormberg series. *Science Journal* **3**(7), 48–54.

ATTRIDGE, J.A., CROMPTON, A.W. & JENKINS, F.A. 1985. The southern African Liassic prosauropod *Massospondylus* discovered in North America. *Journal of Vertebrate Paleontology* **5**(2), 128–132. DOI:10.1080/02724634.1985.10011850

BARON, M.G., NORMAN, D.B. & BARRETT, P.M. 2017. A new hypothesis of dinosaur relationships and early dinosaur evolution. *Nature* **543**, 501–506. DOI:10.1038/nature21700

BARRETT, P.M. 2000. Prosauropod dinosaurs and iguanas: speculations on the diets of extinct reptiles. **In**: Sues, H-D. (ed.), *Evolution of Herbivory in Terrestrial Vertebrates: Perspectives from the Fossil Record*, 42–78. Cambridge, Cambridge University Press.

BARRETT, P.M. 2004. Sauropodomorph dinosaur diversity in the upper Elliot Formation (*Massospondylus* range zone: Lower Jurassic) of South Africa. *South African Journal of Science* **100**, 501–503.

BARRETT, P.M. 2009. A new basal sauropodomorph dinosaur from the upper Elliot Formation (Lower Jurassic) of South Africa. *Journal of Vertebrate Paleontology* **29**, 1032–1045. DOI:10.1671/039.029.0401

BARRETT, P.M. & UPCHURCH, P. 2007. The evolution of feeding mechanisms in early sauropodomorph dinosaurs. *Special Papers in Palaeontology* **77**, 91–112.

BARRETT, P.M. & YATES, A.M. 2006. New information on the palate and lower jaw of *Massospondylus* (Dinosauria: Sauropodomorpha). *Palaeontologia africana* **41**, 123–130.

BARRETT, P.M., UPCHURCH, P. & WANG, X.-L. 2005. Cranial osteology of *Lufengosaurus huenei* Young (Dinosauria: Prosauropoda) from the Lower Jurassic of Yunnan, People's Republic of China. *Journal of Vertebrate Paleontology* **25**, 806–822.

BARRETT, P.M., UPCHURCH, P., ZHOU, X.-D. & WANG, X.-L. 2007. The skull of *Yunnanosaurus huangi* Young, 1942 (Dinosauria: Prosauropoda) from the Lower Lufeng Formation (Lower Jurassic) of Yunnan, China. *Zoological Journal of the Linnean Society* **150**, 319–341. DOI:10.1111/j.1096-3642.2007.00290.x

BENTON, M.J., JUUL, L., STORRS, G.W. & GALTON, P.M. 2000. Anatomy and systematics of the prosauropod dinosaur *Thecodontosaurus antiquus* from the Upper Triassic of southwest England. *Journal of Vertebrate Paleontology* **20**(1), 77–108. DOI:10.1671/0272-4634(2000)020[0077:AASOTP]2.0.CO;2

BONAPARTE, J.F. & POWELL, J.E. 1980. A continental assemblage of tetrapods from the Upper Cretaceous beds of El Brete, northwestern Argentina (Sauropoda-Coelurosauria-Carnosauria-Aves). *Mémoires de la Société Géologique de France, Nouvelle Series* **139**, 19–28.

BOND, G. 1965. Some new fossil localities in the Karoo system of Rhodesia. *Arnoldia* **2**(11), 1–4.

BOND, G. 1973. The palaeontology of Rhodesia. *Rhodesia Geological Survey Bulletin* **70**, 1–121.

BONNAN, M.F. & SENTER, P. 2007. Were the basal sauropodomorph dinosaurs *Plateosaurus* and *Massospondylus* habitutal quadrupeds? *Special Papers in Palaeontology* **77**, 139–155.

BORDY, E.M. & CATUNEANU, O. 2001. Sedimentology of the upper Karoo strata in the Tuli Basin, South Africa. *Journal of African Earth Sciences* **33**, 605–629. DOI:10.1016/S0899-5362(01)00090-2

BOTHA-BRINK, J., SOARES, M.B. & MARTINELLI, A.G. 2018. Osteohistology of Late Triassic prozostrodontian cynodonts from Brazil. *PeerJ* **6**, e5029. DOI:10.7717/peerj.5029

BROOM, R. 1911. On the dinosaurs of the Stormberg, South Africa. *Annals of the South African Museum* **7**, 291–308 + pls XIV–XVII.

BROOM, R. 1912. On the remains of a theropodous dinosaur from the northern Transvaal. *Transactions of the Geological Society of South Africa* **14**, 82–83.

BUTLER, R.J., YATES, A.M., RAUHUT, O.W.M. & FOTH, C. 2013. A pathological tail in a basal sauropodomorph dinosaur from South Africa: evidence of traumatic amputation? *Journal of Vertebrate Paleontology* **33**(1), 224–228. DOI:10.1080/02724634.2012.710691

CABREIRA, S.F., KELLNER, A.W.A., DIAS-DA-SILVA, S., ROBERTO DA SILVA, L., BRONZATI, M., MARSOLA, J.C.A., MÜLLER, R.T., BITTENCOURT, J.S., BATISTA, B.J., RAUGUST, T., CARRILHO, R., BRODT, A. & LANGER, M.C. 2016. A unique late Triassic dinosauromorph assemblage reveals dinosaur ancestral anatomy and diet. *Current Biology* **26**, 3090–3095. DOI:10.1016/j.cub.2016.09.040

CARRANO, M.T., WILSON, J.A. & BARRETT, P.M. 2010. The history of dinosaur collecting in central India, 1828–1947. *Geological Society of London, Special Publications* **343**, 161–173. DOI:10.1144/SP343.9

CASTANET, J. 1994. Age estimation and longevity in reptiles. *Gerontology* **40**(2-4), 174–192. DOI:10.1159/000213586

CATUNEANU, O., WOPFNER, H., ERIKSSON, P.G., CAIRNCROSS, B., RUBIDGE, B.S., SMITH, R.M.H. & HANCOX, P.J. 2005. The Karoo basins of south-central Africa. *Journal of African Earth Sciences* **43**(1–3), 211–253. DOI:10.1016/j.jafrearsci.2005.07.007

CERDA, I.A., CHINSAMY, A., POL, D., APALDETTI, C., OTERO, A., POWELL, J.E. & MARTÍNEZ, R.N. 2017. Novel insight into the origin of the growth dynamics of sauropod dinosaurs. *PLOS ONE* **12**(6), e0179707. DOI:10.1371/journal.pone.0179707

CHAPELLE, K.E.J. & CHOINIERE, J.N. 2018. A revised cranial description of *Massospondylus carinatus* Owen (Dinosauria: Sauropodomorpha) based on computed tomographic scans and a review of cranial characters for basal Sauropodomorpha. *PeerJ* **6**, e4224. DOI:10.7717/peerj.4224

CHINSAMY, A. 1991. The osteohistology of femoral growth within a clade: a comparison of the crocodile *Crocodylus*, the dinosaurs *Massospondylus* and *Syntarsus*, and the birds *Struthio* and *Sagittarius*. Unpublished Ph.D. thesis, University of the Witwatersrand, Johannesburg.

CHINSAMY, A. 1993. Bone histology and growth trajectory of the prosauropod dinosaur *Massospondylus carinatus* Owen. *Modern Geology* **18**, 319–329.

COOPER, M.R. 1981. The prosauropod dinosaur *Massospondylus carinatus* Owen from Zimbabwe: its biology, mode of life and phylo-

genetic significance. *Occasional Papers of the National Museums and Monuments Rhodesia*, *Series B*, *Natural Sciences* **6**, 689–840.
CORMACK, D. 1987. *Ham's Histology*. New York, Lippencott.
CROMPTON, A.W. & ATTRIDGE, J. 1986. Masticatory apparatus of the larger herbivores during Late Triassic and Early Jurassic time. **In**: Padian, K. (ed.), *The Beginning of the Age of the Dinosaurs*, 223–236. Cambridge, Cambridge University Press.
D'EMIC, M.D., WHITLOCK, J.A., SMITH, K.M., FISHER, D.C. & WILSON, J.A. 2013. Evolution of high tooth replacement rates in sauropod dinosaurs. *PLOS ONE* **8**(7), e69235. DOI:10.1371/journal.pone.0069235
DE RICQLES, A.J., MEUNIER, F.J., CASTANET, J. & FRANCILLON-VIEILLOT, H. 1991. Comparative microstructure of bone. **In**: Hall, B.K. (ed.), *Bone (Volume 3): Bone Batrix and Bone Specific Products*, 1–78. Boca Raton, CRC Press.
ELLENBERGER, F., ELLENBERGER, P., FABRE, J., GINSBURG, L. & MENDREZ, C. 1964. The Stormberg Series of Basutoland (South Africa). **In**: Sundaram, R.K. (ed.), *XXII International Geological Congress*, *India*, *1964*. *Part IX*. *Proceedings of Section 9*. *Gondwanas*, 320–330. New Delhi, International Geological Congress.
ERICKSON, G.M., CURRY ROGERS, K. & YERBY, S.A. 2001. Dinosaurian growth patterns and rapid avian growth rates. *Nature* **412**, 429–433. DOI:10.1038/35086558
FRANCILLON-VIEILLOT, H., DE BUFFRENIL, V., CASTANET, J.D., GERAUDIE, J., MEUNIER, F.J., SIRE, J.Y., ZYLBERBERG, L. & DE RICQLES, A. 1990. Microstructure and mineralization of vertebrate skeletal tissues. **In**: Carter, J.G. (ed.) *Skeletal Biomineralization: Patterns*, *Processes and Evolutionary Trends*, 471–530. Washington, D.C., American Geophysical Union.
GAFFNEY, E.S. & KITCHING, J.W. 1994. The most ancient African turtle. *Nature* **369**, 55–58. DOI:10.1038/369055a0
GALTON, P.M. 1985a. Diet of prosauropod dinosaurs from the Late Triassic and Early Jurassic. *Lethaia* **18**, 105–123. DOI:10.1111/j.1502-3931.1985.tb00690.x
GALTON, P.M. 1985b. Cranial anatomy of the prosauropod dinosaur *Plateosaurus*, from the Knollenmergel (Middle Keuper, Upper Triassic) of Germany. *Geologica et Palaeontologica* **19**, 119–159.
GALTON, P.M. 1990. Basal Sauropodomorpha–Prosauropoda. **In**: Weishampel, D.B., Dodson, P. & Osmólska, H. (eds.), *The Dinosauria*, 320–344. Berkeley, University of California Press.
GALTON, P.M. & CLUVER, M.A. 1976. *Anchisaurus capensis* (Broom) and a revision of the Anchisauridae (Reptilia, Saurischia). *Annals of the South African Museum* **69**(6), 121–159.
GALTON, P.M. & UPCHURCH, P. 2004. Prosauropoda. **In**: Weishampel, D.B., Dodson, P. & Osmólska, H. (eds.), *The Dinosauria* (2nd edn), 232–258. Berkeley, University of California Press.
GOW, C.E. 1990. Morphology and growth of the *Massospondylus* braincase (Dinosauria,Prosauropoda). *Palaeontologia africana* **27**, 59–75.
GOW, C.E., KITCHING, J.W. & RAATH, M.A. 1990. Skulls of the prosauropod dinosaur *Massospondylus carinatus* Owen in the collections of the Bernard Price Institute for Palaeontological Research. *Palaeontologia africana* **27**, 45–58.
GRAHAM, M.R., CHOINIERE, J.N., JIRAH, S. & BARRETT, P.M. 2018. The remedial conservation and support jacketing of the *Massospondylus carinatus* neotype. *Palaeontologia africana* **52**, 222–227.
HAUGHTON, S.H. 1918. A new dinosaur from the Stormberg Beds of South Africa. *Annals and Magazine of Natural History*, *Series 9* **2**, 468–469.
HAUGHTON, S.H. 1924. The fauna and stratigraphy of the Stormberg Series. *Annals of the South African Museum* **12**, 323–497.
HUENE, F.v. 1906. Über die Dinosaurier der Aussereuropaïschen Trias. *Geologie und Paläontologie Abhandlungen* (n. s.) **8**, 97–156.
HUENE, F.v. 1914. Das natürliche System der Saurischia. *Zentralblatt für Mineralogie*, *Geologie und Paläontologie* **1914**, 154–158.
HUENE, F.v. 1932. Die fossile Reptil-Ordnung Saurischia, ihre Entwicklung und Geschichte. *Monographien zur Geologie und Paläontologie*, *series 1* **4**, 1–361.
JOHNSON, M.R., VAN VUUREN, C.J., HEGENBERGER, W.F., KEY, R. & SHOKO, U. 1996. Stratigraphy of the Karoo Supergroup in southern Africa: an overview. *Journal of African Earth Sciences* **23**(1), 3–15. DOI:10.1016/S0899-5362(96)00048-6
KERMACK, D. 1984. New prosauropod material from south Wales. *Zoological Journal of the Linnean Society* **82**, 101–117. DOI:10.1111/j.1096-3642.1984.tb00538.x
KITCHING, J.W. 1979. Preliminary report on a clutch of six dinosaurian eggs from the Upper Triassic Elliot Formation, northern Orange Free State. *Palaeontologia africana* **22**, 41–45.
KITCHING, J.W.& RAATH, M.A. 1984. Fossils from the Elliot and Clarens formations (Karoo Sequence) of the north-eastern Cape, Orange Free State and Lesotho, and a suggested biozonation, based on tetrapods. *Palaeontologia africana* **25**, 111–125.
KLEIN, N. & SANDER, P.M. 2008. Ontogenetic stages in the long bone histology of sauropod dinosaurs. *Paleobiology* **34**(2), 247–263.
KNOLL, F. 2004. Review of the tetrapod fauna of the "Lower Stormberg Group" of the main Karoo Basin (southern Africa): implication for the age of the Lower Elliot Formation. *Bulletin de la Société Géologique de France*, **175**(1), 73–83. DOI:10.2113/175.1.73
KNOLL, F. 2005. The tetrapod fauna of the upper Elliot and Clarens formations in the main Karoo Basin (South Africa and Lesotho). *Bulletin de la Société Géologique de France*, **176**(1), 81–91. DOI:10.2113/176.1.81
KNOLL, F. 2010. A primitive sauropodomorph from the upper Elliot Formation of Lesotho. *Geological Magazine* **147**(6), 814–829. DOI:10.1017/S001675681000018X
KUTTY, T.S., JAIN, S.L. & ROY CHOWDHURY, T. 1987. Gondwana sequence of the northern Pranhita-Godavari Valley: its stratigraphy and vertebrate faunas. *The Palaeobotanist* **36**, 214–229.
LUCAS, S.G. & HANCOX, P.J. 2001. Tetrapod-based correlation of the non-marine Upper Triassic of southern Africa. *Albertiana* **25**, 5–9.
LYDEKKER, R. 1885. The Reptilia and Amphibia of the Maleri and Denwa groups. *Memoirs of the Geological Survey of India*, *Palaeontologia Indica (Series IV: Indian pre-Tertiary Vertebrata)* **1**(5), 1–38 + pls. I–VI.
LYDEKKER, R. 1890a. Note on certain vertebrate remains from the Nagpur district. *Records of the Geological Survey of India* **23**, 21–24.
LYDEKKER, R. 1890b. *Catalogue of the Fossil Reptilia and Amphibia in the British Museum (Natural History)*. *Part IV, containing the orders Anomodontia*, *Ecaudata*, *Caudata and Labyrinthodontia*, *and Supplement*. London, British Museum (Natural History).
MALLISON, H. & WINGS, O. 2014. Photogrammetry in paleontology – a practical guide. *Journal of Paleontological Techniques* **12**, 1–31.
MARTÍNEZ, R.N. 2009. *Adeopapposaurus mognai*, gen. et sp. nov. (Dinosauria: Sauropodomorpha), with comments on adaptations of basal Sauropodomorpha. *Journal of Vertebrate Paleontology* **29**(1), 142–164. DOI:10.1671/039.029.0102
McPHEE, B.W., BORDY, E.M., SCISCIO, L. & CHOINIERE, J.N. 2017. The sauropodomorph biostratigraphy of the Elliot Formation of southern Africa: tracking the evolution of Sauropodomorpha across the Triassic-Jurassic boundary. *Acta Palaeontologica Polonica* **62**(3), 441–465. DOI:10.4202/app.00377.2017
McPHEE, B.W., BONNAN, M.F., YATES, A.M., NEVELING, J. & CHOINIERE, J.N. 2015. A new basal sauropod from the pre-Toarcian Jurassic of South Africa: evidence of niche-partitioning at the sauropodomorph-sauropod boundary? *Scientific Reports* **5**, 13224. DOI:10.1038/srep13224
MEYER, H.v. 1837. Mittheilungen, an Professor Bronn gerichtet. *Neues Jahrbuch für Mineralogie*, *Geologie und Paläontologie* **1837**, 314–316.
MUNYIKWA, D. 1997. Faunal analysis of Karoo-aged sediments in the northern Limpopo Valley, Zimbabwe. *Arnoldia* **10**(13), 129–140.
NOVAS, F.E., EZCURRA, M.D., CHATTERJEE, S. & KUTTY, T.S. 2011. New dinosaur species from the Upper Triassic upper Maleri and lower Dharmaram formations of central India. *Earth and Environmental Science Transactions of the Royal Society of Edinburgh* **101**, 333–349. DOI:10.1017/S1755691011020093
OLSEN, P.E. & GALTON, P.M. 1984. A review of the reptile and amphibian assemblages from the Stormberg of southern Africa, with special emphasis on the footprints and the age of the Stormberg. *Palaeontologia africana* **25**, 87–110.
OLSEN, P.E., KENT, D.V. & WHITESIDE, J.H. 2011. Implications of the Newark Supergroup-based astrochronology and geomagnetic polarity time scale (Newark-APTS) for the tempo and mode of the early diversification of Dinosauria. *Earth and Environmental Science Transactions of the Royal Society of Edinburgh* **101**, 201–229. DOI:10.1017/S1755691011020032
OTERO, A. & POL, D. 2013. Postcranial anatomy and phylogenetic relationships of *Mussaurus patagonicus* (Dinosauria: Sauropodomorpha). *Journal of Vertebrate Paleontology* **33**(5), 1138–1168. DOI:10.1080/02724634.2013.769444
OWEN, R. 1842. Report on British fossil reptiles, part II. *Reports from the British Association for the Advancement of Science* **1841**, 60–204.
OWEN, R. 1854. *Descriptive Catalogue of the Fossil Organic Remains of Reptilia and Pisces contained in the Museum of the Royal College of Surgeons*. London, Taylor and Francis.
POL, D. & POWELL, J.E. 2007. Skull anatomy of *Mussaurus patagonicus* (Dinosauria: Sauropodomorpha) from the Late Triassic of Patagonia. *Historical Biology* **19**(1), 125–144. DOI:10.1080/08912960601140085

PRIETO-MÁRQUEZ, A. & NORELL, M.A. 2011. Redescription of a nearly complete skull of *Plateosaurus* (Dinosauria: Sauropodomorpha) from the Late Triassic of Trossingen (Germany). *American Museum Novitates* **3727**, 1–58.
RAATH, M.A. 1974. Fossil vertebrate studies in Rhodesia: further evidence of gastroliths in prosauropod dinosaurs. *Arnoldia* **7**(5), 1–7.
RAATH, M.A., SMITH, C.C. & BOND, G. 1970. A new upper Karoo dinosaur fossil locality on the lower Angwa River, Sipolilo District, Rhodesia. *Arnoldia* **4**(35), 1–10.
REISZ, R.R., EVANS, D.C., SUES, H.-D. & SCOTT, D. 2010. Embryonic skeletal anatomy of the sauropodomorph dinosaur *Massospondylus* from the Lower Jurassic of South Africa. *Journal of Vertebrate Paleontology* **30**(6), 1653–1665.
DOI:10.1080/02724634.2010.521604
REISZ, R.R., EVANS, D.C., ROBERTS, E. M., SUES, H-D. & YATES, A.M. 2012. Oldest known dinosaurian nesting site and reproductive biology of the Early Jurassic sauropodomorph *Massospondylus*. *Proceedings of the National Academy of Sciences of the United States of* America **109**, 2428–2433.
DOI:10.1073/pnas.1109385109
REISZ, R.R., SCOTT, D., SUES, H.-D., EVANS, D.C. & RAATH, M.A. 2005. Embryos of an Early Jurassic prosauropod dinosaur and their evolutionary significance. *Science* **309**, 761–764.
DOI:10.1126/science.1114942
ROWE, T.B., SUES, H.-D. & REISZ, R.R. 2011. Dispersal and diversity in the earliest North American sauropodomorph dinosaurs, with a description of a new taxon. *Proceedings of the Royal Society B* **278**, 1044–1053.
DOI:10.1098/rspb.2010.1867
SCISCIO, L., DE KOCK, M., BORDY, E.M. & KNOLL, F. 2017. Magnetostratigraphy across the Triassic-Jurassic boundary in the main Karoo Basin. *Gondwana Research* **51**, 177–192.
DOI:10.1016/j.gr.2017.07.009
SEELEY, H.G. 1887. On the classification of animals commonly called Dinosauria. *Proceedings of the Royal Society of London* **43**, 165–171.
SEELEY, H.G. 1894. On *Hortalotarsus skirtopodus*, a new saurischian fossil from Barkly East, Cape Colony. *Annals and Magazine of Natural History, Series 6* **14**, 411–419.
SEELEY, H.G. 1895a. On the type of the genus *Massospondylus*. *Annals and Magazine of Natural History, Series 6* **15**, 102–118.
SEELEY, H.G. 1895b. On some vertebrae and limb bones from the Telle River, Cape Colony, provisionally described as *Massospondylus(?) browni* Seeley. *Annals and Magazine of Natural History, Series 6* **15**, 118–125.
SERENO, P.C. 1998. A rationale for phylogenetic definitions, with application to the higher-level taxonomy of Dinosauria. *Neues Jahrbuch für Geologie und Paläontologie, Abhandlungen* **210**(1), 41–83.
SERENO, P.C. 1999. The evolution of dinosaurs. *Science* **284**, 2137–2147.
DOI:10.1126/science.284.5423.2137
SERTICH, J.J.W. & LOEWEN, M.A. 2010. A new basal sauropodomorph dinosaur from the Lower Jurassic Navajo Sandstone of southern Utah. *PLOS ONE* **5**(3), e9789.
DOI:10.1371/journal.pone.0009789
SMITH, N.D & POL, D. 2007. Anatomy of a basal sauropodomorph dinosaur from the Early Jurassic Hanson Formation of Antarctica. *Acta Palaeontologica Polonica* **52**, 657–674.
SUES, H.-D., REISZ, R.R., HINIC, S. & RAATH, M.A. 2004. On the skull of *Massospondylus carinatus* Owen, 1854 (Dinosauria: Sauropodomorpha) from the Elliot and Clarens formations (Lower Jurassic) of South Africa. *Annals of the Carnegie Museum* **73**, 239–257.
UPCHURCH, P., BARRETT, P.M. & GALTON, P.M. 2007. A phylogenetic analysis of basal sauropodomorph relationships: implications for the origin of sauropod dinosaurs. *Special Papers in Palaeontology* **77**, 57–90.
VAN HOEPEN, E.C.N. 1920a. Contributions to the knowledge of the reptiles of the Karroo Formation. 5. A new dinosaur from the Stormberg Beds. *Annals of the Transvaal Museum* **7**(2), 77–92 + pls IX–X.
VAN HOEPEN, E.C.N. 1920b. Contributions to the knowledge of the reptiles of the Karroo Formation. 6. Further dinosaurian material in the Transvaal Museum. *Annals of the Transvaal Museum* **7**(2), 93–141 + pls XI–XXIII.
VARRICCHIO, D.J. 1997. Growth and embryology. **In**: Currie, P.J. & Padian, K. (eds), *Encyclopedia of Dinosaurs*, 282–288. San Diego, Academic Press.
WILSON, J.A. 1999. A nomenclature for vertebral laminae in sauropods and other saurischian dinosaurs. *Journal of Vertebrate Paleontology* **19**(4), 629–653.
DOI:10.1080/02724634.1999.10011178
WILSON, J.A. 2012. New vertebral laminae and patterns of serial variation in vertebral laminae of sauropod dinosaurs. *Contributions from the Museum of Paleontology, University of Michigan* **32**(7), 91–110.
WILSON, J.A., D'EMIC, M.D., IKEJIRI, T., MOACDIEH, E.M. & WHITLOCK, J.A. 2011. A nomenclature for vertebral fossae in sauropods and other saurischian dinosaurs. *PLOS ONE* **6**(2), e17114.
DOI:10.1371/journal.pone.0017114
YATES, A.M. 2003. A new species of the primitive dinosaur *Thecodontosaurus* (Saurischia: Sauropodomorpha) and its implications for the systematics of early dinosaurs. *Journal of Systematic Palaeontology* **1**, 1–42.
DOI:10.1017/S1477201903001007
YATES, A.M. 2004. *Anchisaurus polyzelus* (Hitchcock): the smallest known sauropod dinosaur and the evolution of gigantism amongst sauropodomorph dinosaurs. *Postilla* **230**, 1–58.
YATES, A.M. 2007a. The first complete skull of the Triassic dinosaur *Melanorosaurus* Haughton (Sauropodomorpha: Anchisauria). *Special Papers in Palaeontology* **77**, 9–55.
YATES, A.M. 2007b. Solving a dinosaurian puzzle: the identity of *Aliwalia rex* Galton. *Historical Biology* **19**(1), 93–123.
DOI:10.1080/08912960600866953
YATES, A.M. & BARRETT, P.M. 2010. *Massospondylus carinatus* Owen, 1854 (Dinosauria: Sauropodomorpha) from the Lower Jurassic of South Africa: proposed conservation of usage by designation of a neotype. *Palaeontologia africana* **45**, 7–10.
YATES, A.M. & KITCHING, J.W. 2003. The earliest known sauropod dinosaur and the first steps towards sauropod locomotion. *Proceedings of the Royal Society of London B* **270**, 1753–1758.
DOI:10.1098/rspb.2003.2417
YATES, A.M. & VASCONCELOS, C.C. 2005. Furcula-like clavicles in the prosauropod dinosaur *Massospondylus*. *Journal of Vertebrate Paleontology* **25**(2), 466–468.
DOI:10.1671/0272-4634(2005)025[0466:FCITPD]2.0.CO;2
YATES, A.M., BONNAN, M.F. & NEVELING, J. 2011. A new basal sauropodomorph dinosaur from the Early Jurassic of South Africa. *Journal of Vertebrate Paleontology* **31**(3), 610–625.
DOI:10.1080/02724634.2011.560626
YATES, A.M., HANCOX, P.J. & RUBIDGE, B.S. 2004. First record of a sauropod dinosaur from the upper Elliot Formation (Early Jurassic) of South Africa. *South African Journal of Science* **100**, 504–506.
YATES, A.M., BONNAN, M.F., NEVELING, J., CHINSAMY, A. & BLACKBEARD, M.G. 2010. A new transitional sauropodomorph dinosaur from the Early Jurassic of South Africa and the evolution of sauropod feeding and quadrupedalism. *Proceedings of the Royal Society B* **277**, 787–794.
DOI:10.1098/rspb.2009.1440
YOUNG, C.-C. 1941. A complete osteology of *Lufengosaurus huenei* Young (gen. et sp. nov.) from Lufeng, Yunnan, China. *Palaeontologica Sinica, Series C* **7**, 1–53 + pls. 4–5.
YOUNG, C.-C. 1942. *Yunnanosaurus huangi* Young (gen. et sp. nov.), a new Prosauropoda from the Red Beds at Lufeng, Yunnan. *Bulletin of the Geological Society of China* **22**, 63–104.
ZELENITZKY, D.K. & MODESTO, S.P. 2002. Re-evaluation of the eggshell structure of eggs containing dinosaur embryos from the Lower Jurassic of South Africa. *South African Journal of Science* **98**, 407–408.